Tudor domain containing protein 6 and its essential role in murine spermatogenesis

D I S S E R T A T I O N

Zur Erlangung des akademischen Grades

Doctor rerum naturalium
(Dr. rer. nat.)

vorgelegt

der Fakultät Mathematik und Naturwissenschaften
der Technischen Universität Dresden

von

Diplom-Biologin Daniela Tiedau

geboren am 13. September 1979 in Bad Oeynhausen

eingereicht am 30. Juni 2009

Die Dissertation wurde in der Zeit von Oktober 2005 bis September 2009 im Institut für Physiologische Chemie der Medizinischen Fakultät Carl Gustav Carus in Dresden angefertigt.

Datum der Verteidigung: 13. Oktober 2009
1. Gutachter: Prof. Rolf Jessberger
2. Gutachter: Prof. Gerhard Rödel

Tudor domain containing protein 6 and its essential role in murine spermatogenesis

Expression of the Tudor domain containing protein 6 (TDRD6), which is restricted to the male germ line, starts at day 16 of spermatogenesis, i.e. in pachytene spermatocytes. TDRD6 is a 250 kDa protein, which we recently found to be cleaved at the C-terminal end during germ cell development, resulting in a 230 kDa product. Neither is the process of cleavage itself nor are the functions of the two different forms known. The 230 kDa isoform is the most prominent form in round spermatids, where it localizes to the chromatoid body (CB), i.e. a single filamentous, perinuclear granule. One characteristic component of the CB is the RNA helicase MVH. CBs contain components of the microRNA (miRNA) pathway, including Piwi-interacting RNAs (piRNAs), as well as MIWI, MIWI2, and MILI, the mouse homologs of the Piwi proteins, which bind piRNAs and also act in transposon regulation. We showed that TDRD6 interacts with MIWI and MILI *in vitro*, and a direct interaction with MVH was shown before. To reveal the function of TDRD6, we generated *Tdrd6*$^{-/-}$ mice, which lack the protein. These mice are generally healthy but the males are sterile, due to the absence of mature spermatozoa. The most striking intracellular phenotype of *Tdrd6*$^{-/-}$ mice is the highly aberrant architecture of chromatoid bodies in round spermatids. *Tdrd6*$^{-/-}$ CBs appear as diffuse, disrupted, and less condensed structures. Their interior is largely missing, and only a “ghost”-like structure remains, expected to be significantly impaired in function. Other CB components like MVH, MIWI and MILI are expressed in *Tdrd6*$^{-/-}$ testes, but they cannot localize to the disrupted CBs. This suggests a role for TDRD6 in assembling the chromatoid body complex by recruiting other proteins. The CB is important for storage and translational regulation of mRNA, through interaction with miRNAs. In *Tdrd6*-deficient testes 10 % of all known murine miRNAs are differently expressed, whereas most of the mature miRNAs are up-regulated, indicating less turnover, and thus, accumulation of mature miRNAs. Since some precursor miRNAs are up-regulated as well, we assume, that TDRD6 affects miRNA transcription most likely by indirectly influencing transcriptional regulation of miRNA genes. In *Tdrd6*$^{-/-}$ mice an overall abnormal mRNA gene expression pattern was observed by microarray analyses. Of all mis-regulated genes 36 % are located to the centromer-proximal region of Chr 8, and 11 % are located to the distal end of Chr 1. This mis-regulation might be due to a common transcriptional regulation. The orthologous regions on the human chromosomes show altered chromosomal structures in many different carcinomas. If TDRD6 plays a role in carcinogenesis has to be investigated.

1. Introduction

1.1. Spermatogenesis

Spermatogenesis in mice takes places in the seminiferous tubules of the testis, initiates a few days after birth and continues for the duration of the reproductive life of the animal. Spermatogenesis takes approximate 35 days and consists of the mitotic proliferation of spermatogonial cells, meiosis and spermiogenesis, the haploid spermatid differentiation stage (Braun 1998). The mammalian testis contains two discrete morphological compartments, interstitial tissue and the seminiferous tubules. Interstitial tissue is composed primarily of vascular, lymphatic and connective tissue elements, macrophages, fibroblasts and the androgen secreting interstitial cells of Leydig (Bellve et al. 1977). Within the seminiferous epithelium of the testis, developing germ cells and Sertoli cells are in close association with each other. The proliferation of spermatogonia occurs in the basal compartment of the seminiferous epithelium below the Sertoli junctional complexes (Dym and Fawcett 1970) (figure 1.1).

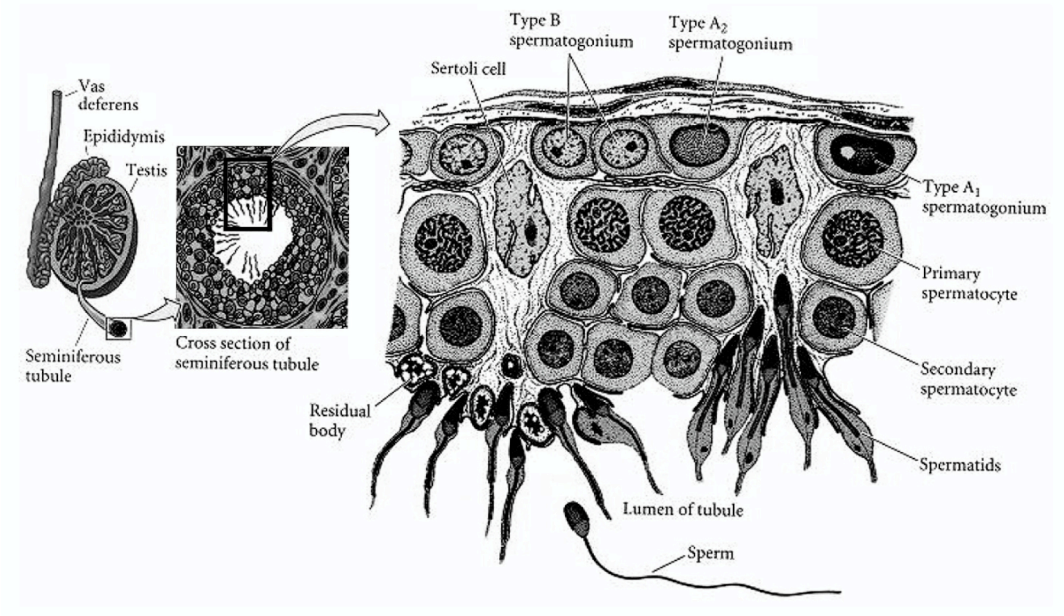

Figure 1.1: **Scheme of the testis structure and a cross section of a seminiferous tubule** (Gilbert 2000). Diploid spermatogonia reside in the basal compartment of the seminiferous tubule; divide mitotically to produce two diploid primary spermatocytes. Each spermatocyte then moves into the adluminal compartment of the tubule and duplicates its DNA and subsequently undergoes meiosis I to produce two haploid secondary spermatocytes. These spermatocytes undergo a second meiotic division to result in haploid round spermatids. The round spermatids go through several differentiation steps and culminate in elongated spermatids and mature spermatozoa, which are released into the lumen of the tubule.

Spermatogonia originate from primordial germ cells (PGCs). In the mouse, PGCs appear at the same time as the three embryonic layers: endoderm, mesoderm and ectoderm. PGCs are visible around 7 days post coitum (dpc) in the extra-embryonic mesoderm. They enter the developing fetal gonad, the genital ridge, at 9.5-11 dpc (Anderson et al. 2000). The testis structure is established while the PGCs proliferate and differentiate into prospermatogonia or gonocytes, which arrest in the G_0/G_1 phase until 2 days after birth (18 dpc). By day 6 postpartum (dpp), these cells migrate to the basement membrane of the seminiferous tubules and become undifferentiated type A spermatogonia, the male germ line stem cells (GSCs) (McLaren 2000). Type A spermatogonia either renew themselves to maintain the pool of stem cells or undergo differentiation to produce spermatozoa (Dym 1994; Feng et al. 2002; Lacham-Kaplan 2004). Spermatogonia differentiate into spermatocytes, which undergo meiosis to produce haploid round spermatids. During mammalian meiosis, homologous chromosomes align, physically associated via formation of the synaptonemal complex (SC). The SC consists of two axial elements (AE), each AE supports the two sister chromatids of one homologue, which are connected by transverse filaments. Meiotic prophase I can be classified into four sequential substages defined by the development of the SC. Chromosome cores appear in leptotene and synapse during zygotene to form the SC. This assembly is completed by pachytene. In diplotene, the two homologues pull apart until they are held together only at the sites of crossing-over/chiasmata (Marcon et al. 2008). After the first meiotic division primary spermatocytes (4n) become secondary spermatocytes (2n), which undergo a second meiotic division. The resulting haploid round spermatids (1n) undertake drastic morphological changes via a process called spermiogenesis to become motile sperm (Unhavaithaya et al. 2009). Spermiogenesis in mouse is roughly divided into processes occurring in round spermatids (step 1-8) and those occurring in elongating spermatids (step 9-16) (Russell 1990) (figure 1.2). In round spermatids, the acrosome starts to differentiate (Kierszenbaum and Tres 1975). The acrosomal vesicle, a cap-like structure derived from the Golgi apparatus, is an organelle that stretches out around the anterior half of the sperm's head. At later steps, the mitochondria become arranged in a spiral around the base of the flagellum, the future tail of the spermatozoa, and the nuclei become elongated, dense and compact (Saade et al. 2007). Spermiogenesis culminates with excision of the residual body and release of the spermatozoa into the lumen of the tubules. The

complexity of the seminiferous epithelium is compounded by the fact that cytokinesis is not completed at each of the successive mitotic and meiotic divisions. Thus, germ cells at comparable stages of differentiation exist as a syncytium in which many cells are interconnected by cytoplasmic bridges (Bellve et al. 1977).

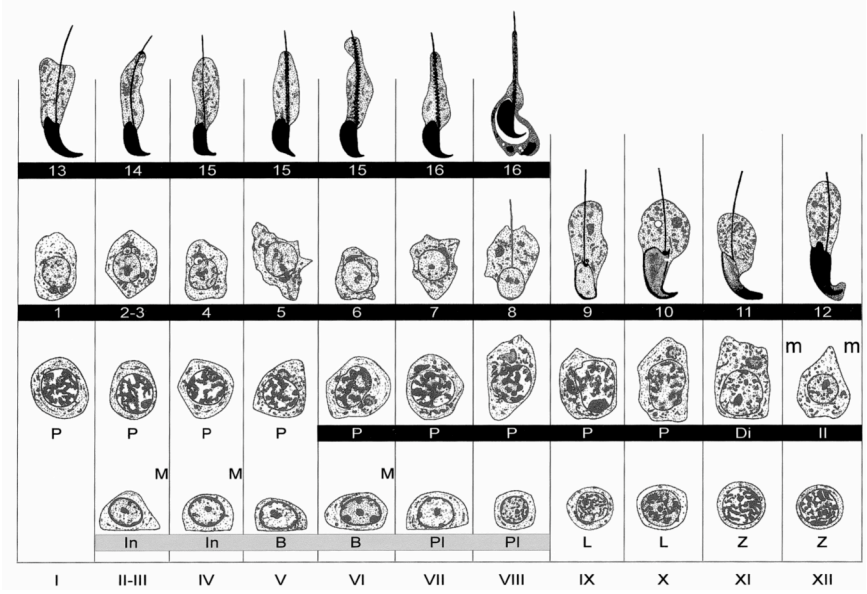

Figure 1.2: **The cycle of the seminiferous epithelium** (Russell 1990). The vertical columns, designated by Roman numerals (I-XII), depict cell associations (stages). A cycle is a complete series of cell associations, which are placed in logical order. The developmental progression of a cell is followed horizontally until the right hand border of the cycle map is reached. It continues at the left of the cycle map one row up. The cycle map ends with the completion of spermiation. Cell progression is divided into 16 steps, based on the form and shape of the acrosome, spermatid head shape and degree of chromatin condensation. The symbols used designate specific phases of cell development (In, intermediate spermatogonia; B, type B spermatogonia; Pl, preleptotene; L, leptotene; Z zygotene; P, pachytene; Di, diplotene; II, meiosis II).

Coincident with the onset of meiosis, however, the early primary spermatocytes traverse the existing Sertoli junctions and enter the adluminal compartment. As differentiation proceeds, the spermatocytes and early spermatids are gradually displaced toward the lumen of the seminiferous tubule until, during late spermiogenesis, the spermatids lie within deep infoldings in the apical cytoplasm of the Sertoli cell (Bellve et al. 1977). Sertoli cells produce many soluble factors necessary for germ cell survival and proliferation, such as stem cell factor (SCF), basic fibroblast growth factor (bFGF), and leukaemia inhibitory factor (LIF) (Hofmann et al. 2003).

1.2. Chromatoid Body

Germ cells of various organisms are characterized by the accumulation of dense material into a cytoplasmic structure called germ plasm or nuage. In non-mammalian organisms, such as *Drosophila melanogaster* and *Caenorhabditis elegans*, germ plasm forms in a particular cytoplasmic region within the oocyte and, after fertilization of the egg, has an essential function in the specification of germ line lineage and the initiation of embryonic development (Ikenishi 1998). No germ plasm-like structure is detectable in unfertilized and fertilized eggs in mice (Nagamori and Sassone-Corsi 2008). Nuage in mammalian spermatogonia, spermatocytes and oocytes is seen among clusters of mitochondria and is called “intermitochondrial cement”, whereas in spermatocytes and spermatids, larger solitary aggregates of nuage, termed “chromatoid bodies” (CB), are prominent in the cytoplasm (Hosokawa et al. 2007).
On the basis of structural features and protein composition, the chromatoid body in the cytoplasm of mouse haploid male germ cells has been suggested to be the mammalian counterpart of germ plasm. The CB is composed of thin filaments that are consolidated into a compact mass or into dense strands of varying thickness that branch to form an irregular network. In the mouse, the CB appears for the first time in the cytoplasm of meiotic pachytene spermatocytes as a fibrous-granular structure (Parvinen 2005) (figure 1.3). After meiosis, the CB condenses into one single finely filamentous, lobulated, perinuclear granule in round spermatids and remains a distinctive feature in the cytoplasm of post-meiotic spermatids until the nucleus begins to elongate (Kotaja and Sassone-Corsi 2007). Although the chromatoid body in spermatogenesis was described more than 100 years ago (Brenda 1891), its origin, function, chemical composition, and fate is still controversial (Parvinen and Jokelainen 1974). The varying localization of the CB during successive stages of spermatogenesis is one of its primary features. The CB moves rapidly in the cytoplasm of spermatids in both parallel and perpendicular fashion related to the nuclear envelop (Parvinen and Parvinen 1979). Actin is a possible motor of this movement, together with a calcium-cAMP dependent mechanism and cytoplasmic microtubules (Parvinen 2005). During this movement the CB has been suggested to collect gene products from the nucleus, and to be involved in nucleocytoplasmic RNA transport (Parvinen 2005). The testis-specific kinesin KIF17b has been shown to shuttle between the nucleus and the chromatoid body and thus, provides a potential

mechanism for the active transport of material from one compartment to the other (Kotaja et al. 2006b). The CB was also reported to move through cytoplasmic bridges to neighbouring cells, suggesting that this organelle could provide a mechanism to share haploid products between adjacent spermatids (Ventela et al. 2003).

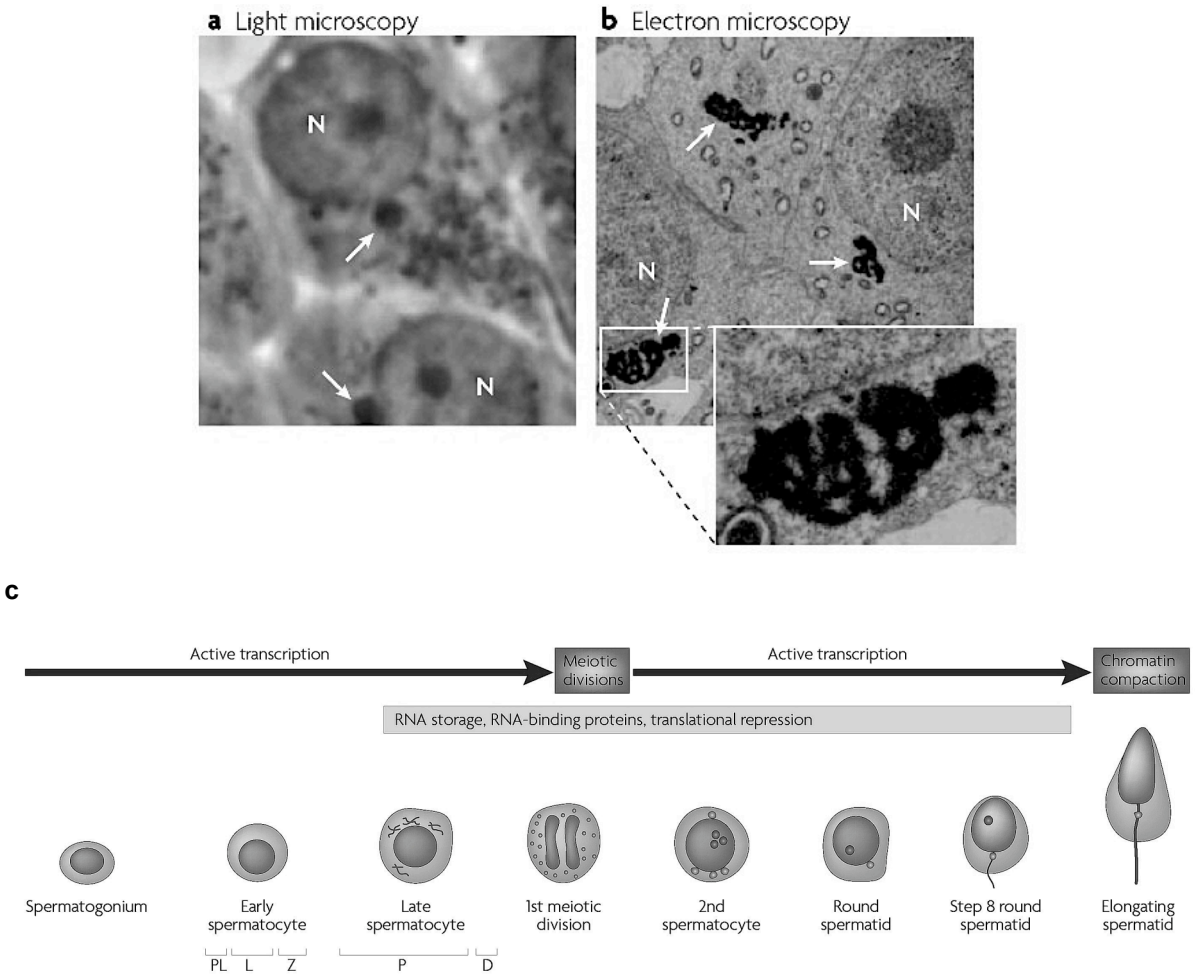

Figure 1.3: **The CB is a dense fibrous structure in the cytoplasm of haploid round spermatids** (Kotaja and Sassone-Corsi 2007). (**a**) For light microscopy, mouse germ cells of early stage II of the seminiferous epithelial cycle, were observed under phase-contrast optics. The CB is shown as a single dense granule that is in close contact with the nuclear envelope in the cytoplasm of round spermatids. (**b**) Electron microscopy was carried out with seminiferous tubule segments from stages I-IV. The CB seems to be composed of thin filaments that are consolidated into dense strands of varying thickness that branch to form an irregular network. (**c**) Schematic representation of transcriptional activity and appearance of the CB during spermatogenesis. CB material is first apparent in late pachytene spermatocytes prior to the first meiotic division as intermitochondrial cement, fibrous structures that disperse during meiotic division. The CB is condensed to its final shape immediately after meiosis, and remains a distinctive feature in the cytoplasm of post-meiotic round spermatids next to the nucleus. It diminishes in size and then disappears in elongating spermatids. D, diplotene; L, leptotene; P, pachytene; PL, preleptotene; Z zygotene.

Studies on the molecular composition of the CB provide an attractive experimental gateway for the understanding of the physiological role played by this organelle (Nagamori and Sassone-Corsi 2008). It has been recently shown that microRNA (miRNA) pathway components, such as the miRNA-processing endonuclease DICER, Argonaute proteins, and miRNAs are concentrated in CBs (Kotaja et al. 2005; Kotaja et al. 2006a). Additionally, components of RNA processing bodies (P-bodies) accumulate in CBs indicating that the germ cell-specific CBs and somatic P-bodies are functionally related (Kotaja et al. 2006a). As P-bodies in somatic cells are thought to integrate RNA decay and regulation by miRNAs, it was proposed that CBs function as platforms for miRNA pathways in germ cells (Kotaja et al. 2005). These notions strengthen the hypothesis of RNA interference and miRNA pathways being mechanisms essential for gene regulation in spermatogenesis (Nagamori and Sassone-Corsi 2008).

Poly(A)-containing mRNAs accumulate in the CBs of spermatids and have suggested that the process of translational repression is organized within this cytoplasmic structure (Kotaja et al. 2006a). This hypothesis was supported by the finding of the cytoplasmic poly(A)-binding protein 2 (PABPC2) in the chromatoid body of spermatids (Kimura et al. 2009), which is involved in translational initiation, translation termination, and mRNA decay (Mangus et al. 2003; Kuhn and Wahle 2004).

1.3. Chromatoid body components

1.3.1. Tudor domain family proteins

Genetic studies in *Drosophila* have identified numerous genes (i.e., *Oskar, Vasa, Nanos, Tudor)* that are involved in the formation of germ cell precursors and pole cells (Rongo and Lehmann 1996). One of these components of *Drosophila* nuages is *Tudor*, which is genetically downstream of *Vasa* (Golumbeski et al. 1991; Bardsley et al. 1993). One characteristic of the TUDOR protein is the presence of ten repeated copies of the tudor domain (Ponting 1997). Tudor domains are related to plant Agenet, Chromo PWWP (conserved Proline and Tryptophane), and MBT (malignant brain tumour) domains, which together form the tudor domain "Royal Family" (Maurer-Stroh et al. 2003). The tudor domain is about 60 amino acids long and was initially found in proteins that associate with nucleic acids (Ponting 1997). Three-dimensional analysis of the domain reveals a barrel-like structure composed of ß-sheets forming a hydrophobic pocket surrounded by negatively charged residues that most likely constitutes a protein-protein interaction surface (Ponting 1997; Selenko et al. 2001; Huyen et al. 2004). A scaffolding function has also been suggested, allowing the assembly of cellular proteins that associate with each tudor domain into macromolecular complexes (Hosokawa et al. 2007; Skorokhod et al. 2008).

Tudor domain proteins have been shown to interact with other proteins and efficient binding requires methylated arginine and lysine residues in the target protein (Brahms et al. 2001; Huyen et al. 2004; Cote and Richard 2005; Kim et al. 2006); (Sprangers et al. 2003). The tudor domain of the Survival motor neuron (SMN) protein binds directly to spliceosomal assembly (Buhler et al. 1999; Brahms et al. 2001; Selenko et al. 2001; Sprangers et al. 2003). It has been shown, that this domain directly binds the arginine-glycine rich tail of the SMN proteins *in vitro* (Buhler et al. 1999; Selenko et al. 2001). A number of tudor domain proteins, like the 53 Binding Protein 1 (53BP1), have been shown to interact with modified histone H3 on methylated Lys79 (Huyen et al. 2004). Several of the first tudor domain containing proteins that were identified, have well known RNA binding motifs. Based on this knowledge, it was suggested that tudor domains may have a role in RNA metabolism (Ponting 1997).

Several tudor domain containing proteins exist in mammalian germ cells, including TDRD1, TDRD2, TDRD3, TDRD4, TDRD5, TDRD6, TDRD7 and TDRD9.

Tudor domain containing protein 1/ mouse tudor repeat 1 (*Tdrd1/Mtr-1*) is a *Tudor*-related gene in mice (Wang and Dreyfuss 2001; Chuma et al. 2003). TDRD1 contains four tudor domains and a zinc finger MYND domain. TDRD1 expression starts in pachytene spermatocytes and stops in round spermatids (Hosokawa et al. 2007) (figure 1.4). TDRD1 expression is confined to male germ cells, and this protein constitutes the chromatoid bodies in round spermatids (Chuma et al. 2003). *Tdrd1* mutant mice lack intermitochondrial cement, but chromatoid bodies are visible. The male mutant mice are sterile and the females are not affected (Chuma et al. 2006). TDRD3 is expressed in various tissues and plays a role in stress granules (Linder et al. 2008). With its single tudor domain it is able to bind methylated proteins (Cote and Richard 2005). TDRD4, also called RNF17, is restricted to the male germline and *Rnf17*-deficient mice are sterile. The protein is localized to the so-called RNF17 granule, another form of nuage in the cytoplasm of male germ cells. It has five tudor domains and it is expressed in pachytene and diplotene spermatocytes. In round spermatids its expression is restricted to step 10 and later spermatids (figure 1.4) (Pan et al. 2005). TDRD5 has one tudor domain and is a germ line-specific protein in mouse, which expression starts around 12.5 days post coitum and continues throughout testis development (figure 1.4). About the function of this tudor domain protein nothing is known (Smith et al. 2004). TDRD7/TRAP (tudor repeat associator with PCTAIRE 2) contains four tudor domains, it is localized to the CB and forms a complex with TDRD1 and TDRD6 (Hirose et al. 2000; Hosokawa et al. 2007). TDRD7 expression starts in early-pachytene spermatocytes, and in mid-late pachytene spermatocytes, the signal exhibits fine granular appearance. In spermatids, TDRD7 forms larger solitary aggregates similarly to TDRD1 and TDRD6, corresponding to the chromatoid bodies (figure 1.4) (Hosokawa et al. 2007). So far nothing is known about expression, localization and function of TDRD2, TDRD8 and TDRD9 in germ cells.

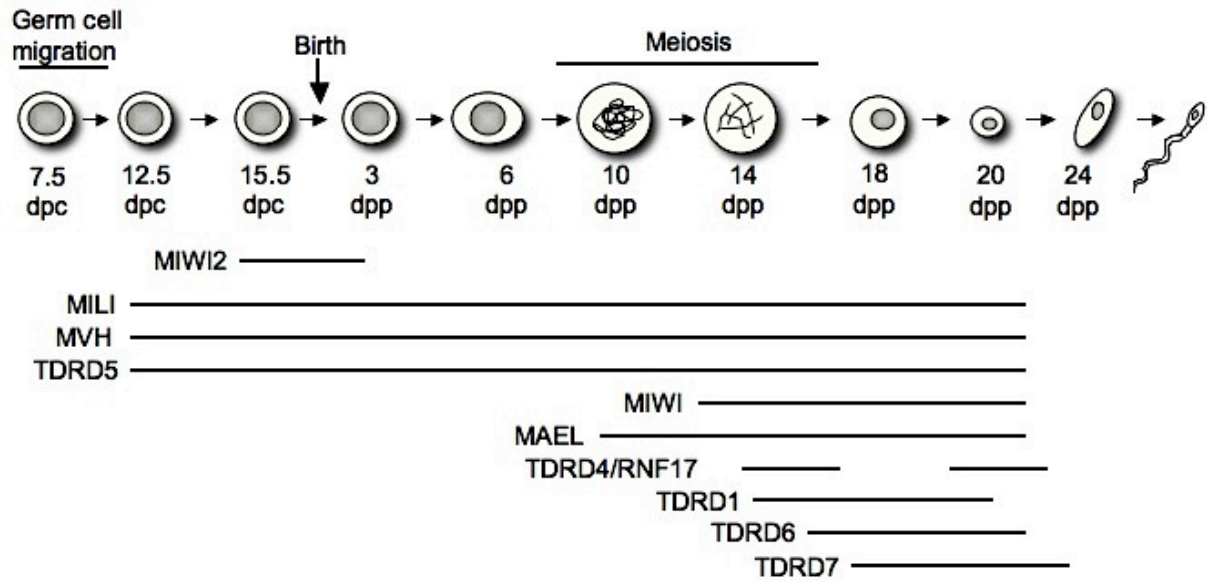

Figure 1.4: **A scheme of spermatogenesis is shown with the timing of expression of MILI, MVH, MIWI2, MIWI, MAEL, TDRD1, TDRD4, TDRD5, TDRD6 and TDRD7**. After migration, primordial germ cells (PGCs) arrive at the gonad around 11.5 dpc and expand prior to undergoing cell-cycle arrest at 15.5 dpc. Germ cells resume division after birth at around 3 dpp and initiate meiotic division at 10 dpp. The first haploid round spermatids appear at day 20 after birth.

TDRD6 has seven of the characteristic tudor domains. It is the closest homolog of *Drosophila* Tudor (Vasileva et al. 2009). The human TDRD6 was initially identified as a tumour-dependent antigene present in serum of colon carcinoma patients, called NY-CO-45 (Scanlan et al. 2002). In primary cells, it is specifically expressed in germ cells (Hosokawa et al. 2007) and appears first in primary late spermatocytes (17.5 dpp) as multiple fine filamentous cytoplasmic granules. In postmeiotic round spermatids at 20.5 dpp, the TDRD6 signal appears as bright, distinct perinuclear dots (figure 1.4). TDRD6 was not detected in female mice (Vasileva et al. 2009). TDRD6 (2134 aa) was reported to migrate as a 250 kDa protein in SDS gel electrophoresis (Hosokawa et al. 2007). Whereas in the extracts from mice aged 17 dpp, the expected 250 kDa TDRD6 protein was detected, extracts from older mice display a strong band of 230 kDa and a weak band of 250 kDa. Mass spectrometric analysis of the two immunoprecipitated proteins confirmed that both are products of the *Tdrd6* gene (Vasileva et al. 2009). There is no indication for alternative splice products from our and other studies (Hosokawa et al. 2007; Vasileva et al. 2009).

1.3.2. Mouse Vasa homolog

Another component of *Drosophila* nuage is VASA. It is a member of the DEAD-box family of genes encoding an ATP-dependent RNA helicase. VASA is required for the assembly and function of the pole plasm in *Drosophila* (Lasko and Ashburner 1988) (Liang et al. 1994). In addition, on the basis of structural conservation, genes homologous to *Vasa* have been identified in many animal species, such as *C.elegans*, Xenopus, zebrafish and mouse (Roussell and Bennett 1993; Fujiwara et al. 1994; Komiya et al. 1994; Olsen et al. 1997; Yoon et al. 1997)**.** The mouse vasa homolog (MVH) protein exhibits specific expression in developing germ cells (Fujiwara et al. 1994). The expression of MVH is maintained in both male and female germ cells ranging from PGCs of 12.5 dpc gonads to postmeiotic round spermatids and primary oocytes (Tanaka et al. 2000) (figure 1.4). Targeted mutation of the *Mvh* gene in the mouse yields a drastic interruption of spermatogenesis by the zygotene stage, before the formation of the CB (Tanaka et al. 2000). Oogenesis and formation of germ cells are not affected in *Mvh*-null mice, possibly underscoring the differences in the germ-cell-fate determination systems between fruit fly and mouse (Kotaja and Sassone-Corsi 2007).

1.3.3. Piwi proteins

As seen in other organisms, the expression of the three murine Piwi proteins, MIWI (PIWIL1), MILI (PIWIL2), and MIWI2 (PIWIL4), is largely germ line restricted (Kuramochi-Miyagawa et al. 2001; Sasaki et al. 2003). MILI is expressed from 12.5 days post coitum until round spermatid stage (figure 1.4), at which point the majority of MILI localizes in the chromatoid body (Kuramochi-Miyagawa et al. 2001; Wang et al. 2009). MILI is not only expressed in spermatocytes and spermatogonia, but also in primordial germ cells of both sexes (Kuramochi-Miyagawa et al. 2001). Spermatogenesis in *Mili*-null mice was blocked completely at the early prophase of the first meiosis, from the zygotene to early pachytene stage, and the mice were sterile. However, PGC development and female germ cell production were not disturbed (Kuramochi-Miyagawa et al. 2004).

MIWI2 could be detected in male germ cells beginning around 14.5 – 15.5 dpc, but was absent from female germ cells as well as somatic cells and the embryonic gonads. MIWI2 expression declined soon after birth, reaching undetectable levels in 4-day-old mice (figure 1.4) (Aravin et al. 2008). *Miwi2*-deficient mice display a meiotic-progression defect in early prophase of meiosis I and a progressive loss of germ cells with age (Carmell et al. 2007).

MIWI is a cytoplasmic protein that is first detectable at 14 dpp, a stage that corresponds to the appearance of pachytene spermatocytes (Deng and Lin 2002). The MIWI protein is clearly detectable until step 13 elongating spermatids (figure 1.4). MIWI is not detectable in Sertoli cells or interstitial cells. *Miwi*-null mice display spermatogenic arrest at the beginning of the round spermatid stage (Deng and Lin 2002).

Deficiency in either of two Piwi family members, MILI or MIWI2, leads to loss of DNA methylation marks on transposons and results in increase of transposition activity. These observations led to the hypothesis that Piwi proteins might serve as sequence-specific guides that direct the *de novo* DNA methylation machinery to transposable elements (Aravin et al. 2007; Aravin et al. 2008; Kuramochi-Miyagawa et al. 2008)

1.3.4. Maelstrom

In the *Drosophila* female germ line, maelstrom (MAEL) is found predominantly in nuage, but its function is unknown (Findley et al. 2003). MAEL contains a domain with similarity to a high mobility group (HMG) box DNA-binding domain. First MAEL expression was observed in the early stages of meiotic prophase I (leptotene to midpachytene). Round spermatids contain MAEL in the CB (figure 1.4). *Mael*-null mice show a meiotic arrest of spermatogenesis due to failure of chromosome synapsis, as well as derepression of transposable elements (TEs), like observed in MILI and MIWI2 mutant mice (Soper et al. 2008).

1.3.5. Interplay of chromatoid body components

To find interacting partners of TDRD6 immunoprecipitation analyses were done by our group, using an antibody against the middle part of TDRD6 and total testis extract. MVH, MIWI and MILI as possible interaction partners were found. Additionally a direct interaction of MVH and TDRD6 was shown by (Hosokawa et al. 2007), and an *in vitro* interaction of MIWI and MILI with TDRD6 was confirmed by our group (Vasileva et al. 2009).
TDRD6 was found to form a ribonucleoprotein complex with TDRD1 and TDRD7 (Hosokawa et al. 2007). In a mouse mutated in *Mvh*, TDRD6 and TDRD7 aberrantly localizes in cytoplasmic granules, indicating that MVH is required for proper localization of these two tudor domain proteins (Hosokawa et al. 2007).

1.4. Transcriptional regulation in spermatogenesis

The complex and highly elaborated differentiation program of male germ cells involves multiple and finely tuned levels of gene control (Sassone-Corsi 2002). During late steps of spermiogenesis there is a striking cessation of transcription, occurring in concert with drastic epigenetic modifications that result in chromatin compaction (Kimmins and Sassone-Corsi 2005). Concomitantly there is an extensive posttranscriptional storing and processing of mRNAs (Steger 2001). One possibility to regulate gene expression is the involvement of small RNAs, which are known to function in several pathways for gene silencing. These non-coding RNAs, which are 19-31 nucleotides long, behave as sequence-specific triggers for mRNA degradation, translational repression, heterochromatin formation, and transposon control (Chu and Rana 2007). Small RNAs can be classified into different groups based on their origin or the components to which they are coupled. The most abundant small RNA groups include microRNA (miRNA), small-interfering RNAs (siRNAs), repeat-associated siRNAs (rasiRNAs) and Piwi-interacting RNAs (piRNAs). MiRNAs and siRNAs facilitate translation repression in various organisms, by cleaving their target mRNAs. RasiRNAs are longer than siRNAs and silence repetitive and mobile genetic elements in yeast, plants, and flies (Aravin et al. 2001; Hamilton et al. 2002; Reinhart and Bartel 2002). Recent studies have shown that fly rasiRNAs are similar to the

mammalian piRNAs, which associate with germ line specific Piwi proteins to silence transposons during spermatogenesis (Chu and Rana 2007; O'Donnell and Boeke 2007). For this thesis it will be focused mainly on miRNAs and piRNAs.

1.4.1. microRNAs (miRNAs)

Genes for miRNAs are located on all chromosomes, and half of all miRNAs are identified in clusters that can be transcribed as polycistronic primary transcripts. It has been shown that miRNAs located in the same genomic cluster, can be transcribed and regulated independently (Song and Wang 2008). MiRNA genes are found in introns of non-coding or coding genes and in exons on non-coding genes (Rodriguez et al. 2004). MiRNAs are transcribed by RNA polymerase II or III as precursor molecules with 5' m^7G capping structures and 3' poly-A tails (Cai et al. 2004; Lee et al. 2004). These long transcripts of primary miRNA genes (pri-miRNA) are subsequently cleaved by the complex Drosha-DGCR8 (DGCR8 is also known as Pasha in *Drosophila* and *C.elegans*) to produce a stem-loop structured precursor, the preliminary miRNA (pre-miRNA) which is ~ 70-nt long. After the first processing step in the nucleus, pre-miRNAs with a short hairpin structure are recognized by the nuclear export factor, Exportin-5 (EXP5), which delivers pre-miRNA through nuclear pores to the cytoplasm (Yi et al. 2003; Lund et al. 2004). Upon export, pre-miRNAs are then processed by DICER, a highly conserved, cytoplasmic RNase III, that chops long double stranded (ds) RNAs into ~ 22-nt duplexes of mature miRNAs (Kim et al. 2009) (figure 1.5).

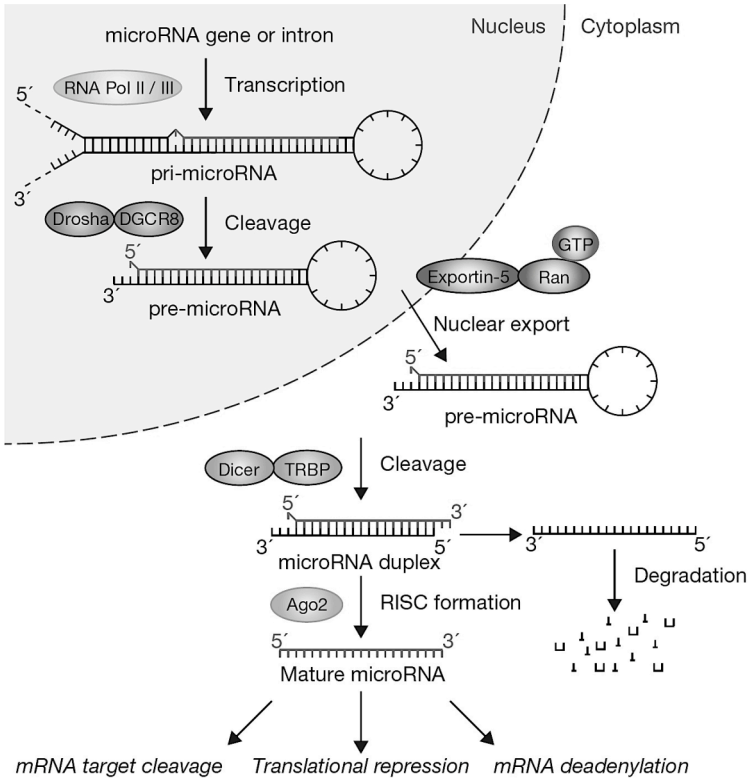

Figure 1.5: **The canonical pathway of microRNA processing** (Winter et al. 2009). This maturation includes the production of the primary miRNA transcript (pri-miRNA) by RNA polymerase II or III and cleavage by the complex Drosha-DGCR8 in the nucleus. The resulting preliminary (pre-) miRNA is exported from the nucleus by Exportin-5-Ran-GTP. In the CB, the RNase DICER in complex with TRBP cleaves the pre-miRNA hairpin to its mature length. The functional strand of the mature miRNA is loaded together with Argonaute (AGO2) proteins into the RNA-induced silencing complex (RISC), where it guides RISC to silence target mRNAs through mRNA cleavage, translational repression or deadenylation, whereas the passenger strand is degraded.

Mature miRNAs are assembled into the miRISC (miRNA-induced silencing complex), which subsequently act on targets by translational repression or mRNA cleavage. During the RISC-loading stage, only one strand of the miRNA duplex is successfully incorporated into the RISC, while the other strand is eliminated. MiRISC contains several proteins such as DICER, the double-stranded RNA-binding protein TRBP (transactivation-response element RNA-binding protein), and Gemin3, but the components directly associated with miRNAs are Argonaute proteins, which were shown to be localized to the chromatoid body (Carmell et al. 2002; Kotaja et al. 2006b). These proteins share the so-called PAZ and PIWI domains and are classified into two subfamilies depending on sequence similarity to either *Arabidopsis* Argonaute *1* or *Drosophila* Piwi (Carmell et al. 2002; Sasaki et al. 2003). In mammals, Argonaute 1 subfamily members, AGO1 to AGO4, have been shown to be involved in the RNAi/miRNA pathways (Liu et al. 2004; Meister et al. 2004; Kotaja et al. 2006a). A general feature of the miRNA-target RNA interaction is imperfect base

pairing between the miRNA and its target mRNA. The sequence specificity for target recognition by the guide miRNA strand is determined by nucleotides 2-8 of its 5' region, referred to as the "seed sequence" (Carthew and Sontheimer 2009).

At least three mechanisms are supported for miRNA-mediated gene silencing (Chu and Rana 2007; Winter et al. 2009). The first model is, that both cap- and internal ribosome entry site (IRES)-dependent protein synthesis from the polycistronic reporter construct can be repressed by miRNA and these translational repressed mRNAs are associated with polysomes (Petersen et al. 2006). The second model is, that translational repression is mediated by binding of the Ago protein of the RISC to the mRNA cap structure (Kiriakidou et al. 2007). These observations support a mechanism where Ago competes with eIF4E (eukaryotic initiation factor 4 E) for cap-binding and suppress translation (Chu and Rana 2007). The third model is, that miRNAs could trigger destabilization of target mRNA by a deadenylation mechanism (Behm-Ansmant et al. 2006; Wu et al. 2006).

Given the complexity of miRISC structure and function, it is tempting to propose that these mechanisms of gene silencing by miRNA take place simultaneously or perhaps synergistically (Winter et al. 2009).

1.4.2. Piwi-interacting RNAs (piRNAs)

Not all Argonaute proteins in *Drosophila* and mammals are ubiquitously expressed. One group of these proteins, PIWI, is the germ line-specific subclass of Argonaute proteins. The Piwi family genes encode basic proteins that contain a highly conserved PAZ domain of 110-amino acid residues in the middle region of the proteins and a 300-amino acid PIWI domain in the C-terminal region (Kuramochi-Miyagawa et al. 2004). Mammalian Piwi proteins were reported to interact with a new class of RNAs that were longer than miRNAs (Aravin et al. 2006; Girard et al. 2006). These Piwi-interacting RNAs are called piRNAs. Like other members of the Ago family, Piwi proteins associate with small RNAs that act as guides in silencing target mRNA. Sequence analysis of piRNAs shows a high percentage of uridine residues at the 5' termini (Faehnle and Joshua-Tor 2007), and genomic mapping shows that piRNAs are concentrated at a few loci. Primary piRNAs are generated from dedicated loci, called piRNA clusters, which contain a high density of transposon-related sequences (Brennecke et al. 2007). Primary piRNAs join Piwi proteins and

guide these to the selection of their targets. Two outcomes follow recognition of a transposon mRNA by a piRNA. First, the mRNA is cleaved, resulting in its destruction. The cleavage event also promotes the production of a secondary piRNA derived from the mRNA itself (Brennecke et al. 2007; Gunawardane et al. 2007). Though this is in the sense orientation with respect to the transposon, it can target antisense piRNAs that can again target transposons. As a whole, this creates a so-called “ping-pong cycle” that optimizes the piRNA population to target active elements (Brennecke et al. 2007; Aravin et al. 2008).

1.5. Transposons

Mammalian transposable elements consist of DNA transposons and retrotransposons. DNA transposons move by a “cut and paste” mechanism utilizing transposase (Mizuuchi 1992; Smit and Riggs 1996). Although roughly 3 % of the human genome is composed of DNA transposons, they are remnants of ancient elements, and it is unlikely that any remain transpositionally active. In contrast to DNA transposons, retrotransposons encode a reverse transcriptase (RT) activity and move by a “copy and paste” process involving an RNA intermediate. The original retrotransposon is maintained *in situ* where it is transcribed. The transcript is then reverse transcribed and integrated into a new genomic location (Whitcomb and Hughes 1992; Luan and Eickbush 1995). Approximately 42 % of the human genome is composed of retrotransposons, and, although most of these elements are inactive, some retain the ability to retrotranspose (Sassaman et al. 1997). Retrotransposable elements can be classified as either autonomous or nonautonomous. Elements are considered autonomous if they encode certain activities necessary for their mobility. There are two classes of autonomous retrotransposons: LTR (long terminal repeat) and non-LTR retrotransposons. Mammalian LTR retrotransposons are structurally similar to retroviruses. These retrotransposons include elements such as mouse intracisternal A-particle (IAPs). The non-LTR retrotransposon class contains LINEs (long interspersed nucleotide elements), like LINE-1 in mice (Malik et al. 1999; Smit 1999). In addition to the autonomous retrotransposons, there are a large number of nonautonomous retrotransposons in mammalian genomes. These elements do not encode any proteins. Therefore, they require activities encoded by other autonomous retrotransposons for their mobility. The most prominent members of this class are Alu

elements in humans and their B1 counterpart in mice (Rowold and Herrera 2000; Ostertag and Kazazian 2001). Non-LTR retrotransposons usually have two open reading frames (ORFs), one encoding a nucleic acid binding protein, and the other encoding an endonuclease and a reverse transcriptase. Mammalian LINE-1 elements apparently integrate at a very large number of sites in the genome because their endonuclease prefers to cleave DNA at a short consensus sequence (5'-TTTT/A-3', where / designates the cleavage site) (Feng et al. 1996; Jurka 1997).

Epigenetic stable repression of transposable elements in mammals requires CpG DNA methylation (Walsh et al. 1998; Bourc'his and Bestor 2004). Transposon methylation patterns are extensively remodelled during mammalian development. Following fertilization, gametic methylation patterns are mostly lost (Lane et al. 2003). *De novo* methylation patterns are then established around implantation and subsequently maintained in somatic cells throughout the life of the organism. The germ line undergoes a wave of transposon demethylation soon after its emergence during embryogenesis (Hajkova et al. 2002). In males, after migrations of primordial germ cells into embryonic gonads and their initial expansion, germ cells arrest their cell cycle around 14.5 days post coitum (dpc) as spermatogonia, only resuming division 2-3 days after birth (dpp). This is the critical window during which male gametic methylation patterns are established (Lees-Murdock et al. 2003; Kato et al. 2007). Several members of the DNA methyltransferase family, DNMT3A, DNMT3B, and DNMT3L, act in *de novo* methylation of transposable elements. DNMT3A and DNMT3B are important in both germ and somatic cells. DNMT3L operated as a central regulator of *de novo* methylation specifically in the germ line. Recent studies have begun to unravel the biochemistry of *de novo* DNA methylation, which might be preceded by specific histone modifications (Jia et al. 2007; Ooi et al. 2007), but it is still not clear how transposon sequences are specifically recognized to receive such modifications. In the male germ line, deficiency in either of two Piwi family members, MILI or MIWI2, results in loss of the DNA methylation marks on transposons, and mutant animals display a phenotype remarkably similar to that of *Dnmt3L*-deficient mice, a globally failure to establish *de novo* methylation of transposons in their germ cells (Kuramochi-Miyagawa et al. 2004; Carmell et al. 2007; Aravin et al. 2008; Kuramochi-Miyagawa et al. 2008). These data led to the hypothesis that Piwi/piRNA complexes might serve as sequence-specific guides that direct the *de novo* DNA

methylation machinery to transposable elements (Aravin and Bourc'his 2008; Kuramochi-Miyagawa et al. 2008)

1.6. Aims and structure of this thesis

Aim of this thesis was to investigate and understand the role of TDRD6 in spermatogenesis in mice. Since it is a male germ line restricted protein in various organisms, we suggested that it might play an important role in germ cell development. Until now, not so many details about expression pattern and function of TDRD6 are known. To get first information about the function of this protein, a *Tdrd6*-deficient mouse model was generated. Several phenotypic analyses were carried out, e.g. examination of the organization and shape of the chromatoid body. Furthermore other major components of the chromatoid body were investigated, if they were modified in the *Tdrd6*-deficient mouse. For instance other known proteins, that localize to the CB, components of the miRNA pathway and variation in transposon activity. Whole genome microarray analyses were done, to get information about modified gene expression in the *Tdrd6*-deficient mouse.
To get knowledge about differently localization of the two existing isoforms of TDRD6, antibodies specific for each terminus of the protein were generated.

2. Material and Methods

2.1. Construction of a *Tdrd6*-deficient mouse model

To generate the *tdrd6*$_{null}$ allele the first of five exons was disrupted (ENSEMBLE gene ID ENSMUSG00000040140), which contains 95% of the *Tdrd6* cDNA sequence. Homologous genomic sequences amplified by PCR (Table 2.4) were cloned into the targeting vector pTV-Uni (Gadue et al. 2006) (Figure 2.1). This plasmid was kindly provided by A. Vasileva (MSSM, NY). The final targeting vector consisted of: (i) the Diphtheria toxin A gene (*Dta*) for negative selection; (ii) a 5' "short arm" of homology encompassing 1.4 kb upstream of the start codon; (iii) a truncated human CD4 cDNA; (iv) a loxP flanked puromycin resistance gene; and (v) a "long arm" of homology encompassing 5 kb downstream of exon 1 of the *Tdrd6* locus.

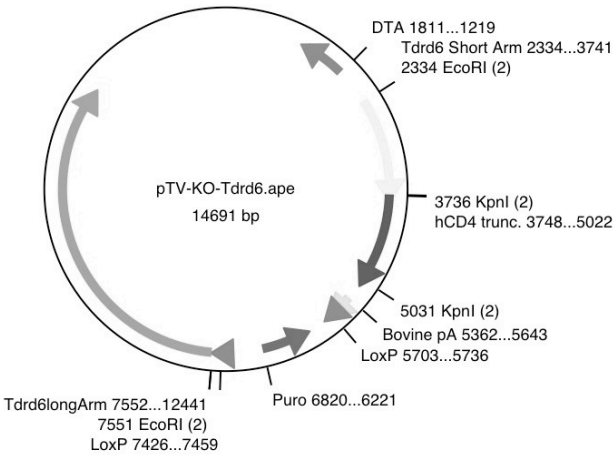

Figure 2.1: **Targeting vector pTV-KO-Tdrd6.**

The production of targeted embryonic stem (ES) cells clones was performed in accordance with standard procedures (Joyner 2000). Briefly, the targeting vector was linearized by digestion with *Pvu*I and was electroporated into 129SvEv embryonic stem cells (Taconic Inc.). After selection with 0.75 µg/ml puromycin, 300 drug-resistant clones were picked and cultured separately in replica. Whereas clones in one of the replica plates were cultured further on, the other replica plate was used for isolation of DNA. Positive clones were identified by PCR (Table 2.4) and absence of random integration was confirmed by Southern Blotting. One positive clone was

found and the respective clone from the replica plate was injected into a C57BL/6 blastocyst. The resulting chimeras were crossed with C56BL/6 mice.

2.2. Generation of TDRD6 specific antibodies

Two *Tdrd6* cDNA fragments encompassing amino acid residues 52-171 (TDRD6-Nterm) and 2058-2182 (TDRD6-Cterm) were subcloned into the *Escherichia coli* expression vector pGEX-4T-3 (Invitrogen) (figure 2.2 and table 2.4). These plasmids were kindly provided by A. Vasileva (MSSM, NY).

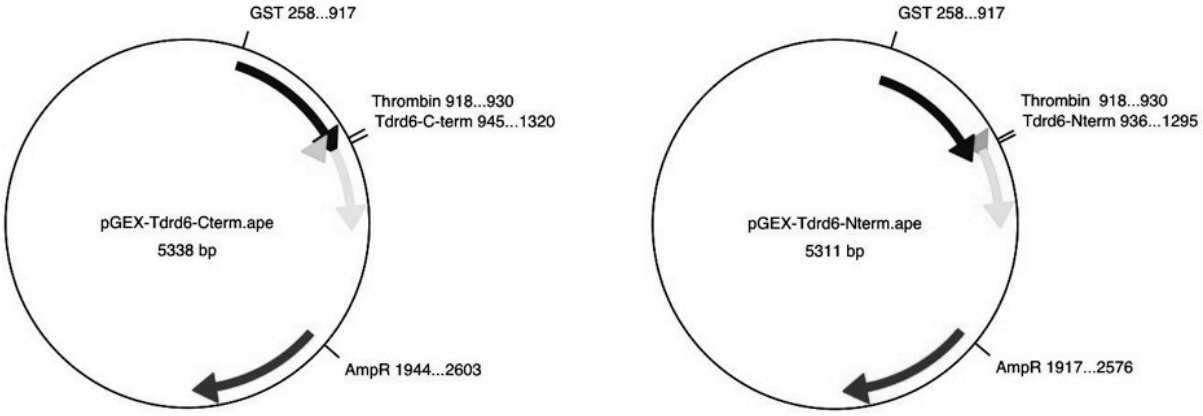

Figure 2.2: **Expression vector pGEX with TDRD6-Cterm and -Nterm peptides for antibody production, respectively.**

The GST-tagged peptides TDRD6-Nterm and TDRD6-Cterm were overexpressed in Stbl2^{TM} competent cells (Invitrogen) by induction with IPTG and purified on glutathione agarose. The TDRD6-Cterm was eluted with 30 mM glutathione, the TDRD6-Nterm was insoluble under native conditions and was solubilized in 6 M urea. After dialyzing against dialyzing buffer I, the peptides were used for immunization. 100 µg peptide (total volume 500 µl, filled up with PBS) were mixed with 500 µl of Freund's complete adjuvants and injected into two rabbits for each peptide. Table 2.1 shows the numeration of the used rabbits.

Rabbit numeration	Peptide
#27477	TDRD6-Cterm No. 1
#27507	TDRD6-Cterm No. 2
#27459	TDRD6-Nterm No. 1
#27515	TDRD6-Nterm No. 2

Table 2.1: **Number of rabbits and corresponding peptides**.

The initial immunization was followed by series of bleedings and injections with the according peptide mixed with an equal volume of Freund's incomplete adjuvants. The injections were repeated every four weeks and in addition 20 ml blood was drawn from ear vessels. After coagulation of the blood, the serum was separated by centrifugation and stored at -20 °C. The obtained sera were purified with Protein A-agarose. In detail, the serum was mixed 1:10 with PBS-T and applied to a Poly-Prep® Chromatography column (Bio-Rad) filled with 500 µl Protein A-agarose. After washing with 10 ml of 100 mM Tris pH 8.0 and 10 ml of 10 mM Tris pH 8.0, the antibodies were eluted with 10 ml of 100 mM Glycine pH 2.9. Fractions of 1 ml were collected in tubes filled with 100 µl of 1 M Tris pH 8.0 for neutralization. After examining the fractions by sodium dodecylsulfate polyacrylamide gel electrophoresis (SDS-PAGE), the fractions containing antibodies were pooled and dialyzed against 500 ml dialyzing buffer I. Concentrations were measured using a spectrophotometer and the antibodies were stored in aliquots at -20°C.

The TDRD6-Cterm serum was additionally purified using Cyanogen bromide-activated-Sepharose coupled to the TDRD6-Cterm peptide. In detail, after overexpression of the TDRD6-Cterm peptide, it was dialyzed against buffer II overnight. The Cyanogen bromide-activated-Sepharose beads were solved in 1 mM HCl and washed with the same solution. The peptide and the beads were mixed and incubated overnight on a rotating wheel at 4°C. The binding efficiency was measured by comparing the optical dense of the supernatant before and after incubation. A binding efficiency of 50 % was achieved. The beads were washed twice with wash buffer I, and once with wash buffer II. The remaining active groups were blocked with 100 mM Tris pH 8.0 overnight at 4 °C. After washing the beads with PBS, they were filled in a Poly-Prep® Chromatography column (Bio-Rad) and washed with each 10 vol of 10 mM Tris pH 7.5, 100 mM Glycine pH 2.9, 10 mM Tris pH 8.8, 100 mM Tris pH 11.5. To neutralize the beads, they were washed with 10 mM Tris pH 7.5 until the pH reaches 7.5. Before loading the rabbit serum to the beads it was diluted 1:10 with 10 mM Tris pH 7.5. Sodium azide to a final vol of 0.1 % was added to avoid growing of bacteria. After applying the serum very slowly to the beads, they were washed with 20 vol 10 mM Tris pH 7.5 and 20 vol 0.5 M NaCl, 10 mM Tris pH 7.5. Antibodies were eluted with 10 vol 100 mM Glycine pH 2.9 and 1 ml fractions were collected in tubes filled with 100 µl 1 M Tris pH 8.0 for neutralization. After washing the beads with 10 mM Tris pH 8.8, the remaining antibodies were eluted by adding 10 vol of

100 mM Tris pH 11.5 and fractions were collected like described before. The fractions were examined by SDS-PAGE, pooled and dialyzed against buffer I overnight. The antibodies were stored in aliquots at -20°C. After washing the beads with 10 mM Tris pH 7.5, the column can be stored by applying PBS with proteinase inhibitors and 0.1 % sodium azide at 4°C.

PBS (Phosphate Buffered Saline)	137 mM NaCl, 2.7 mM KCl, 100 mM Na_2HPO_4, 2 mM KH_2PO_4
Dialyzing buffer I	PBS, 10 % glycerol, proteinase inhibitors
Dialyzing buffer II	PBS, 0.05 M Na_2HPO_4, 0.5 M NaCl, pH 8.3
PBS-T	PBS, 0.1 % Tween-20
Proteinase Inhibitors	0.5 mM vanadate, 2 mM PMSF, 10 mM $Na_2S_2O_5$, 50 µg/ml TLCK, Complete (Roche)
Wash buffer I	0.5 M Na_2HPO_4 pH 8.0
Wash buffer II	1 M NaCl, 0.05 M Na_2HPO_4 pH 7.5

2.3. Periodic acid-Schiff/Hematoxylin staining

Testes were dissected and fixed in Bouin's solution overnight at 4°C, washed in 70 % ethanol for 24h and embedded in paraffin. Testes were cut into 7 µm sections and deparaffinized using standard xylene/ethanol procedures. In detail, slides were placed 2 times for 10 min each in xylene, 99 % Ethanol, 96 % Ethanol and 70 % Ethanol. Finally the slides were washed with distilled water and placed in 0.5 % periodic acid for 5 min. After washing the slides in 3 changes of water, they were incubated in Schiff's reagent for 15 min. Slides were incubated 2 x with 0.55 % Potassium metabisulfite for 1 min to remove excess reagent and washed in running tap water for 10 min to allow the color to develop. After counterstaining with acidified Harris Hematoxylin for 10 sec, slides were dehydrated using 96 % Ethanol, 99 % Ethanol and xylene for 10 min each and mounted with Roti-Histokitt II.

2.4. Apoptosis assay

To analyze apoptosis, testes were fixed with 3.7 % formaldehyde diluted in PBS overnight at 4°C, washed with 70 % Ethanol for 24 h and embedded in paraffin. Apoptosis analysis on 7 µm sections was performed using the TACS 2 TdT-DAB kit according to manufacturer's recommendations (Trevigen Inc.).

2.5. FACS analysis

For staining of individual germ cell populations, testis single cell suspensions were prepared as previously described (Bastos et al. 2005) with some modifications. Briefly, two testes were isolated and incubated in 2 ml digestion buffer for 25 min at 32 °C with gentle shaking. After spinning for 5 min at 100 x *g*, the tubules were resuspended in 2 ml digestion buffer and incubated for further 25 min. The suspension was filtered through a 40 µm nylon mesh to remove clumps. After washing once in HBSS, the cell pellet was resuspended in incubation buffer to a final concentration of 2 millions per 1 ml, supplemented with 0.5 µg/ml Hoechst No.33342. The cells were incubated for 1 h at 32°C in the dark. Cells were pelleted at 100 x *g* for 5 min and resuspended in incubation buffer supplemented with propidium iodid for staining of dead cells. Suspensions were sorted on the LSR II (BD Biosciences) with UV laser excitation wavelength 355 nm and emission filters Hoechst-Blue 405B and Hoechst-Red 430A, and analyzed using FACSDiVa software (BD Biosciences).
For staining of germ cells with an antibody against human CD4, single cell suspension was prepared as described above. Cells were resuspended in incubation buffer with anti-hCD4-FITC (1:100) and incubated for 30 min at 32°C. Cells were analyzed using the LSR II.

Digestion buffer	Hanks Balanced Salt Solution (HBSS), 20 mM Hepes pH 7.2, 1.2 mM $MgSO_4x7H_2O$, 1.3 mM $CaCl_2x2H_2O$, 6.6 mM sodium pyruvate, 0.05 % sodium lactate, 0.4 mg/ml Collagenase I, DNase I
Incubation buffer	Digestion buffer, 1 % glutamine, 1 % fetal calf serum

2.6. Extraction of proteins from testis

For nuclear extracts, mice were dissected and both testes were minced using a dounce homogenizer (loose) in 1 ml PBS. After centrifugation at 200 x *g*, 4°C for 5 min, cells were resuspended in 1ml cold buffer B. Cells were dounced with a tight pestel 20-30 times. To pellet nuclei cells were centrifuged for 3 min at 5900 x *g*. The supernatant correspond to the cytoplasmic fraction. Nuclei were resuspended in 250 µl buffer C. 1/10 Vol of ammonium sulfate pH 7.4 was added, mixed immediately and incubated on ice for 30 min with occasional shaking. Centrifugation in an ultracentrifuge at 40000 x *g*, 4°C for 30 min followed. The supernatant correspond to the nuclear fraction. Fractions can be stored at -80°C after supplement of 10 % glycerol and 100 mM NaCl.

For total cell lysates (RIPA extract), two testes were dounced (tight pestel) in 500 µl complete RIPA buffer. After incubation on ice for 10 min, lysates were centrifuged for 20 min at highest speed, 4 °C. The proteins resided in the supernatant and after addition of 100 mM NaCl and 10 % glycerol, the extracts can be stored at -20°C. Protein concentration was measured with Roti®-Quant according to manufacturers recommendations using a micro plate spectrophotometer.

Buffer B	5 mM KCl, 40 mM Tris pH 7.5, 2 mM EDTA, 0.5 mM vanadate, 2 mM PMSF, 10 mM $Na_2S_2O_5$, 50 µg/ml TLCK, 2 mM DTT, Complete (Roche)
Buffer C	5 mM KCl, 0.5 mM EDTA, 15 mM Tris pH 7.5, 2 mM PMSF, 10 mM $Na_2S_2O_5$, 50 µg/ml TLCK, 1 mM DTT, Complete (Roche)
RIPA buffer	50 mM Tris pH 8.0, 150 mM NaCl, 0.5 % deoxycholate, 1 % NP-40, 0.1 % SDS, 50 mM NaF, 0.2 % PMSF, TLCK, $Na_2S_2O_5$

2.7. Immunoblotting of protein extracts

Protein pattern were analyzed using SDS-PAGE. 40 µg of protein extract were separated on a 7.5 % SDS gel. Gels were either stained with Coomassie Brilliant Blue or blotted to a Hybond^{TM}-C membrane using the Mini Trans-Blot® Electrophoretic Transfer cell (Bio-Rad) for 2 h with 100 Volt. After staining with Ponceau red, the membrane was blocked for 1 h with blocking buffer. Three wash steps with PBS-T followed and the first antibody was incubated overnight at 4°C. Next day the membrane was washed and incubated with the secondary antibody diluted in PBS-T for 1 h at RT. After washing with PBS-T, the membrane was covered with detection reagent for 1 min and luminescence was detected using the KODAK Image Station 2000MM.

PBS-T	1x PBS, 0.1 % Tween-20
Blocking buffer	PBS-T, 5 % milk powder
Ponceau red	2 % Ponceau S, 30 % Trichloroacetic acid, 30 % Sulfosalicylic acid in H_2O

For immunoblot analysis following antibodies were used:

Antibodies for Immunoblot	Provider	Dilution
Rabbit polyclonal α -MVH/DDX4	Abcam	1 µg/ml
Rabbit polyclonal α -PIWIL2	Abcam	1 µg/ml
Rabbit polyclonal α -RNF17	J. Wang, UPenn	1:1000
Rabbit polyclonal α -HIWI	Abcam	0.5 µg/ml
Rabbit polyclonal α -MAEL	Abcam	1 µg/ml
Rabbit polyclonal α -TDRDN PA #27459		5 µg/ml
Rabbit polyclonal α -TDRDC AG #27507		8 µg/ml
Rabbit polyclonal α -SP1	Bethyl Lab.	1 µg/ml
α -rabbit-HRP	Jackson Lab	1:10000
α -mouse-HRP	Jackson Lab	1:10000

Table 2.2: Antibodies and the respective concentrations used for immunoblotting.

2.8. Immunofluorescence of testis sections

Native testes were frozen in Tissue Tek O.C.T.™ compound and cut in 7 µm sections using the Leica CM1900 Cryostat. After fixation in ice-cold methanol/acetone for 10 min, slides were washed in PBS 3 x 5 min. Slides were blocked in prewarmed PBTG at 37°C for 5 min. Antibodies were diluted in PBTG, covered with Parafilm and incubated overnight at 4°C in a humid chamber. For staining with the LINE-1 antibody, slides were fixed with 3.7 % PFA for 20 min on ice. After incubation in PBS/Triton for 4 min, slides were washed 3 x 10 min with PBS. The antibody was diluted in PBS with 2 % goat serum and incubation was carried out overnight at 4 °C. Slides were washed 4 x 5 min with PBTG at 37°C and incubated with the secondary antibody diluted in PBTG for 1 h at 37°C in a humid chamber. After washing 4 x 3 min with PBTG, slides were mounted with Fluoromount and covered with a coverslip. Fluoromount was supplemented with DAPI to visualize nuclei. Stainings were analyzed using the fluorescence microscope Axiophot (Zeiss) with the corresponding AxioVision 4.6 software.

Methanol/Acetone	4 Vol Methanol, 1 Vol Acetone
3.7 % PFA	3.7 % Paraformaldehyde in PBS
PBS/Triton	0.1 % Triton in PBS
PBTG	0.1% BSA, 0.5% Fish Gelatine, 0.05% Tween 20 in PBS

For immunofluorescence (IF) analyses following antibodies were used:

Antibodies for Immunofluorescence	Provider	Dilution	Fixative
Rabbit polyclonal α - MVH	Abcam	1 µg/ml	Methanol/Acetone
Rabbit polyclonal α - HIWI (MIWI)	Abcam	2 µg/ml	Methanol/Acetone
Rabbit polyclonal α - MAEL	Abcam	2 µg/ml	Methanol/Acetone
Rabbit polyclonal α - TDRDN (PA)		0.4 mg/ml	Methanol/Acetone
Rabbit polyclonal α - TDRDC #27477 (AG)		4.2 µg/ml	Methanol/Acetone
Rabbit polyclonal α - L1 Orf1p	S. Martin (Berkeley Univ.)	1:500	3.7 % PFA
Mouse IgG1 hybridoma α - SYCP3	C. Heyting (Wageningen Univ.)	1:1 PBS-T	Methanol/Acetone
Secondary antibodies			
Goat α - rabbit IgG-Biotin	Dianova (Jackson Lab)	1:500	
Donkey α - mouse IgG - Biotin	Dianova (Jackson Lab)	1:500	
Goat α - rabbit IgG - Cy3	Dianova (Jackson Lab)	1:500	
ExtrAvidin® - Cy3	Sigma	1:1000	
ExtrAvidin® - FITC	Sigma	1:1000	

Table 2.3: Antibodies and the respective dilutions and fixation methods used for IF.

2.9. DNA isolation from testes and tails

Testes were isolated from mice and a single cell suspension by dounce homogenization was prepared. Cells were harvested by centrifugation and resuspended in lysis buffer (10^6 cells/50 µl) and incubated overnight at 55°C with intense shaking. For DNA isolation from mice tails, tails were incubated in 500 µl lysis buffer at 55 °C overnight. After centrifugation for 2 min at 16000 x *g* the supernatant was transferred to a fresh tube.

For both protocols, an equal volume of Phenol-Chloroform (1:1) was added, mixed and centrifuged for 5 min at highest speed. The upper aqueous phase was transferred to a new tube. An equal volume of Chloroform was added, the two phases were mixed and after centrifugation, the supernatant was transferred to a fresh tube. DNA was precipitated with 2 vol of 96 % ethanol. The mixture was centrifuged at 16000 x *g* for 5 min and the pellet was washed with 70 % ethanol. The DNA was dried and resuspended in an appropriate volume of TE buffer. DNA concentration was measured using a Nanodrop.

Lysis buffer testis	10 mM Tris-HCl pH 8.0, 10 mM EDTA, 100 mM NaCl, 40 mM DTT, 2 % SDS, 20 µg/ml Proteinase K
Lysis buffer tail	50 mM Tris-HCl pH7.5, 50 mM EDTA, 0.5 % SDS, 0.2 M NaCl, 0.2 mg/ml Proteinase K
TE buffer	10 mM Tris-HCl pH 7.5, 0.1 mM EDTA

2.10. Genotyping

For genotyping the mice, tail DNA was isolated and analyzed by polymerase chain reaction (PCR) using the Taq DNA Polymerase from Invitrogen. For the wild-type locus a band of 685 bp and for the knockout locus a band of 292 bp is expected. For primer sequences refer to table 2.4. Following reagents were mixed and PCR settings were applied (Eppendorf Mastercycler® ep):

Reagents	25 µl total	PCR settings		
DNA	0.5 µl			
10 x buffer	2.5 µl			
50 mM $MgCl_2$	1.25 µl	94°C	3 min	
10 pmol Primer forward (Tdrd6ShArmgeno_for)	0.5 µl	94°C	30 sec	⎤
10 pmol Primer reverse I (hCD4_rev)	0.25 µl	63°C	30 sec	⎥ x 35 cycles
10 pmol Primer reverse II (Tdrd6genoWT_rev)	0.25 µl	72°C	1 min	⎦
dNTPS (10 mM of dATP, dCTP, dGTP, dTTP)	0.5 µl	72°C	10 min	
DMSO	1.25 µl			
Taq polymerase	0.1 µl			
water	17.9 µl			

2.11. Southern Blotting

2.11.1. Probe labeling

The Southern Blot (Southern 1975) was an additional method to analyze the genotype of the mice. For this, the targeting vector pTV-Uni-Tdrd6 (Figure 2.1) was digested with *Eco*RI and *Kpn*I. The resulting 1.4 kb fragment was gel-extracted using the gel extraction kit from Qiagen. 50 ng of the DNA fragment was used for labeling with α-32P-dCTP (PerkinElmer) by using the Prime-It labeling kit from Stratagene, following the manufacturer's recommendations. For the Line-1 Southern Blot the probe was designed like described previously (Carmell et al. 2007) using primers listed in table 2.4.

2.11.2. Hybridization

Southern Blot was done as described previously (Sambrook and Russell 2001). 15 µg (Genotyping Southern Blot) or 5 µg (*Line*-1 Southern Blot) of testis or tail DNA was digested with the appropriate restriction enzymes (Genotyping: *Bgl*II, *Line*-1: *Msp*I, *Hpa*II) overnight. DNA was run on a 0.8 % agarose gel prepared in 1 x TBE. After taking a picture using UV light, the gel was incubated in denaturing solution for 30 min on a shaker at RT. Other incubation steps in neutralization solution for 2 x 15 min followed. The gel was placed upside-down on a piece of Whatman 3 MM paper, both were put on a tray within a bigger dish, making a bridge in 20 x SSC. The membrane was placed on the gel and was covered with 3 layers of pre-wetted

Whatman 3 MM paper and a stack of paper tissues. The stack was covered with a glass plate and a weight of approximately 1 kg was placed on top. The transfer was done overnight. The next day the DNA was fixed on the membrane by cross-linking with UV light. After rinsing the membrane in 2 x SSC, it was pre-hybridized for a few hours in a rotating oven at 60°C with PerfectHyb® buffer. The radioactive labeled probe was diluted in 10 ml fresh PerfectHyb® buffer and hybridized to the membrane overnight at 60°C in a rotating oven. The next day the probe was collected and was stored at -20°C in a protected box. The membrane was rinsed in wash buffer I for 1 min, and 2 times incubated with wash buffer II for 30 min at 60°C. After washing, the membrane was exposed for several hours up to overnight to a Phosphor screen. The Southern Blot was analyzed using a PhosphorImager (Molecular Dynamics) and the ImageQuant 5.1 software.

10 x TBE	0.89 M Tris, 0.89 M Boric acid, 2 mM EDTA, pH 8.9
Denaturing solution	500 mM NaOH, 1.5 M NaCl
Neutralization solution	500 mM Tris-HCl pH7.2, 1.5 M NaCl, 1 mM EDTA
20 x SSC	3 M NaCl, 0.3 M $C_6H_5Na_3O_7$ x 2 H_2O (Sodium citrate)
Wash buffer I	2 x SSC, 0.1 % SDS
Wash buffer II	100 mM Na_2HPO_4, 0.1 % SDS

2.12. Electron microscopy

Seminiferous tubules were dissected from mouse testis, fixed in 0.1 M phosphate buffer (pH 7.4) containing 2 % glutaraldehyde for 1.5 h and post-fixed in 1 % osmium tetroxide in water for 1 h. Samples were dehydrated through a graded series of ethanol and thin-layer embedded in Epon/Araldite as described (Muller-Reichert et al. 2003). Ultrathin sections (70 nm) were stained using 2 % uranyl acetate in 70 % methanol followed by lead citrate and imaged in a TECNAI 12 transmission electron microscope (FEI) operated at 100 kV.

2.13. Gene expression analyses

2.13.1. Whole mouse genome analyses

To analyze gene expression in *Tdrd6*-deficient mice, total testis RNA of 18-days-old mice was purified using TRIzol® reagent according to the manufacturer's recommendations. The integrity of RNA was analyzed by running on the Bioanalyzer 2100 (Bio-Rad). RNA was labeled using the One-Color Microarray-Based Gene Expression Analysis System from Agilent Technologies (Agilent 2007) according to manufacturer's recommendation. Briefly, cDNA of total testis RNA was synthesized and labeled with Cyanine 3-CTP and hybridized to 4x44K whole mouse genome microarrays (Agilent). Data were analyzed using the GeneSpring 7.3 software (Agilent).

2.13.2. Quantitative real time PCR

RNA from testes was purified using TRIzol® reagent according to the manufacturer's recommendations. DNA was digested with DNase I, and reverse transcription was carried out using the Superscript RT from Invitrogen. Primers used for analyzing gene expression are listed in table 2.4. For quantitative real time PCR the SYBR green kit from Qiagen was used according to the manufacturer's recommendations. Samples were analyzed using the Corbett RG-3000 system.

2.13.3. MiRNA expression analyses

Total testis RNA was isolated from 18-days-old mice using TRIzol® reagent according to the manufacturer's recommendations. MiRNA expression analyses were carried out using the miRXplore™ Standard Service (Miltenyi Biotech GmbH). Data were normalized by applying the 50th percentile of background value and by performing the Lowess normalization. Additionally, data from mature miRNA analyses were validated by quantitative real time-PCR according to (Sharbati-Tehrani et al. 2008) using the Corbett RG-3000 system. Briefly, reverse transcription on total testis RNA

was performed with an oligonucleotide (RT6-miR-x) that hybridizes to the 3' end of the respective miRNA. For subsequent qRT-PCR (QuantiTect SYBR Green PCR Kit, Qiagen) another miRNA-specific primer as well as two universal primers were used (Table 2.4). Precursors of miRNAs were analyzed according to (Davis et al. 2008). The results of qRT-PCR assays presented are an average of three independent RNA preparations and each sample was analyzed in triplicates. Statistical analyses were performed using One-way ANOVA followed by Bonferroni post tests (GraphPad Prism software).

2.14. Bioinformatic analyses

Following bioinfomatic databases were used:

- Ensemble (www.ensembl.org/index.html) and MGI (www.informatics.jax.org/): Information about gene sequences and localization

- miR-Base database (http://microrna.sanger.ac.uk/): miRNA accession numbers, as well as cluster and promoter analyses.

- TargetScanS (www.targetscan.org) and TarMir (www.tarmir.rgcb.res.in/): miRNA/mRNA target prediction

- miRDB (http://mirdb.org/miRDB/): prediction of mRNAs and their hypothetical miRNAs (Wang 2008)

- MAPPER (http://snpper.chip.org/mapper/mapper-main): analyses of putative transcription factor binding sites in promoter regions of mRNAs

ShArm forward	5'- GAATTCTTCAAGGATAAGCTCAACGTGGAGAA
ShArm Reverse	5'- CGCCAACCGAGAGCT
LongArm forward	5'- GAAAATTTAAATACAAAGAAGTTAGCTCAGATTTG
LongArm reverse	5'- CAGTTTAAACGCTAACATGCTAACACTA
hCD4 reverse	5'- GGGAAGCTGTACAGGTCAGTTCCA
Tdrd6ShArmgeno forward	5'- GGCTGCTACCAGTCGCGAGTC
Tdrd6genoWT reverse	5'- ATGGAGGAGCAACACATCCAGGAC
Tdrd6 RT-fwd	5'- GAAGGAAGGAAGTGCGGGAGC
Tdrd6 RT-rev	5'- CACCTCCACACGCCTCCTCC
Cterm-fwd BglII	5'- GCCAGAtctGGAAGGAAGTGCG
C-term-revXhoI	5'- ATGCTCGAGTCATATGTTCAGC
Nterm-fwdBglII	5'-TCGAGATCTACTCCGGGGCTGC
Nterm-revXhoI	5'-CCTCGAGGGGCAGGTGGAAGA
Actin-F (qRT-PCR)	5'- AGGCATTGCTGACAGGATGCAG
Actin-R (qRT-PCR)	5'- AGCACTTGCGGTGCACGATG
GAPDH-F (qRT-PCR)	5'- GAGAAACCTGCCAAGTATGATG
GAPDH-R (qRT-PCR)	5'- GGAGTTGCTGTTGAAGTCGC
MP-F (miR-qRT-PCR)	5'- TGTCAGGCAACCGTATTCACC
MP-R (miR-qRT-PCR)	5'- CGTCAGATGTCCGAGTAGAGG
5S rRNA-F (miR-qRT-PCR)	5'- GCCCGATCTCGTCTGATCT
5S rRNA-R (miR-qRT-PCR)	5'- AGCCTACAGCACCCGGTATT
RT-miR-29b-1(miR-qRT-PCR)	5'- TGTCAGGCAACCGTATTCACCGTGAGTGGTAACACT
RT-miR-29c(miR-qRT-PCR)	5'- TGTCAGGCAACCGTATTCACCGTGAGTGGTTAACCG
RT-miR-34a(miR-qRT-PCR)	5'- TGTCAGGCAACCGTATTCACCGTGAGTGGTACAACC
RT-miR-34c(miR-qRT-PCR)	5'- TGTCAGGCAACCGTATTCACCGTGAGTGGTCCTGGC
RT-miR-322(miR-qRT-PCR)	5'- TGTCAGGCAACCGTATTCACCGTGAGTGGTTCCAAA
RT-miR-342(miR-qRT-PCR)	5'- TGTCAGGCAACCGTATTCACCGTGAGTGGTCCTGGC
Short-miR-29b1R(miR-qRT-PCR)	5'- CGTCAGATGTCCGAGTAGAGGGGGAACGGCGTAGCACCATTTGAAATCAG
Short-miR-29c-R(miR-qRT-PCR)	5'- CGTCAGATGTCCGAGTAGAGGGGGAACGGCGTAGCACCATTTGAAATCGG
Short-miR-34a-R(miR-qRT-PCR)	5'- CGTCAGATGTCCGAGTAGAGGGGGAACGGCGTGGCAGTGTCTTAGCTCC
Short-miR-34c-R(miR-qRT-PCR)	5'- CGTCAGATGTCCGAGTAGAGGGGGAACGGCGAATCACTAACCACACAGC
Short-miR-322-R(miR-qRT-PCR)	5'- CGTCAGATGTCCGAGTAGAGGGGGAACGGCGCAGCAGCAATTCATGTTT
Short-miR-342-R(miR-qRT-PCR)	5'- CGTCAGATGTCCGAGTAGAGGGGGAACGGCGAGGGGTGCTATCTGTGAT
Pri-miR-29b1-F(miR-qRT-PCR)	5'- TGTAAGCCTCGTGCTCACTG
Pri-miR-29b1-R(miR-qRT-PCR)	5'- GAAGGTGAAGTCCGTGCAAT
Pre-miR-29b1-F(miR-qRT-PCR)	5'- AGGAAGCTGGTTTCATCTGG
Pre-miR-29b1-R(miR-qRT-PCR)	5'- AGAACACTGATTTCAAATG
Pri-miR-29c-F(miR-qRT-PCR)	5'- AGCAAGGAAGGGGTAAGAGC
Pri-miR-29c-R(miR-qRT-PCR)	5'- ACCGACTGGTGGTGTTCTTC
Pre-miR-29c-F(miR-qRT-PCR)	5'- ATCTCTTACACAGGCTGACC
Pre-miR-29c-R(miR-qRT-PCR)	5'- TCCCCCTACATCATAACCGA
Pri-miR-34a-F(miR-qRT-PCR)	5'- TCCTGACTCAGCCTCCTTGT
Pri-miR-34a-R(miR-qRT-PCR)	5'- TGACACACTCCTCCAGCACT
Pre-miR-34a-F(miR-qRT-PCR)	5'- CCAGCTGTGAGTAATTCTTT
Pre-miR-34a-R(miR-qRT-PCR)	5'- ACAATGTGCAGCACTTCTAG
L15UTR-F	5'- GGCGAAAGGCAAACGTAAGA
L15UTR-R	5'- GGAGTGCTGCGTTCTGATGA

Table 2.4: Primer sequences used for these thesis.

3. Results

3.1. Generation of TDRD6 C- and N-terminal antibodies

TDRD6 is expressed exclusively in testis cells during spermatogenesis. In the transition from diploid to haploid cells, the protein is cleaved by an unknown process. We speculate, that Caspase I cleaves TDRD6 at the C-terminal end, since there is a predicted cleavage site in a respective distance from this end. To verify if the cleavage really occur at the C-terminal end, we generated two different antibodies specific for each terminus of the protein.

The respective peptides for the TDRD6 N-terminal and C-terminal antibodies were overexpressed in bacteria and purified on glutathione agarose. Figure 3.1 shows the purified peptides after separation with SDS-polyacrylamide gel electrophoresis stained with Coomassie Brilliant Blue. The expected size of the peptides is 40 kDa.

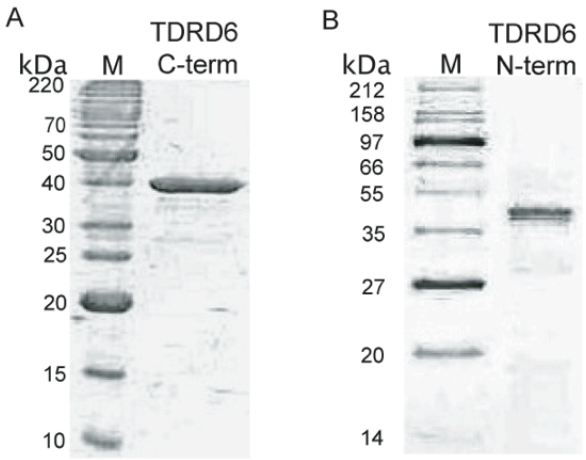

Figure 3.1: Purified peptides of TDRD6-Cterm (A) and TDRD6-Nterm (B).
Peptides are separated with SDS-PAGE and stained with Coomassie Blue.

After injection of the peptides into rabbits, mixed with Freund's Adjuvants as an immunopotentiator (see table 2.1 for details), the obtained blood sera were purified using Protein A-agarose. Figure 3.2 shows the first three fractions of antibodies purified with Protein A-agarose beads for each immunized rabbit. The heavy (50 kDa) and light chains (25 kDa) of the antibodies are visible. These purified antibodies are a mixture of all existing antibodies in the rabbit, since Protein A-agarose is suitable of

binding all IgG molecules. Table 3.1 gives information of the total amount of antibodies, which were obtained from 25-30 ml serum of each rabbit purified with Protein A-agarose.

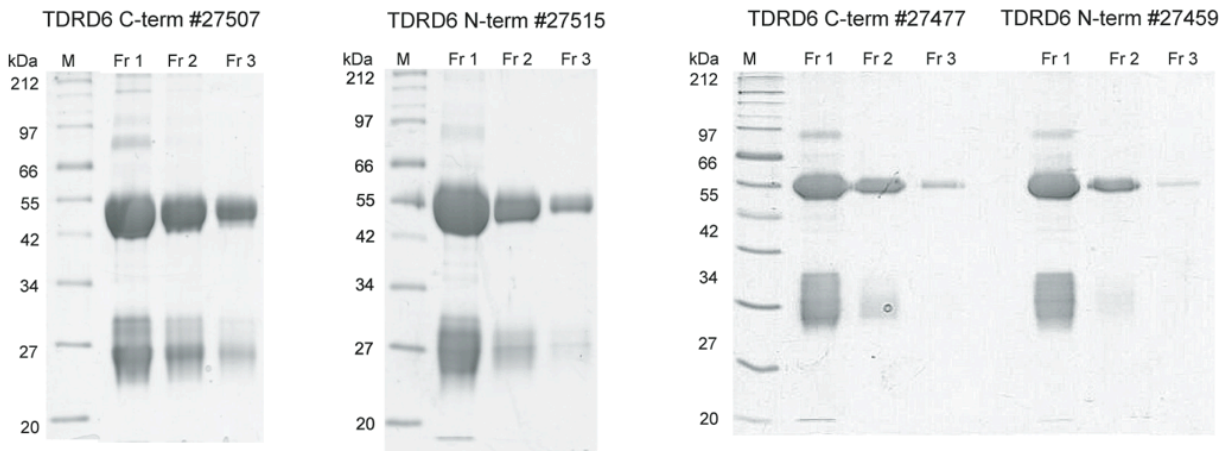

Figure 3.2: **With Protein A-agarose purified antibodies from all four rabbits.** Antibodies are separated with SDS-PAGE and stained with Coomassie Blue; heavy and light chains are visible.

Rabbit numeration	Peptide	Amount of antibody
#27477	TDRD6-Cterm No. 1	1,3 mg
#27507	TDRD6-Cterm No. 2	1,8 mg
#27459	TDRD6-Nterm No. 1	2,2 mg
#27515	TDRD6-Nterm No. 2	2,1 mg

Table 3.1: **Obtained amount of antibodies from 25-30 ml serum of each rabbit**.

To purify TDRD6 specific antibodies, the respective TDRD6-Cterm peptide was coupled to Cyanogen bromide-activated-Sepharose. For TDRD6-Nterm peptides the antibody purification using this method was not successful. Figure 3.3 shows the five first fractions of the TDRD6-Cterm antibody purification using serum of rabbit #27507. Heavy chains of the antibodies are apparent, the light chains are very faint; the total amount of purified antibody from 18 ml serum of the first three bleedings was 0,19 mg.

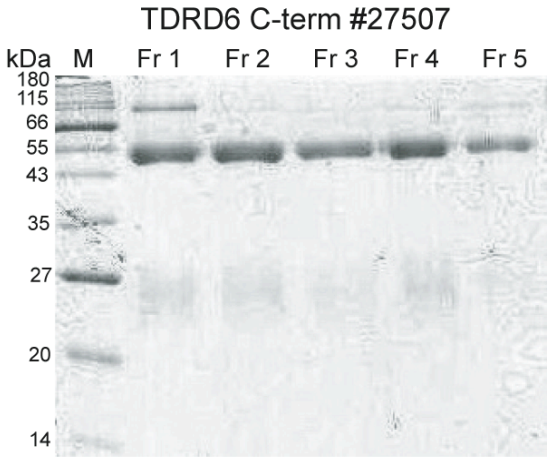

Figure 3.3: Antigen-column purified antibodies of TDRD6-Cterm #27507 serum. Antibodies are separated with SDS-PAGE and stained with Coomassie Blue; heavy and light chains of antibodies are visible.

The achieved antibodies were tested by Immunoblotting using total testis protein extract. Protein extract from kidney was used as a negative control. Figure 3.4 (A) shows the result of probing the membrane with α-TDRD6-Cterm (#27507) and α-TDRD6-Nterm (#27459), purified by Protein A-agarose. The blot probed with α-Nterm antibody shows the two different TDRD6 isoforms at 250 and 230 kDa. The 230 kDa isoform gives a more prominent band, since in total testis extract there are much more cells expressing the shorter TDRD6 protein. As expected, the blot probed with TDRD6-Cterm antibody shows only the 250 kDa isoform, which confirmed our hypothesis that the cleavage occurs at the C-terminal end of TDRD6.

Figure 3.4 (B) shows frozen testis sections stained with either TDRD6-Nterm or TDRD6-Cterm antibodies. As expected, the TDRD6-Nterm antibody shows a prominent staining of the chromatoid body in round spermatids, as a single red dot. In the displayed figure for TDRD6-Nterm, the respective tubules are not in the stage to show a cytoplasmic staining of primary spermatocytes, which are stained with the synaptonemal complex protein 3 (SYCP3). The staining with the TDRD6-Cterm antibody shows no signal of the 230 kDa TDRD6 isoform, which is present in round spermatids. Therefore, in these images the primary spermatocytes show a diffuse cytoplasmic staining, which correspond to the 250 kDa TDRD6 isoform. Again, our hypothesis about the cleavage of TDRD6 at the C-terminal end is approved, since the TDRD6-Cterm antibody just recognize the 250 kDa isoform.

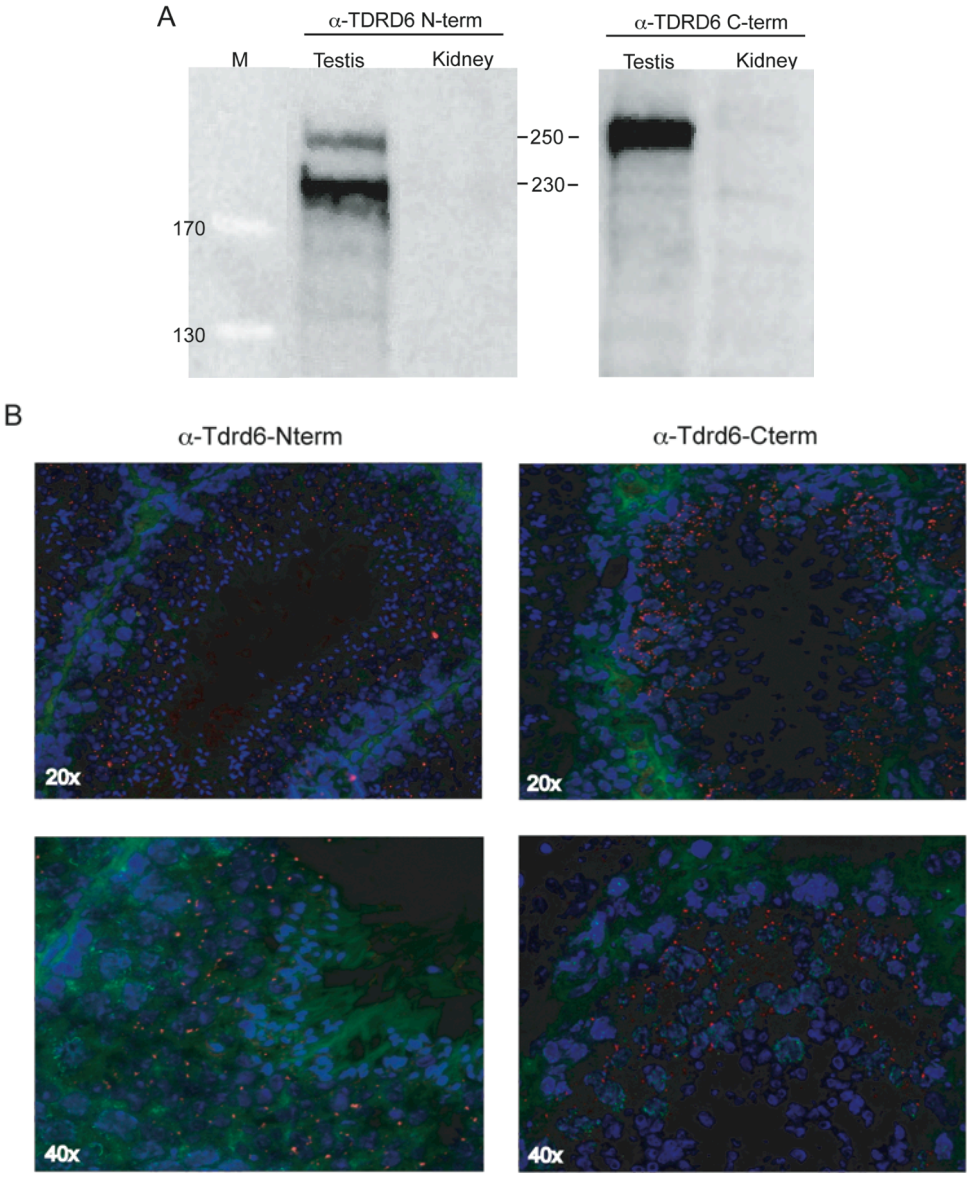

Figure 3.4: Analyses of two TDRD6-specific antibodies. Immunoblot (A) of testis and kidney total cell extract of *Tdrd6*$^{+/+}$ mice with two different TDRD6 antibodies. Incubation with α-TDRD6-Nterm antibody shows the two different isoforms of TDRD6, whereas incubation with α-TDRD6-Cterm shows the 250 kDa isoform. Immunofluorescence (B) of *Tdrd6*$^{+/+}$ testes sections with α-TDRD6-Nterm or α–Cterm antibody, counterstained with synaptonemal complex protein 3 (SYCP3) with 20-fold and 40-fold magnification. With α-TDRD6-Nterm antibody spermatocytes and spermatids show a signal for TDRD6, whereas with TDRD6-Cterm antibody only spermatocytes show a diffuse cytoplasmic TDRD6 signal.

3.2. Generation of a *Tdrd6* knockout mouse model

The *Tdrd6* knockout mouse model was established to analyze the role of TDRD6 during spermatogenesis. Figure 3.5 shows in detail the targeted disruption of the *Tdrd6* locus. Exon 1, representing 95 % of the *Tdrd6* gene, was replaced with the hCD4 gene, lacking the cytoplasmic tail responsible for intracellular signaling.

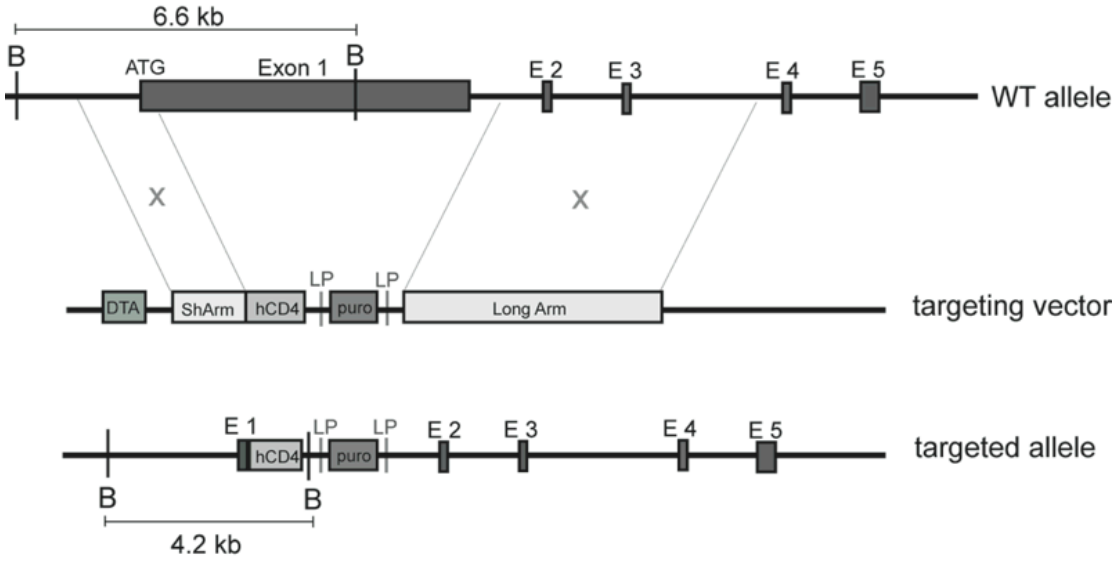

Figure 3.5: **Schematic representation of the wild-type allele, the targeting vector and the mutated *Tdrd6* allele.** B, *Bgl*II cleavage site for later Southern Blot analyses.

After electroporation of the targeting vector into embryonic stem cells and selection for clones carrying the vector, one positive clone among 300 was identified bearing one targeted allele. This clone was injected into a BL6 blastocyst and the resulting offspring transmitted the mutation into the germ line. As shown in figure 3.6 the *Tdrd6* mRNA and protein are present in *Tdrd6*$^{+/-}$, but absent from *Tdrd6*$^{-/-}$ testis.

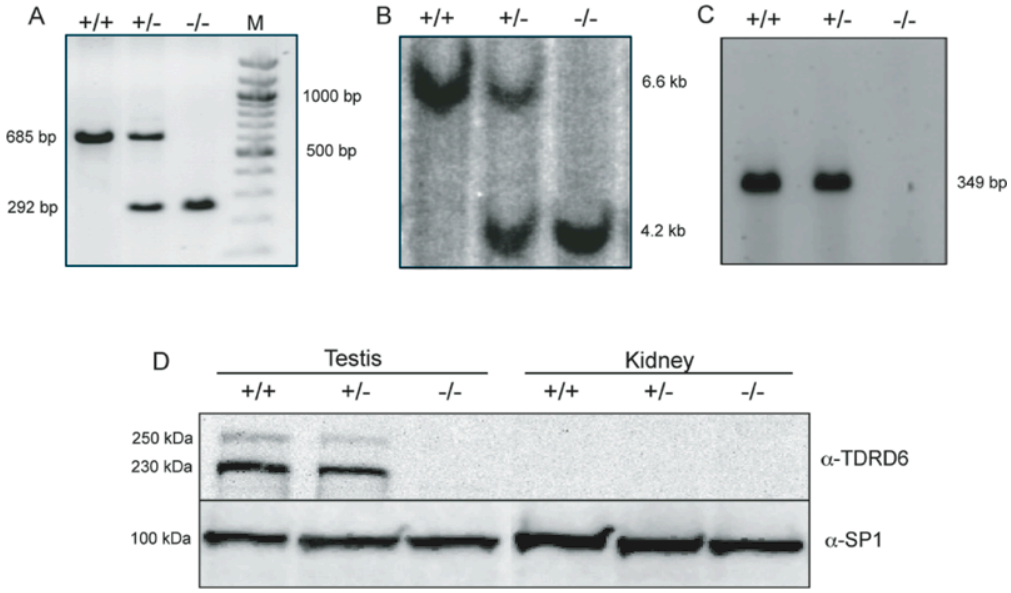

Figure 3.6: Analyses of *Tdrd6*$^{+/+}$, *Tdrd6*$^{+/-}$ and *Tdrd6*$^{-/-}$ mice. (A) PCR for the *Tdrd6* locus. For the wild-type locus a band of 685 bp and for the knockout a band of 292 bp is expected. (B) Southern Blotting using a probe for *Tdrd6*. For the wild-type locus a band of 6.6 kb and for the knockout a band of 4.2 kb is expected. (C) RT-PCR shows a 349 bp band for *Tdrd6*$^{+/+}$ and *Tdrd6*$^{+/-}$, but not for *Tdrd6*$^{-/-}$ mice. (D) Immunoblotting using an α-TDRD6-Nterm antibody (#27459). The two isoforms of TDRD6 are visible, with the more prominent 230 kDa isoform.

3.3. Characterization of the *Tdrd6*$^{-/-}$ mouse phenotype

3.3.1. Mouse colony

Tdrd6$^{-/-}$ mice are viable and show apparently normal development except in male gonads. Interbreeding of *Tdrd6*$^{+/-}$ mice produces offspring of normal litter size and yields the Mendalian ratios of *Tdrd6*$^{+/+}$, *Tdrd6*$^{+/-}$ and *Tdrd6*$^{-/-}$ mice. Whereas the female *Tdrd6*$^{-/-}$ mice are fertile, the males are sterile. *Tdrd6*$^{-/-}$ testes of 20-day-old males are the same size as those from wild-type littermates, which suggests normal development of spermatogonia, primary, and secondary spermatocytes. However, at six weeks of age, the *Tdrd6*$^{-/-}$ males present up to 25 % smaller testes than those of control littermates.

3.3.2. Expression of hCD4 under the *Tdrd6* promoter

Due to the insertion of the truncated *hCD4* gene, lacking the cytoplasmic tail responsible for intracellular signaling, into the genomic locus of the *Tdrd6* gene, the expression of hCD4 is driven by the endogenous *Tdrd6* promoter. Therefore, *Tdrd6*$^{+/-}$ derivates of this strain may serve as a very useful tool to identify, sort, and investigate separate postpachytene germ cell populations. Fluorescence activated cell sorting (FACS) analysis (figure 3.7) of testis, kidney and human peripheral blood monocytes (hPBMC) shows, that testis cells express the hCD4 on their surface. Kidney cells were used as a negative control and the hPBMC, which normally express hCD4, as a positive control.

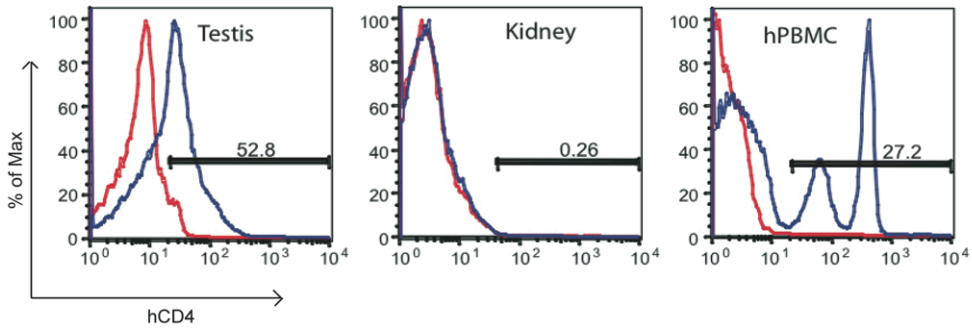

Figure 3.7: **FACS analysis of α-hCD4 stained total testis cell suspension from *Tdrd6*$^{+/-}$ mice**. Kidney cell suspension and human peripheral blood monocytes (hPBMC) were used as controls. In blue, hCD4 positive stained cells in testis, as well as in the positive control. In red, hCD4 negative cells.

3.3.3. Histology of testes sections

To get first information about the assembly of the *Tdrd6*$^{-/-}$ testes, histological analyses were done by staining paraffin-embedded testes sections with periodic acid-Schiff (PAS) and Hematoxylin. Periodic acid-Schiff stains all carbohydrates in pink and Hematoxylin stains basophilic structures like nuclei in blue. In figure 3.8 *Tdrd6*$^{+/-}$ and *Tdrd6*$^{-/-}$ testis sections with tubules in various stages are shown. Mature spermatozoa are completely absent from the lumen of the tubules and from the epididymes of *Tdrd6*$^{-/-}$ mice. Elongated spermatids are almost completely missing, which leads to sterility of the *Tdrd6*$^{-/-}$ mice. Some giant cells are visible in the tubules of *Tdrd6*$^{-/-}$ mice, which are most probably apoptotic cells. The absence of mature sperm was additionally observed by electron microscopy of testis tubules (figure 3.9).

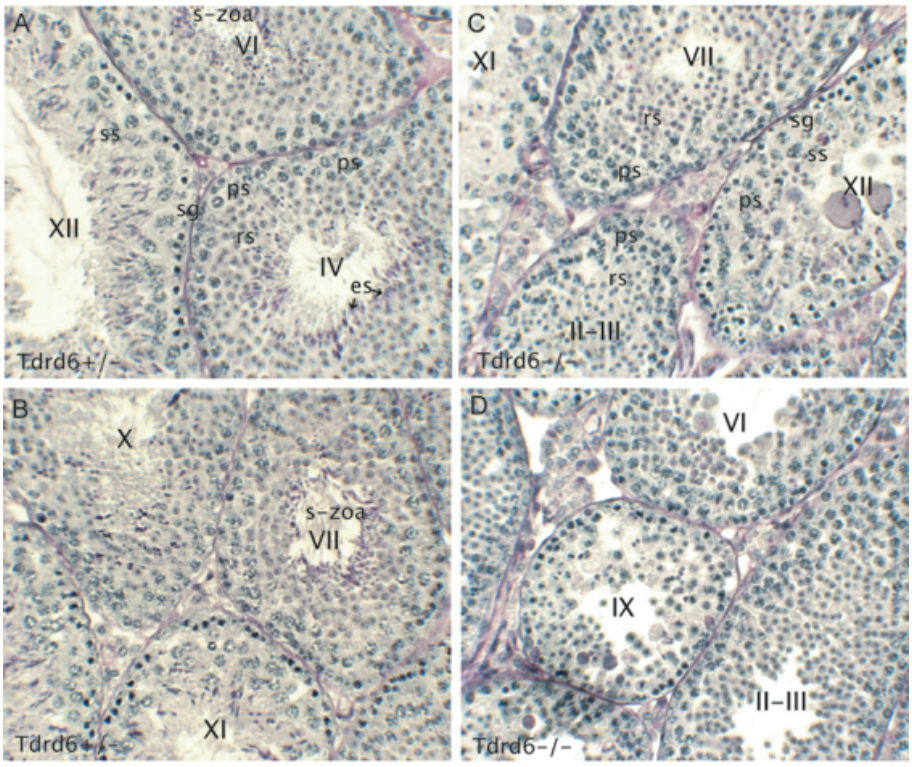

Figure 3.8: Testes from adult *Tdrd6*$^{+/-}$ (A,B) and *Tdrd6*$^{-/-}$ (C,D) littermates were stained with periodic acid-Schiff (PAS) reagent and hematoxylin. Seminiferous tubule stages are indicated by roman numerals in the center. Testes sections of *Tdrd6*$^{-/-}$ mice lack elongated spermatids and mature sperm. Sg, spermatogonia; ps, primary spermatocytes; ss, secondary spermatocytes; rs, round spermatids; es, elongated spermatids; s-zoa, spermatozoa.

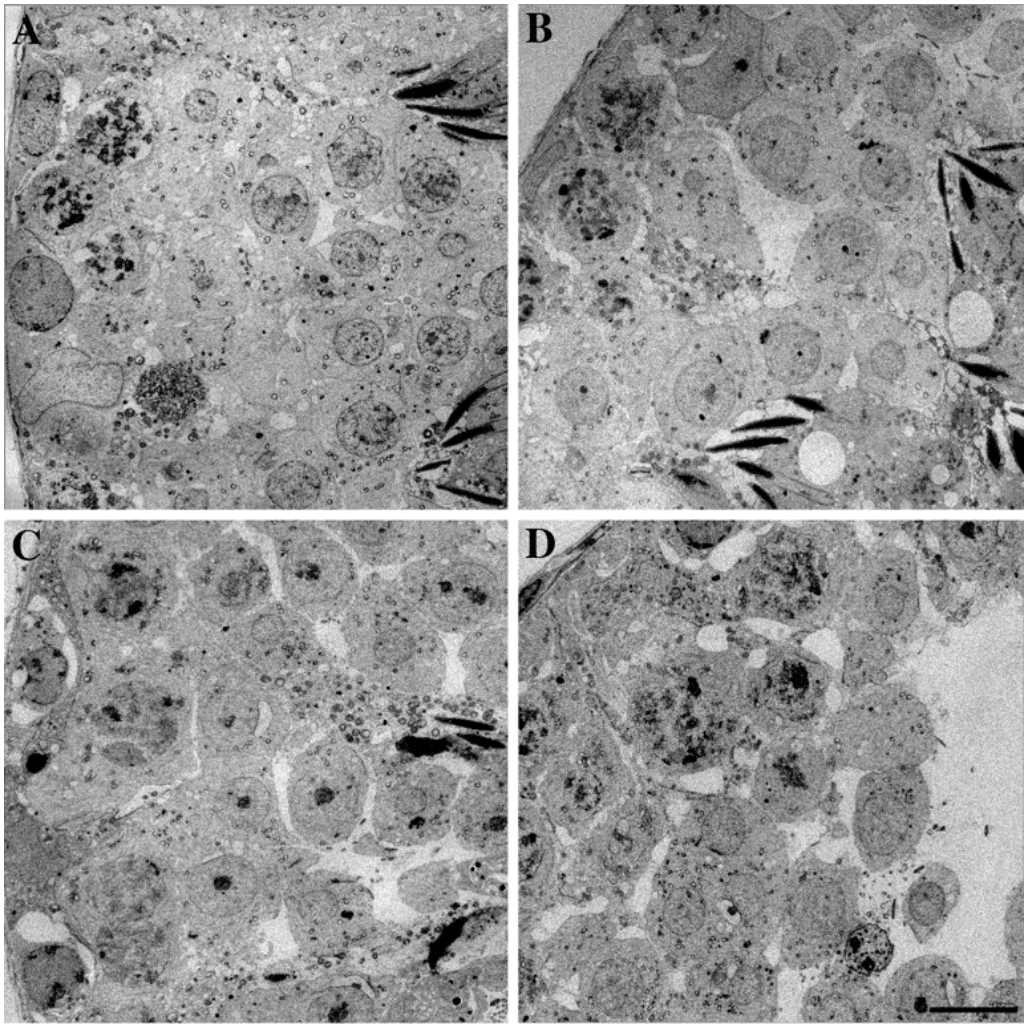

Figure 3.9: **Electron microscopy of seminiferous tubules.** In stage I seminiferous tubules of *Tdrd6*$^{+/-}$ (A) and *Tdrd6*$^{-/-}$ mice (B) elongated spermatids are apparent. Due to a block in spermiogenesis, stage V seminiferous tubules of *Tdrd6*$^{-/-}$ mice (D) lack elongated spermatids, while they are present in *Tdrd6*$^{+/-}$ mice (C) (bar 10 µm).

3.3.4. Germ cell populations in *Tdrd6*$^{-/-}$ mice

The absence of elongated spermatids in adult mice was confirmed by Fluorescence activated cell sorting (FACS) using the LSR II. Testis cells of 10-week-old mice were isolated by collagenase treatment, stained with Hoechst dye and analyzed based on their DNA content. Figure 3.10 shows the FACS plot of the different germ cell populations of *Tdrd6*$^{+/-}$ and *Tdrd6*$^{-/-}$ mice. Spermatogonia and somatic cells are not highlighted. Spermatocytes I are the largest cells with a DNA content of 4 n and represent 8.75 % in the *Tdrd6*$^{+/-}$ and 12 % in the *Tdrd6*$^{-/-}$ mouse. After meiosis division I they become spermatocytes II with a DNA content of 2 n (8.79 % *Tdrd6*$^{+/-}$, 14.4 % *Tdrd6*$^{-/-}$). Round spermatids (RS) are small cells with a DNA content of 1 n and, in these preparations, are the most abundant cell population with 40.1 % in the *Tdrd6*$^{+/-}$ and 44 % in *Tdrd6*$^{-/-}$ mice. The population of elongated spermatids (ES), present with 11.6 % in the *Tdrd6*$^{+/-}$ mouse, is remarkably reduced to 1.38 % in the *Tdrd6*$^{-/-}$ mouse. This confirmed our observations from the electron microscopy that most of the elongated spermatids are missing in *Tdrd6*$^{-/-}$ testis.

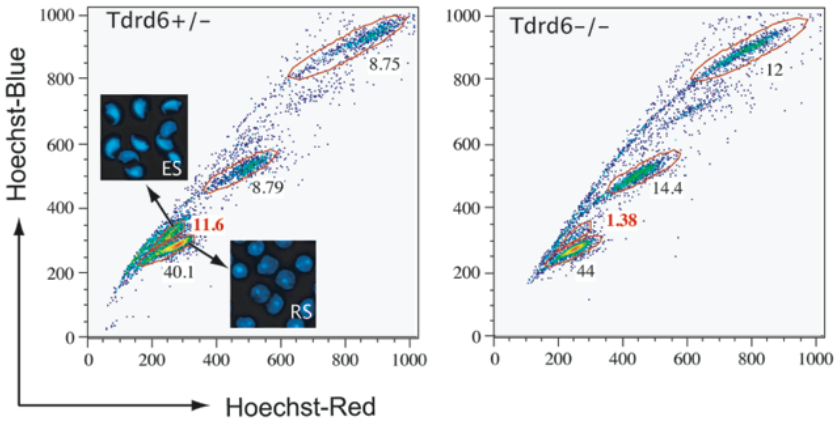

Figure 3.10: **Comparison of the distribution of germ cell populations in 10-weeks-old heterozygous (*Tdrd6*$^{+/-}$) and homozygous (*Tdrd6*$^{-/-}$) mice.** Only very few elongated spermatids are found in tubules of *Tdrd6*$^{-/-}$ mice.

3.3.5. Analyses of apoptosis in *Tdrd6*$^{-/-}$ testes sections

Since an arrest in the spermiogenesis of *Tdrd6*$^{-/-}$ mice at the stage of round to elongated spermatids was observed, we asked for an increase in apoptotic cells. TUNEL (Terminal deoxynucleotidyl transferase dUTP nick end labeling) labeling was used to determine the timing of abnormal cell death in the first wave of spermatogenesis. In apoptotic cells, DNA fragmentation occurs, and by filling the resulting nicks with labeled nucleotides and following incubation with horseradish peroxidase, these cells develop a brown staining. We analyzed mice of different age, from 18 days to 22 days post partum. Figure 3.11 shows testes sections of 19 days old *Tdrd6*$^{+/-}$ and *Tdrd6*$^{-/-}$ mice counterstained with methyl green, in brown apoptotic cells. Until day 18 post partum no difference in the number of abnormal cell death was visible (figure 3.11 C). From day 19 post partum on, a 4-fold increase of apoptotic cells in *Tdrd6*$^{-/-}$ testes sections in comparison to *Tdrd6*$^{+/-}$ sections was observed. Statistic analyses revealed a significant increase (day 19 *, P-value 0.0459, day 20 ***, P-value <0.0001, day 22 **, P-value 0.0036).

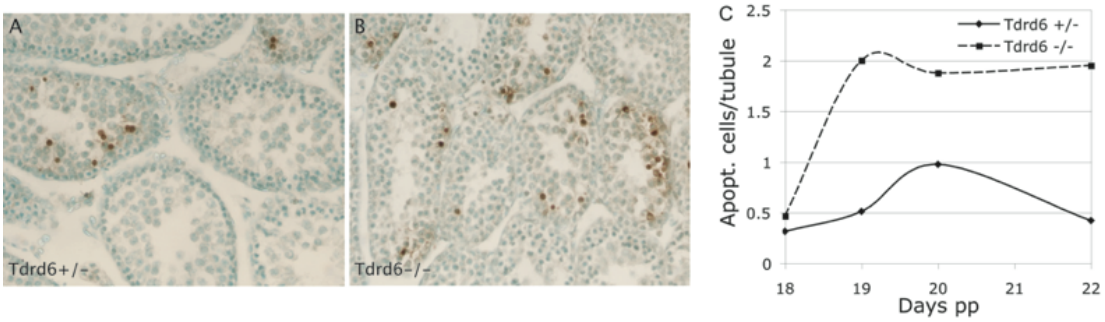

Figure 3.11: **Apoptosis in *Tdrd6*$^{+/-}$ (A) and *Tdrd6*$^{-/-}$ (B) testes**. Testes from 19-day-old heterozygous and homozygous mutant littermates were stained with the TUNEL technique. Figure C shows a quantification of apoptosis in the testes of juvenile mice. From day 19 on, *Tdrd6*-deficient mice show a 4-fold increase of apoptotic cells.

3.3.6. Electron microscopic analysis of the chromatoid body

Since TDRD6 is localized to the chromatoid body in round spermatids we subjected this structure closer examination using high-resolution morphological analysis by transmission electron microscopy. In figure 3.12 chromatoid bodies of *Tdrd6*$^{+/-}$ and *Tdrd6*$^{-/-}$ mice using different magnifications are displayed. CBs were observed at similar frequencies, and in the same close proximity to the nuclear membrane in round spermatids of *Tdrd6*$^{+/-}$ and *Tdrd6*$^{-/-}$ mice of the same stage. In *Tdrd6*$^{-/-}$ spermatocytes and round spermatids, subcellular structures such as synaptonemal complex and acrosomes do not differ from control mice. The most striking difference in round spermatids of *Tdrd6*$^{-/-}$ mice is the disrupted appearance of the chromatoid bodies. Whereas the CBs in *Tdrd6*$^{+/-}$ littermates consist of dense, amorphous material, they appear in *Tdrd6*$^{-/-}$ mice as diffuse structures. The CBs look disrupted, less condensed, and incorrectly assembled, a “ghost”-like structure. Therefore, we conclude that TDRD6 is essential for the correct assembly of the CBs in round spermatids, and their further differentiation into elongated spermatids.

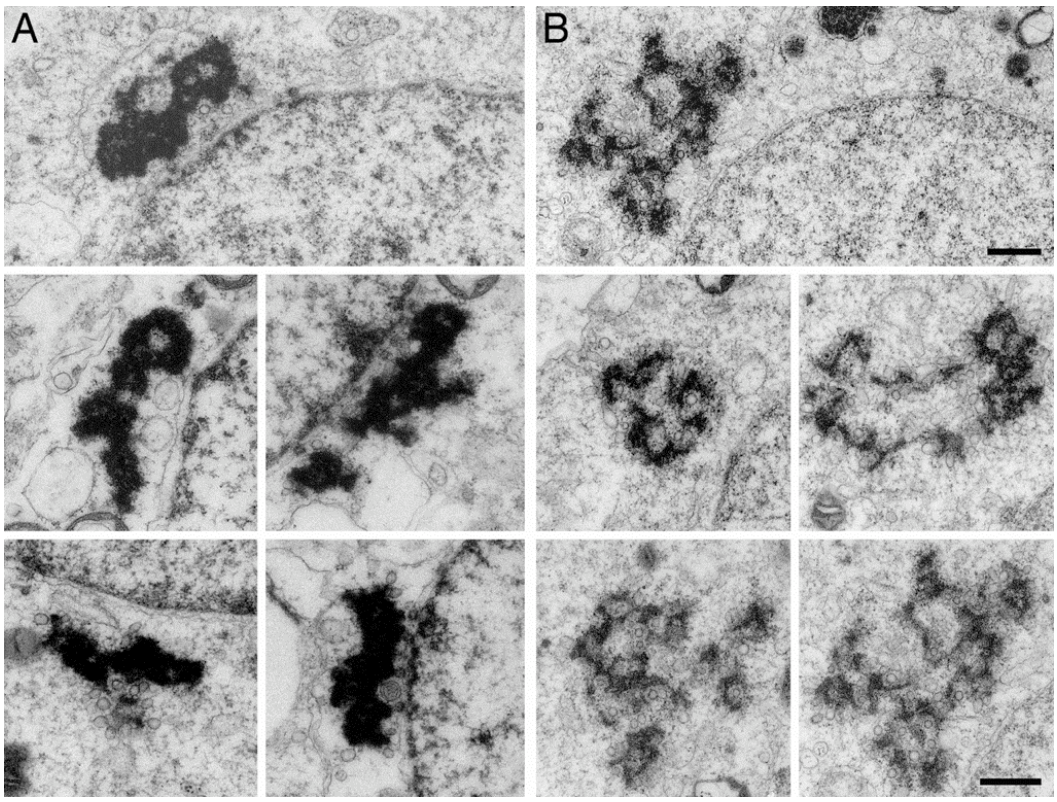

Figure 3.12: **Electron microscopy of the chromatoid body**. (A) and (C) show the fully condensed chromatoid bodies near the nuclear membrane in stage I round spermatids in *Tdrd6*$^{+/-}$ mice. (B) and (D) show the dispersed chromatoid bodies in round spermatids of the same stage in *Tdrd6*$^{-/-}$ mice. Scale bar represents 500 nm.

3.3.7. Expression of chromatoid body components

Many other proteins localize to the chromatoid body in round spermatids, e.g. mouse vasa homolog (MVH), MIWI and Maelstrom. Since we observed, that in the *Tdrd6*-deficient mouse the CB is dispersed and does not look like in wild-type mice, it was obvious to investigate the abundance of other CB components in *Tdrd6*$^{-/-}$ mice. Figure 3.13 shows immunoblot analysis of 40 µg of testis and kidney nuclear protein extract from *Tdrd6*$^{+/+}$, *Tdrd6*$^{+/-}$ and *Tdrd6*$^{-/-}$ mice. Different antibodies for CB components (MVH, MIWI, MAEL), as well as control proteins (SP1, TDRD4/RNF17) were applied. All investigated CB components MVH, MIWI and MAEL are expressed in the same amount in the *Tdrd6*$^{-/-}$ protein extract as in the control mice (figure 3.13). We conclude that TDRD6 has no effect on the expression of these investigated proteins.

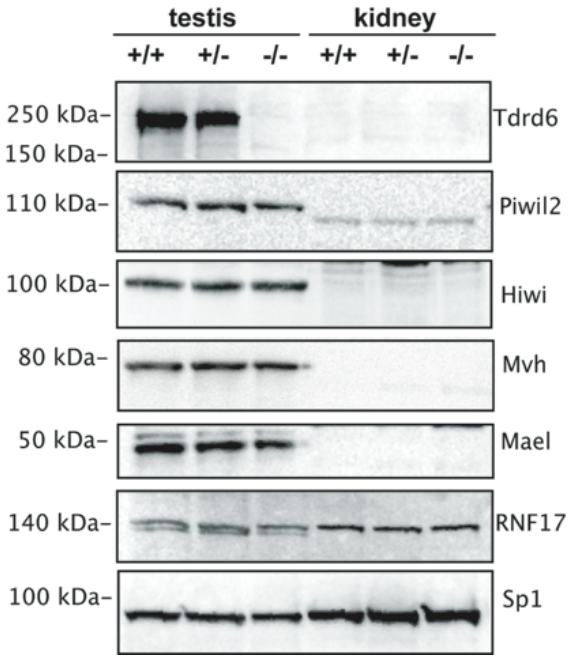

Figure 3.13: **Immunoblot of nuclear extracts from testis and kidney from *Tdrd6*$^{+/+}$, *Tdrd6*$^{+/-}$ and *Tdrd6*$^{-/-}$ mice.** Extracts were probed with specific antibodies for chromatoid body markers TDRD6, PIWIL2 (MILI) HIWI (MIWI), MVH, MAEL, and for control RNF17 and SP1. No differently expression of CB markers is observed in *Tdrd6*$^{-/-}$ mice.

3.3.8. Localization of chromatoid body components

As shown in figure 3.13, other chromatoid body components like MVH, MIWI and Maelstrom are expressed in *Tdrd6*-deficient mice. Next the localization of these proteins was examined. In wild-type mice these proteins localize to the CB in round spermatids, which is disrupted in *Tdrd6*$^{-/-}$ mice. Figure 3.14 shows immunofluorescence staining of testis section from *Tdrd6*$^{+/-}$ and *Tdrd6*$^{-/-}$ mice using a 40-fold magnification. The sections are stained with antibodies against MVH, MIWI and MAEL (Cy3 in red). Each slide is counterstained with the synaptonemal complex protein 3 (SYCP3; FITC in green) to highlight the chromosomes in primary spermatocytes. In *Tdrd6*$^{+/-}$ testis sections a clear “single dot” signal is visible for MVH, MIWI and Maelstrom in round spermatids, which indicates the chromatoid body. However, in *Tdrd6*$^{-/-}$ testis sections a diffuse cytoplasmic staining is visible, but the prominent dots in round spermatids disappeared. For MIWI the typical cytoplasmic staining in primary spermatocytes is not affected. Thus, localization, but not expression of CB components, and certainly CB architecture itself depend on TDRD6.

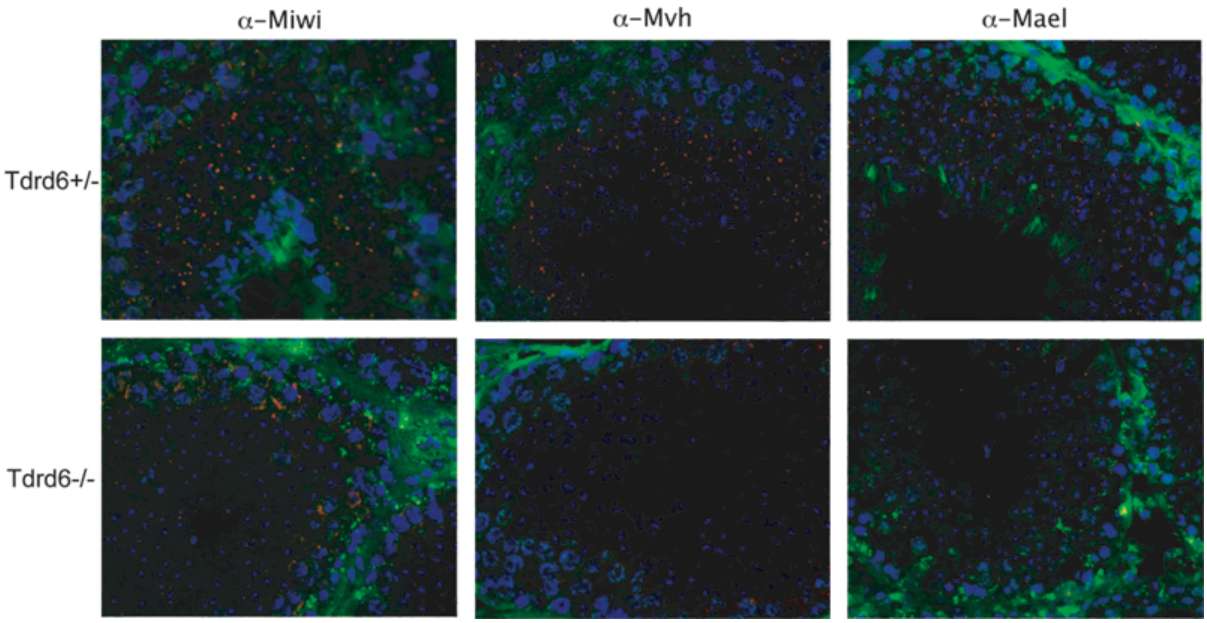

Figure 3.14: **Mislocalization of CB proteins in *Tdrd6*$^{-/-}$ spermatids**. Testis frozen sections from *Tdrd6*$^{+/-}$ and *Tdrd6*$^{-/-}$ were immunostained with α-MVH, α-MIWI or α-MAEL antibodies (red). For all three proteins, the typical pattern of CB staining seen in the control testes is disrupted in *Tdrd6*$^{-/-}$. SYCP3 (green) was used to visualize synaptonemal complexes on chromosomes, and nuclei were stained in DAPI (blue).

3.3.9. Transposon expression in *Tdrd6*-deficient mice

Piwi domain containing proteins MILI and MIWI2, as well as MAEL, are known to regulate retrotransposon activation (Aravin et al. 2007; Carmell et al. 2007; Soper et al. 2008). In the respective knockout mice, activity of retrotransposons like LINE-1 (L1) or intracisternal A-particle (IAP) is strongly increased, due to loss of methylation. Transposable elements are thought to be maintained in a silent state by DNA methylation of CpG islands in the promoter region.

We investigated the transcription activity of LINE-1 (L-1) by CpG methylation diagnostic Southern blotting. For this, testis and tail DNA were digested using either *Msp*I or *Hpa*II. These enzymes are isoschizomers, which recognize the same sequence (CCGG) but have different methylation sensitivities. Whereas *Msp*I is not sensitive for methylated cytosines, *Hpa*II is blocked and cannot cleave a methylated CpG site. By digesting with these two enzymes and Southern blotting with a probe against the 5'UTR of L-1, one can conclude about the methylation pattern of CpG islands in the promoter region and therefore about the activity of this transposon. The probe recognizes four bands of 156 bp generated by *Hpa*II/*Msp*I sites in the 5'UTR, and a band of 1206 bp that is generated by one cleavage site in the 5'UTR and one site in the coding sequence (Carmell et al. 2007). Obviously, there is no difference in the methylation pattern of the L-1 5'UTR between *Tdrd6*-deficient and control mice (figure 3.15). As expected, after digestion of testis and tail DNA with *Msp*I, the correct bands appeared after hybridization with the L-1 probe. Since in the *Hpa*II digested DNA no bands appear, we can conclude, that the 5'UTR of Line-1 is properly methylated in both, *Tdrd6*$^{+/-}$ and *Tdrd6*$^{-/-}$ mice.

Additionally, we examined LINE-1 expression in *Tdrd6*$^{-/-}$ mice by immunofluorescence staining of frozen testes sections with an antibody against LINE-1 (Branciforte and Martin 1994). Primary spermatocytes of a certain stage show a cytoplasmic staining of LINE-1, visible in figure 3.15 (B) with a 10-fold magnification. No obvious difference in this staining is visible between *Tdrd6*$^{+/-}$ and *Tdrd6*$^{-/-}$ mice. So far, we can conclude that there is no significant up-regulation of LINE-1 transposon activity in *Tdrd6*-deficient.

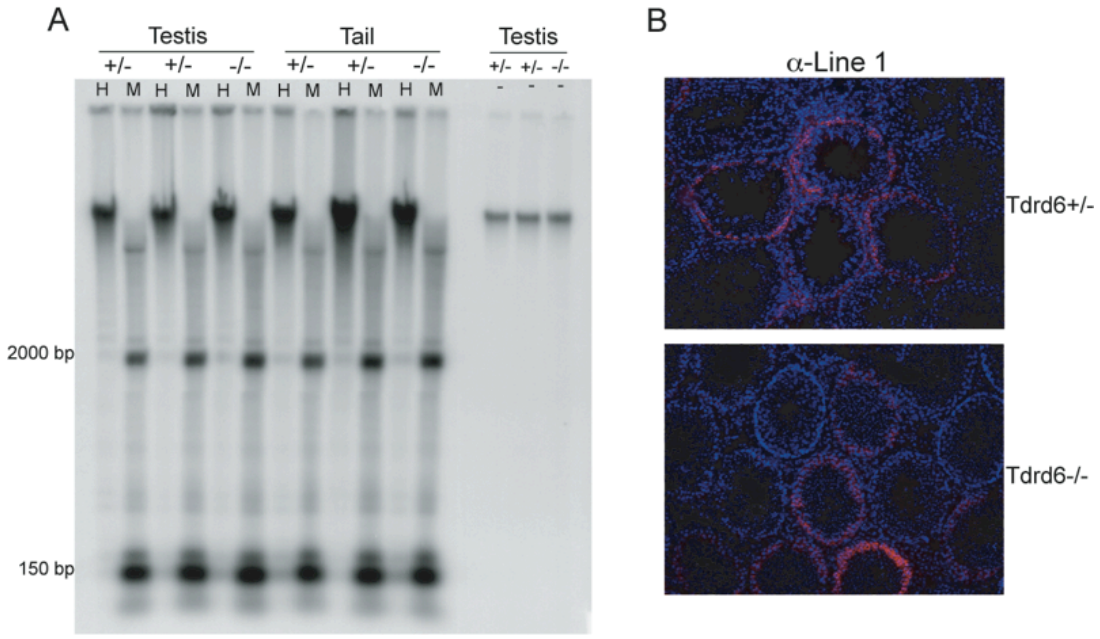

Figure 3.15: LINE-1 transposon methylation and expression in *Tdrd6*$^{-/-}$ mice. In figure (A) testis and tail DNA of *Tdrd6*$^{+/-}$ and *Tdrd6*$^{-/-}$ mice were analyzed by Southern Blotting after digestion with *Hpa*II and *Msp*I, using a radioactive labeled probe against *Line*-1. No difference in the methylation pattern in the promoter region of *Line-1* is observed. In (B) testes sections of *Tdrd6*$^{+/-}$ and *Tdrd6*$^{-/-}$ were stained with an α-LINE-1 antibody (red), nuclei are visualized with DAPI. No difference in LINE-1 expression is visible.

3.4. Gene expression analysis

3.4.1. MiRNA expression analysis

RNA and RNA-processing enzymes reside in the CBs, including proteins involved in the miRNA pathway. The abnormal architecture of the CB in *Tdrd6*$^{-/-}$ spermatids and the mislocalization of MVH, MIWI and MAEL may affect the regulation of miRNAs. For this purpose, total testis RNA of three pairs of 18-days-old *Tdrd6*$^{-/-}$ and *Tdrd6*$^{+/-}$ mice was isolated. MiRNA expression was analyzed using the miRXplore^{TM} Standard Service (Miltenyi Biotech GmbH), which are designed to detect only mature miRNAs and not miRNA precursor forms. This age was chosen to avoid any side effects due to apoptosis, because later (from 19 days of age) an increase in apoptotic cells was observed. Table 3.2 shows the result of all differently expressed mature miRNAs. Of the ~ 793 miRNAs known or predicted for mice (TarMir database), 54 miRNAs were found up-regulated (>1.5-fold), but only five are down-regulated (<0.7-fold). One interesting finding was, that one third of all differentially expressed mature miRNAs are located in different clusters on chromosome X. The X chromosome is known to be rich in miRNAs specific for testis in mice (Mishima et al. 2008). The largest cluster

of mis-regulated miRNA genes on Chr X is the so-called miRNA cluster-19 (miRc-19; miR-463, -470, -471, -472, -878-5P, -881*, -743b-3P, -883a-5P, -883b-3P). These miRNAs are either testis-specific or highly preferentially expressed in testis, suggesting that these miRNAs may have a role limited to spermatogenesis (Ro et al. 2007a).

Mmu-miR	GeneID	Fold	Genomic Locus	Mmu-miR - Cluster	Features	IG/IT
-29c	39300	4,3	1:196,863,234-196,863,828	-29b-2, -29c		IG
-30a*	39306	2,7	1:123,279,108-23,279,178			IG
-128	39210	1,8	1:130,098,938-130,099,007			IT
-466a-3P	38815	1,9	2: 10,388,571-10,438,791	-466a, -466b, -4667a, -669, -297a, -297c, -466b-1, -466d		IT
-466a-5P	35833	4,1				IT
-466b-3P	39949	2,3				IT
-466b-5P	38810	1,7				IT
-467a	38825	1,6				IT
-200a	38505	2,5	4:155,428,014-155,429,859	-200a, -200b, -429		IT
-200b	38723	2,5				IT
-30e*	39308	3,1	4:120,442,139-120,445,302	-30c-, 30e		IT
-34a*	39306	1,3	4:149,442,563-149,442,664			IG
-339-5P	39327	2,1	5:139,845,604-139,845,699			IT
-29b-1	38569	1,9	6: 31,012,660-31,013,093	-29a, -29b-1	CpG,TSS	IT
-489	38535	2,4	6: 3,671,301-3,672,003	-489, -653		IG
-148a	35857	1,9	6: 51,219,811-51,219,909		CpG,TSS	IG
-202	38506	2,8	7:147,143,588-147,143,659		TSS	IG
-140	35847	2,4	8:110,075,144-110,075,213			IT
-191	39255	0,7	9:108,470,650-108,471,192	-191, 425	CpG	IG
-34c*	39350	1,8	9: 50,911,139-50,911,750	-34a, -34c	CpG,TSS	IG
-125b	35830	0,7	9: 41,390,009-41,390,085		TSS	IT
-451	39370	1,6	11: 77,886,507-77,886,743	-144, -451		IG
-497	35866	3,0	11: 70,048,219-70,048,637	-195, -497		IG
-21	35883	2,3	11: 86,397,569-86,397,660			IT
-152	35861	2,0	11: 96,711,707-96,711,779		CpG,TSS	IT
-301a	38983	1,6	11: 86,926,506-86,926,591		CpG.TSS	IT
-379	38528	2,0	12:110,947,270-110,982,005	-134, -154, -299, -300, -323, -329, -369, -377,-376a, -376b, -376c, -379, -380, -381, -382, -409, -410, -411 -412, -453,-476, -485, -487b, -494, -495, -496, -539,-541, -543, -544,-654, -666, -667, -668, -679, -758		IG
-487b	38377	1,8				IG
-494	39394	2,5				IG
-203	38328	2,1	12:113,369,091-113,369,166		CpG,TSS	IG
-342-3P	38991	0,6	12:109,896,830-109,896,928			IT
-7a	38644	2,8	13: 58,494,140-58,494,247			IG
-15a	35864	1,8	14: 62,250,717-62,250,947	-15a, -16-1		IG
-17*	38715	1,9	14:115,442,893-115,443,728	-17, -18a, -19a, -19b-1, -20a, -92a-1	CpG,TSS	IG
-19a	38326	2,1			CpG,TSS	IG
-125a	39208	0,6	17: 17,967,152-17,967,843	Let-7e, -99b, -125a	TSS	IG
-204	38727	0,7	19: 22,825,095-22,825,162			IT
-101b	38961	2,8	19: 29,209,769-29,209,865			IT
-362-3P	38773	2,5	X: 6,814,809-6,825,623	-188, -362, -500, -501, -532		IT
-18b	38720	1,7	X: 50,094,870-50,095,744	-18, -19b, -20b, 92a, -106a, -363	TSS	IG
-20b	38708	2,2			TSS	IG
-106a	38708	1,5			TSS	IG
-201	38725	2,2	X: 65,241,271-65,241,626	-201, -547		IG
-322	35904	1,7	X: 50,401,174-50,407,526	-322, -351, -450a, -450b, -503, -542	CpG,TSS	IG
-351	38995	2,7			CpG,TSS	IG
-503	38849	2,2			CpG,TSS	IG
-463	38807	2,9	X: 64,029,932-63,067,200	-463, -470, -471, -472, -473a, -473b, -880, -881, -883a, -883b, -871, -878, -889		IG
-470	38833	1,5				IG
-471	38834	3,3				IG
-472	38683	3,7				IG
-878-5P	38687	2,0				IG
-881*	40027	2,3				IG
-743b-3P	38681	2,1				IG
-883a-5P	40153	3,4				IG
-883b-3P	38698	1,8				IG
-465a-5P	38533	4,1	X: 64,079,130-64,092,300	-465a, -465b-1, -465b-2, -465c-1, -465c-2		IG
-465b-5P	38810	1,7				IG
-361	35910	1,5	X:110,188,433-110,188,502			IT
-805	39885	2,0	MT:16,115-16,209			IG

Table 3.2: **Differentially expressed miRNAs in testes of 18 days old *Tdrd6*$^{-/-}$ mice**. The genomic loci and feature sets used to annotate miRNAs are available through the miRBase database. (CpG, CpG island; TSS, transcriptional start sites; IG, intergenic; IT, intronic; *, minor miR* sequences). Highlighted in grey are affected miRNA cluster.

To validate the microarray data we carried out quantitative real time PCR (qRT-PCR) for six randomly chosen mature miRNAs, five up-regulated (miR-29b, -29c, -34a, -34c and -322) and one down-regulated (miR-342) referred to the microarray results. These six miRNAs are known to be expressed in testes of mice (Landgraf et al. 2007). To evaluate whether up-regulation of such miRNAs occur on the level of precursors or mature miRNAs, the pri- and pre-miRNAs, along with the mature forms of three miRNAs (miR-29b, -29c, -34a), were analyzed using primers for real time PCR, which are specific for each form (figure 3.16). A significant increase of all investigated precursors was measured. For the mature miRNAs the referred tendency of up- or down-regulation was confirmed to be significant. Since we could not only prove changes in expression of mature miRNA, but also in expression of the precursors in testes of *Tdrd6*$^{-/-}$ mice, we assume that TDRD6 is important for transcriptional regulation of some miRNAs either due to direct influence – but this is unlikely, since Tdrd6 is not visible in the nucleus – or more likely due to an indirect influence, e.g. a common transcriptional regulation of miRNA genes through transcription factors. Promoter analyses of all investigated mis-regulated miRNA genes in the *Tdrd6*-deficient mice, did not reveal any common features, like transcription factors, transcriptional start sites or CpG islands. Furthermore, no similarities were found between all mis-regulated miRNAs in respect to their localization either intergenic or intronic in the genome (miR-Base database).

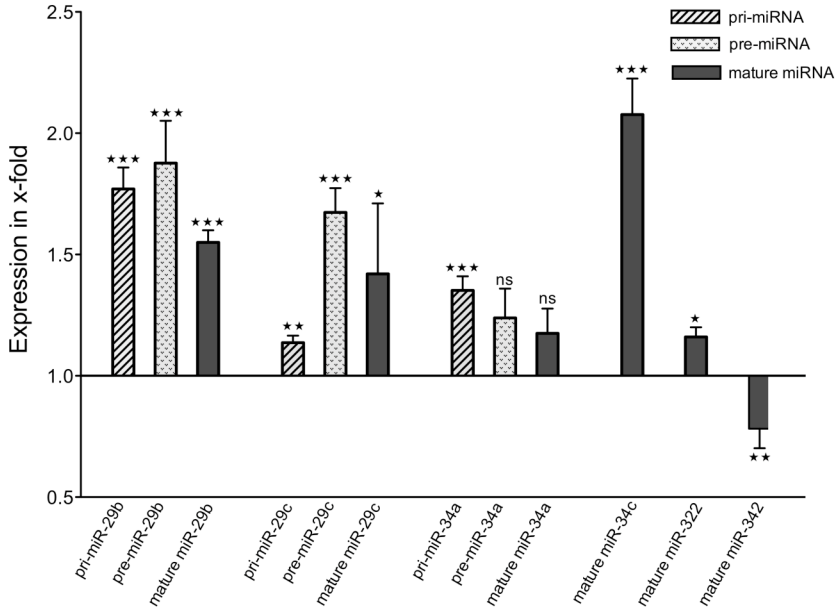

Figure 3.16: **Differentially expressed precursors and mature miRNAs in testes of *Tdrd6*$^{-/-}$ mice.** Analysis was performed with total testis RNA from 18 days old *Tdrd6*$^{+/-}$ and *Tdrd6*$^{-/-}$ mice. Precursors (Pri- and pre-miRNAs) as well as mature miRNAs were analyzed. The values for the *Tdrd6*$^{+/-}$ control were set to 1.0 and the respective increase or decrease in *Tdrd6*$^{-/-}$ mice are represented as mean +/- SEM (standard error mean). (*** P value <0.001, ** P value 0.001 to 0.01, * P value 0.01 to 0.05; ns, not significant P value >0.05).

Targets of miRNAs can be achieved due to analysis of sequence homology between mature miRNA and mRNA. These are just hypothetical predictions, and false positive hits are possible. The analysis was performed using the TargetScanS database, which predicts biological targets of miRNAs by searching for the presence of conserved sites that match the seed region of each miRNA. For each investigated miRNA more than 500 hypothetical target mRNAs are found. Several families of miRNAs are aberrantly regulated, including the miR-29, miR-34, and miR-463 families. The predicted targets of these miRNAs generally include many testis-specific RNAs, as well as RNA-processing enzymes like DICER (miR-29). The miR-463 hypothetically targets TDRD6 itself, and the absence of TDRD6 may cause accumulation of this miRNA. Another finding was that miR-34a, which is up-regulated in the *Tdrd6*$^{-/-}$ mouse could theoretically target CUE domain containing protein 1 (Cuedc1; Chr 11), which was found 4-fold down-regulated in our mRNA microarray analyses. MiRNAs like the miR-34 family are known to play a role in tumorigenesis, by directly binding to the p53 tumour suppressor gene (He et al. 2007). The miR-29 family members were described to directly target DNA-modifying enzymes like DNA methyltransferases 3 a and b (Fabbri et al. 2007), which together can influence tumour progression by modifying methylation patterns.

3.4.2. Whole mouse genome analysis

The chromatoid body is a structure where mRNAs are stored and processed. In *Tdrd6*-deficient mice a disrupted CB was observed, which cannot recruit specific proteins. Since the CB seems to be not fully functional we decided to investigate, if an overall change in mRNA expression is detectable. We isolated total testis RNA from 18-days-old *Tdrd6*$^{-/-}$, *Tdrd6*$^{+/-}$ and *Tdrd6*$^{+/+}$ mice and analyzed gene expression with the One-Color Microarray-Based Gene Expression Analysis System (Agilent 2007). With a threshold of 2-fold up- and down-regulation and a P-value of 0.05, 109 mRNAs were found differently expressed. Of these mRNAs, 59 encode known proteins, 45 encode undetermined cDNAs (Riken consortium library), and 5 cDNAs are unknown at all. Of all differently expressed mRNAs, 69 genes are up-regulated and 40 genes are down-regulated (table 3.3). The genes are distributed all over the genome, but interestingly 36 % of all genes are located to the centromer-proximal end of Chromosome 8 (Chr 8) and 11 % are located to the distal end of chromosome

1(figure 3.17). Within the 40 genes located on Chr 8, 19 are protein-coding cDNAs, but the remaining 21 genes encode unknown cDNAs listed in the Riken consortium library (www.brc.riken.go.jp/lab/dna/en/resourceen.html).

Accession no.	x-fold up	x-fold down	Genomic locus	Name
A_51_P257613		2,25	1: 95,721,817 - 95,748,925	D-2-hydroxyglutarate dehydrogenase (D2hgdh) [NM_178882]
A_52_P546610		2,91	1: 99,717,672 - 99,992,090	Peptidylglycine alpha-amidating monooxygenase (Pam) [NM_013626]
A_51_P471386	2,23		1: 106,665,396 - 106,892,058	Cadherin 20 (Cdh20) [NM_011800]
A_52_P516473	2,01		1: 120,524,522 - 120,581,744	Mus musculus adult male kidney cDNA, RikF530007A16 [AK143960]
A_52_P243992	2,11		1: 122,518,317 - 122,586,980	Mus musculus 10 days embryo whole body cDNA, Rik2610027F03 [AK011565]
A_51_P222280		2	1: 133,151,179 - 133,176,140	Inhibitor of kappaB kinase epsilon (Ikbke) [NM_019777]
A_51_P316661	7,19		1: 135,247,087 - 135,256,902	Renin 1 structural (Ren1) [NM_031192]
A_52_P192265		3,14	1: 135,247,214 - 135,256,900	Renin 2 tandem duplication of Ren1 (Ren2) [NM_031193]
A_52_P165824	2,05		1: 135,260,411 - 135,276,892	Ethanolamine kinase 2 (Etnk2) [NM_175443]
A_52_P616544		6,59	1: 137,006,988 - 137,010,716	Protein tyrosine phosphatase receptor type V (Ptprv) [NM_007955]
A_51_P150653		2,55	1: 137,006,988 - 137,010,716	Protein tyrosine phosphatase receptor type V (Ptprv) [NM_007955]
A_51_P103541	2,13		1: 137,949,361 - 138,016,399	Dihydropyridine sensitive skeletal muscle calcium channel (Cacna1s) [L06234]
A_52_P298112	2,35		2: 17,649,013 - 17,653,091	Mus musculus adult male pituitary gland cDNA, Rik5330423N20 [AK077332]
A_51_P451374		6,56	2: 76,208,069 - 76,221,822	Developmentally regulated RNA binding protein 1 (Drbp1) [NM_153405]
A_51_P255646	4,88		2: 86,285,196 - 86,286,137	Olfactory receptor 1065 (Olfr1065) [NM_146408]
A_52_P614777	2,53		3: 59,885,783 - 59,891,481	Succinate receptor 1 (Sucnr1), mRNA [NM_032400]
A_51_P440682	2,8		4: 122,536,290 - 122,563,300	CAP, adenylate cyclase-associated protein 1 (yeast) (Cap1) [NM_007598]
A_52_P658320	2,23		5: 108,870,073 - 108,877,910	Major facilitator superfamily domain containing 7 (Mfsd7) [NM_172883]
A_52_P25774	3,49		6: 27,225,121 - 28,084,545	Glutamate receptor, metabotropic 8 (Grm8) [NM_008174]
A_52_P374882	2,33		6: 29,010,220 - 29,023,876	Leptin (Lep) [NM_008493]
A_52_P568977		2,34	6: 88,674,702 - 88,716,702	Mus musculus adult male testis cDNA, Rik1700074K19 [AK006949]
A_52_P590535	2,3		6: 91,162,758 - 91,222,534	Fibulin 2 (Fbln2) [NM_007992]
A_51_P305979	2,06		7: 110,759,924 - 110,760,865	Olfactory receptor 620 (Olfr620) [NM_146812]
A_52_P672232		2,16	8: 3,538,783 - 3,540,361	Mus musculus cDNA clone IMAGE:3987110, partial cds. [BC020092]
A_51_P145662		3,69	8: 3,716,084 - 3,720,651	C-type lectin domain family 4, member g (Clec4g) [NM_029465]
A_52_P70381	2,5		8: 4,238,761 - 4,251,423	Mus musculus 10 days neonate skin cDNA, Rik4732455E07 [AK028772]
A_52_P730698	3,11		8: 4,332,259 - 4,334,807	Mus musculus adult retina cDNA, RikA930012B14 [AK044424]
A_52_P947377		6,94	8: 8,377,090 - 8,391,691	Mus musculus 7 days neonate cerebellum cDNA, RikA730008F11 [AK042586]
A_52_P448994	3,98		8: 11,245,002 - 11,245,605	Mus musculus 15 days embryo head cDNA, RikD930007H16 [AK086129]
A_52_P373251	2,47		8: 12,757,014 - 12,868,728	Mus musculus cDNA, RikM5C1054M05 [AK147497]
A_51_P361286	8,29		8: 18,846,279 - 18,884,413	1-acylglycerol-3-phosphate O-acyltransferase 5 (Agpat5) [NM_026792]
A_52_P578763		5,09	8: 22,194,739 - 22,195,667	Defensin, alpha 1 (Defa1) [NM_010031]
A_52_P307801		3,56	8: 22,235,000 - 22,275,000	Defensin related cryptdin, related sequence 2 (Defcr-rs2), mRNA [NM_007847]
A_51_P102081		3,37	8: 22,235,000 - 22,275,000	Defensin related cryptdin, related sequence 2 (Defcr-rs2), mRNA [NM_007847]
A_51_P377158		2,33	8: 22,235,000 - 22,275,000	Defensin related cryptdin, related sequence 10 (Defcr-rs10), mRNA [NM_007845]
A_52_P476535	3,9		8: 22,331,293 - 22,332,142	Defensin-related cryptdin 23 (Defcr23), mRNA [NM_001012307]
A_51_P467086		2,11	8: 22,427,122 - 22,427,971	Defensin related cryptdin 3 (Defcr3), mRNA [NM_007850]
A_52_P398018		4,27	8: 24,351,798 - 24,367,552	Mus musculus activated spleen cDNA, RikF830033L24 [AK089856]
A_51_P352296		2,17	8: 24,521,990 - 24,560,099	Secreted frizzled-related sequence protein 1 (Sfrp1) [NM_013834]
A_52_P577673	13,2		8: 27,187,044 - 27,189,849	Mus musculus 13 days embryo lung cDNA, RikD430019N09 [AK084963]
A_51_P300960		2,2	8: 32,260,787 - 32,272,345	Mus musculus cDNA sequence BC019943 (BC019943) [NM_144927]
A_51_P410900	3,79		8: 32,297,850 - 32,371,955	Fucosyltransferase 10 (Fut10) [NM_001012517]
A_52_P369761		2,25	8: 32,931,245 - 33,028,826	Mus musculus 0 day neonate cerebellum cDNA, RikC230011J18 [AK141037]
A_52_P369769		2,55	8: 32,947,675 - 33,028,826	Mus musculus 0 day neonate cerebellum cDNA, RikC230013P13 [AK048708]
A_52_P498492	5		8: 34,346,172 - 34,495,969	Werner syndrome homolog (Wrn) [NM_011721]
A_51_P202101	32,85		8: 34,841,021 - 34,841,344	Mus musculus adult male testis cDNA, Rik1700104B16 [AK018937]
A_52_P76104	16,18		8: 38,166,850 - 38,167,524	Mus musculus adult male testis, Rik4933404M01 [AV278908]
A_51_P236185	18,66		8: 40,194,244 - 40,195,861	Mus musculus adult male diencephalon cDNA, Rik9330142E06 [AK034021]
A_52_P763167		3,32	8: 41,446,342 - 41,449,492	Mus musculus adult male aorta and vein cDNA, RikA530095A18 [AK041257]
A_52_P609482	3,7		8: 41,633,626 - 41,635,533	Mus musculus 0 day neonate cerebellum cDNA, RikC230079M10 [AK048897]
A_52_P77764	3,19		8: 41,947,721 - 42,007423	Solute carrier family 7 member 2 (Slc7a2) [NM_007514]
A_52_P294510	6,68		8: 42,276,791 - 42,300,507	Fibrinogen-like protein 1 (Fgl1) [NM_145594]
A_51_P120688	2,077		8: 42,462,790 - 42,466,106	Mus musculus 15 days embryo head cDNA, RikD930046J11 [AK086706]
A_51_P267544		2,69	8: 42,482,813 - 42,502,428	FSHD region gene 1 (Frg1) [NM_013522]
A_52_P629849		48,38	8: 44,380,422 - 44,392,334	Zinc finger protein 42 (Zfp42) [NM_009556]
A_52_P117576	2,41		8: 47,702,645 - 47,725,042	Caspase 3 (Casp3) [NM_009810]
A_52_P68087	2,36		8: 48,072,279 - 48,180,249	Ectonucleotide pyrophosphatase/phosphodiesterase 6 (Enpp6) [NM_177304]
A_51_P132530	2,3		8: 48,909,836 - 48,910,829	Mus musculus adult male stomach cDNA, Rik2210404A22 [AK008821]
A_52_P351791	2,26		8: 72,142,768 - 72,149,444	Mus musculus 0 day neonate thymus cDNA, RikA430055D15 [AK079745]
A_52_P553859	2,38		8: 74,200,195 - 74,214,474	Tyrosine-protein kinase JAK3 (Janus kinase 3) (JAK-3) [TC1539197]
A_52_P835473		2,14	8: 91,562,636 - 91,565,980	Mus musculus 13 days embryo heart cDNA, RikD330014J04 [AK052259]
A_51_P157081	2,43		8: 109,643,010 - 109,643,792	Mus musculus adult male hippocampus cDNA, RikC630050I24 [AK021281]
A_52_P135282		2,04	8: 112,471,817 - 112,486,072	MARVEL (membrane-associating) domain containing 3 (Marveld3) [NM_212447]
A_52_P611783	4,3		9: 45,207,957 - 45,218,361	FXYD domain-containing ion transport regulator 2 (Fxyd2) [NM_052824]
A_52_P177021	2,07		9: 50,329,723 - 50,336,756	6-pyruvoyl-tetrahydropterin synthase (Pts) [NM_011220]
A_52_P488572	4,22		9: 110,523,641 - 110,526,897	Engulfment and cell motility 1, ced-12 homolog (Elmo1) [NM_080288]
A_52_P482055	2,04		X: 70,310,126 - 70,313,529	Paraneoplastic antigen MA3 (Pnma3) [NM_153169]
A_51_P292146	2,14		10: 7,924,551 - 8,238,623	Uronyl-2-sulfotransferase (Ust) [NM_177387]
A_51_P265374	2,03		10: 23,571,278 - 23,589,637	Vanin 3 (Vnn3) [NM_011979]
A_52_P673043		2,11	10: 114,515,699 - 114,622,078	Tryptophan hydroxylase 2 (Tph2) [NM_173391]
A_52_P907995	2,16		11: 75,556,521 - 75,558,910	Mus musculus 9 days embryo whole body cDNA, RikD030051F04 [AK083592]
A_51_P175667		2,72	11: 87,619,930 - 87,639,617	Lactoperoxidase (Lpo) [NM_080420]

A_51_P379409		3,98	11: 87,912,751 - 88,006,408	CUE domain containing 1 (Cuedc1) [NM_198013]
A_51_P324082		2,22	11: 98,014,028 - 98,054,607	Peroxisome proliferator activated receptor binding protein (Pparbp) [NM_013634]
A_52_P37517		2,01	11: 99,084,313 - 99,085,778	Mus musculus adult male thymus cDNA, Rik5830412H02 [AK017922]
A_52_P100156		2,12	11: 99,267,978 - 99,283,573	Keratin complex 1, acidic, gene 12 (Krt1-12) [NM_010661]
A_51_P489138	2,06		12: 77,681,475 - 77,811,534	Spectrin beta 1 (Spnb1) [NM_013675]
A_52_P682239	2,05		13: 8,202,124 - 8,206,010	Mus musculus 12 days embryo spinal ganglion cDNA, Rik130050D08 [AK051460]
A_52_P628546	3,18		13: 21,605,091 - 21,622,989	Zinc finger protein 192 (Zfp192) [NM_139141]
A_51_P505521	2,15		13: 22,132,492 - 22,133,189	Mus musculus cDNA clone UI-M-CC0-ayb-f-07-0-UI 5'. [BF467941]
A_52_P67892	2,46		13: 23,710,085 - 23,712,947	Mus musculus, clone IMAGE:3465495 [BC032927]
A_52_P660047	2,52		13: 64,350,054 - 64,369,453	Mus musculus adult male kidney cDNA, RikF530007I15 [AK143964]
A_51_P470989		5,1	13: 120,217,407 - 120,249,127	Polyadenylate binding protein-interacting protein 1 (Paip1) [NM_145457]
A_52_P212284		3,4	13: 120,217,407 - 120,249,127	Polyadenylate binding protein-interacting protein 1 (Paip1) [NM_145457]
A_52_P603540		2,41	14: 6,956,283 - 6,964,644	Mus musculus Rik4930555G01 [NM_175393]
A_51_P305239	2		14: 25,436,790 - 25,440,915	Mus musculus adult male testis cDNA, Rik4931403M11 [AK016429]
A_52_P334499	2,08		16: 58,995,230 - 59,000,442	Olfactory receptor 183 (Olfr183) [NM_146485]
A_52_P533250		2,5	16: 73,683,735 - 73,684,194	Mus musculus Rik1700041G16 [NM_175196]
A_52_P314299	2,21		16: 91,465,349 - 91,470,366	Mus musculus adult male hypothalamus cDNA, RikA230049K01 [AK038602]
A_52_P236288	5,32		16: 93,343,992 - 93,353,434	Mus musculus 10 day old male pancreas cDNA, Rik1810053B23 [AK007854]
A_52_P447375		13,15	16: 93,608,082 - 93,610,594	Carbonyl reductase 1 (Cbr1) [NM_007620]
A_52_P300533	2,09		16: 93,792,395 - 93,795,133	Mus musculus adult male tongue cDNA, Rik2310043M15 [AK009785]
A_51_P236483		2,64	17: 24,035,699 - 24,056,407	Mus musculus cDNA sequence BC005655 [NM_145386]
A_51_P201672		15,466	17: 25,073,247 - 25,074,281	Mus musculus adult male testis cDNA, Rik1700009P10 [AK005803]
A_52_P680761		27,41	17: 43,752,288 - 43,767,248	Mus musculus tudor domain containing 6 (Tdrd6) [NM_198418]
A_51_P320340	2,05		17: 47,047,434 - 47,061,875	Mus musculus retinal degeneration (Rds), mRNA [NM_008938]
A_52_P405655	2,51		18: 81,163,115 - 81,183,317	Mus musculus sal-like 3 (Drosophila) (Sall3) [NM_178280]
A_52_P159365	3,61		18: 81,163,115 - 81,183,317	Mus musculus sal-like 3 (Drosophila) (Sall3) [NM_178280]
A_52_P843410	2,22		19: 35,098,034 - 35,100,114	Mus musculus 16 days neonate thymus cDNA, RikA130049N17 [AK037788]
A_51_P277139	8,22		19: 50,614,297 - 50,615,375	Mus musculus adult male testis cDNA, Rik4933436E20 [AK017078]
A_52_P119039	2,03		not placed	Mus musculus 15 days embryo male testis cDNA, Rik8030402P03 [AK078743]
A_52_P125897	2,12		not placed	Mus musculus cDNA clone IMAGE:5039788 [BI107100]
A_52_P597818	2,89		not placed	Mus musculus cDNA sequence AF067063 [NM_001001449]
A_52_P129428	5,13		not placed	Mus musculus 16 days embryo head cDNA, RikC130058L18 [AK048420]
A_51_P317562	2,07			Unknown
A_52_P14506	2,12			Unknown
A_52_P616932	2,23			Unknown
A_52_P1141541	2,31			Unknown
A_51_P338963	2,61			Unknown

Table 3.3: Differentially expressed mRNAs in testes of 18 days old *Tdrd6*$^{-/-}$ mice are listed, sorted by their genomic localization. The accession numbers, fold change and genomic loci are listed. Highlighted in grey are all mis-regulated genes on chromosome 1 and 8.

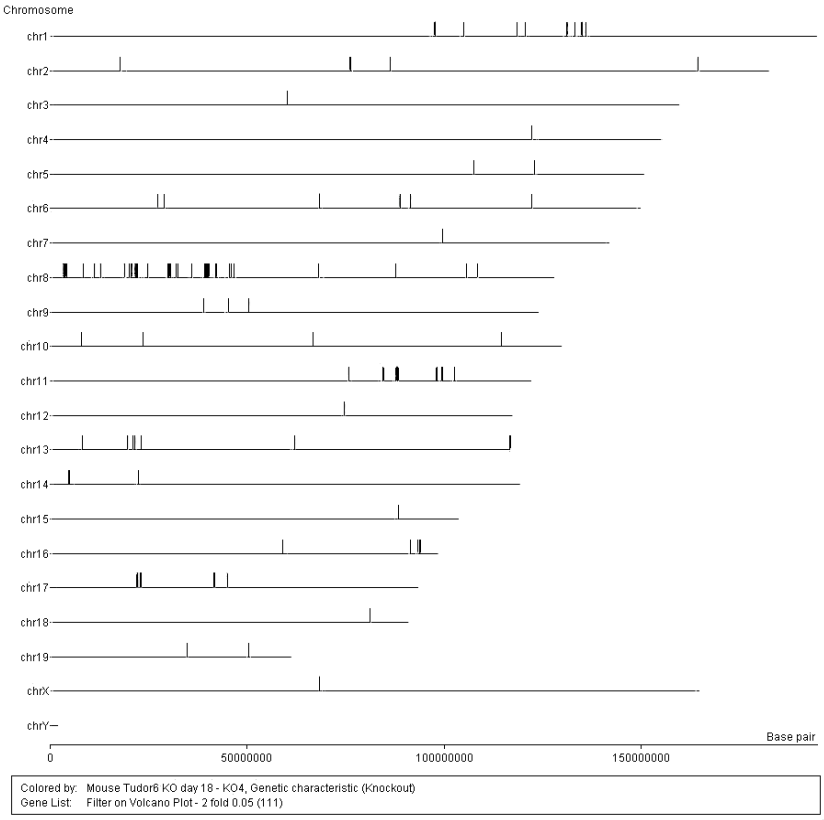

Figure 3.17: Genomic distribution of all differentially expressed genes in the testes of 18-days-old *Tdrd6*$^{-/-}$ mice. 36 % of the genes are located on Chr 8, and 11 % are located on Chr 1. The threshold was set to 2-fold up- or down-regulated and the P-value was set to 0.05.

Randomly four genes from chromosome 8 were chosen; three of the most up-regulated genes (*Fgl1*, *Rik4933404M01* and *Rik1700104B16*) and the most down-regulated gene (*Zfp42*), and the tendency of their mis-regulation in *Tdrd6*$^{-/-}$ mice was significantly confirmed by quantitative real time PCR (figure 3.18).

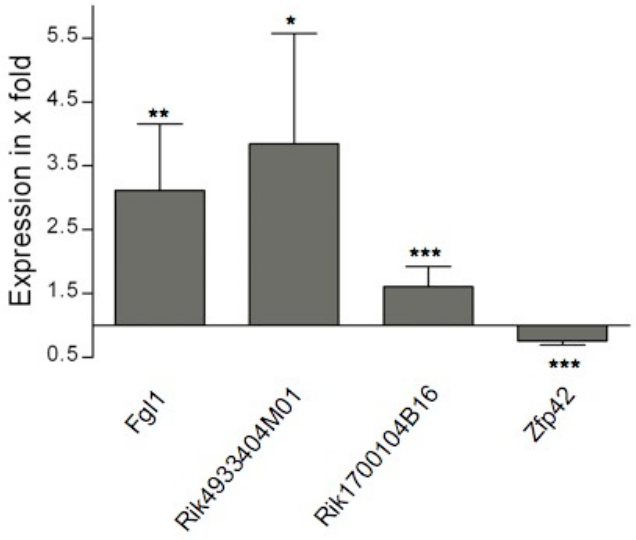

Figure 3.18: Differentially expressed genes in testes of *Tdrd6*$^{-/-}$ mice. Analysis was performed with total testis RNA from 18 days old *Tdrd6*$^{+/-}$ and *Tdrd6*$^{-/-}$ mice. The values for the *Tdrd6*$^{+/-}$ control were set to 1.0 and the respective increase or decrease in *Tdrd6*$^{-/-}$ mice are represented as mean +/- SEM (standard error mean). (*** P value <0.001, ** P value 0.001 to 0.01, * P value 0.01 to 0.05; ns, not significant P value >0.05).

Some of the mis-regulated genes play roles in carcinogenesis. Zinc finger protein 42 (ZFP42), also called Rex-1, is a transcription factor responsible for stem cell potency, which was described to be strongly expressed in human spermatocytic seminomas (Jessberger 2008; Kristensen et al. 2008). *Zfp42* is 48-fold down-regulated in *Tdrd6*-deficient mice. Fibrinogen-like 1 (FGL1) is a liver-specific gene that is frequently down-regulated in hepatocellular carcinoma (Yan et al. 2004). It is described as a tumour-suppressor gene on the short arm of human Chr 8. The mouse *Fgl1* mRNA is 6,7-fold up-regulated in the *Tdrd6*-deficient mice. Inhibitor of kappaB kinase epsilon (IKBKE) has been recently identified as an oncogene, which is frequently overexpressed in ovarian cancer cell lines (Guo et al. 2009). *Ikbke* is localized to the long arm of Chr (1q12) and is 2-fold down-regulated in the *Tdrd6*$^{-/-}$ mice.

The observation that 36 % of all mis-regulated genes are located on Chromosome 8 and 11 % on chromosome 1 was very surprising, since nothing is known about the effect of TDRD6 on particular chromosomes. TDRD6 has not been seen in the nuclei of cells, and thus a direct effect on regulation of Chr 1 or Chr 8 is unlikely. An indirect influence of TDRD6 would be possible through common promoter features all of mis-regulated genes, e.g. transcription factors (TF). To analyze putative TF of all differently expressed genes, bioinformatic analyses were done using the MAPPER database. This program predicts all hypothetical TF binding sites (TFBSs) in the promoter region of certain genes by comparing sequence homology.

We analyzed 25 mis-regulated genes, as well as five control genes, which are not on Chr 8 (*Tdrd6,* Chr 17; *Pax4*, Chr 6; *Cldn14*, Chr 16) or are localized to the same region of Chr 8, but are not mis-regulated (*Tusc3, Rnf122*) in the microarray analyses of the *Tdrd6*$^{-/-}$ mice. The promoter region within 2000 bp upstream of the start codon of each gene was analyzed. For all genes more than 600 predicted binding sites for transcription factors were found, most of the TF showed more than one hit. All mis-regulated genes had 35 putative transcription factors in common (Table 3.4). The aim was to identify transcription factors that regulate only the differently expressed genes in the *Tdrd6*$^{-/-}$ mice. When comparing the results of the TF binding site analyses from the mis-regulated genes with the control genes, no transcription factor was found that was specific for the mis-regulated genes. Three transcription factors (Freac-4, Nrf2 and SU_h) revealed binding sites in the promoter region 2000 bp upstream of the start codon in all 25 mis-regulated genes, but were missing in the promoter region of one of the control genes. So far, we cannot conclude anything about possible regulation through any of these transcription factors, since all of them are present in at least 4 of 5 control genes.

Trancription factor	mis-regulated genes	Ctrl gene Tusc3	Ctrl gene Rnf43	Ctrl gene Rnf122	Ctrl gene Pax4	Ctrl gene Cldn14
AML1	√	√	√	√	√	√
Androgen	√	√	√	√	√	√
Athb-1	√	√	√	√	√	√
Broad-compl_1	√	√	√	√	√	√
c-ETS	√	√	√	√	√	√
COUP-TF	√	√	√	√	√	√
Dof 2	√	√	√	√	√	√
Dof 3	√	√	√	√	√	√
Dorsal_2	√	√	√	√	√	√
Evi-1	√	√	√	√	√	√
FREAC-4	√	√	√	√	–	√
HFH-1	√	√	√	√	√	√
HFH-2	√	√	√	√	√	√
HMG-IY	√	√	√	√	√	√
IRF-2	√	√	√	√	√	√
MEF2	√	√	√	√	√	√
Myc-Max	√	√	√	√	√	√
MZF_5-13	√	√	√	√	√	√
NF-1	√	√	√	√	√	√
Nkx	√	√	√	√	√	√
Nrf2	√	–	√	√	√	√
Pax-2	√	√	√	√	√	√
PPAR gamma	√	√	√	√	√	√
RORalfa-1	√	√	√	√	√	√
RREB-1	√	√	√	√	√	√
Sox-17	√	√	√	√	√	√
Sox-5	√	√	√	√	√	√
Sox-9	√	√	√	√	√	√
SPI-B	√	√	√	√	√	√
Spz1	√	√	√	√	√	√
SQUA	√	√	√	√	√	√
SRY	√	√	√	√	√	√
Staf	√	√	√	√	√	√
SU-h	√	–	√	√	√	√
Thing1-E47	√	√	√	√	√	√

Table 3.4: Common putative transcription factor binding sites of 25 mis-regulated genes of the *Tdrd6*$^{-/-}$ mice mRNA analyses and their abundance in 5 control genes. As a control, two not mis-regulated genes from the same centromer-proximal region on Chr 8 were chosen (*Tusc3, Rnf122*) and three genes from other chromosomes. Three TF are highlighted in grey because they do not bear hypothetical binding sites in one of the control genes.

Using the miRDB database, one can search for hypothetical miRNAs, which can bind to mRNAs of interest. Analyses for 52 known proteins, which are mis-regulated in the *Tdrd6*$^{-/-}$ mice, were performed. Unknown mis-regulated cDNAs from the microarray analyses could not be investigated by this database. Table 3.5 shows all investigated mis-regulated mRNAs in the *Tdrd6*-deficient mice, which found complementary hits in the database analyses. MiRNAs are listed, which can hypothetically target these mRNAs, and are also mis-regulated in the *Tdrd6*$^{-/-}$ mice. For 16 mRNAs corresponding miRNAs could be found.

Probably not all miRNAs are indeed responsible for the mis-regulation of the listed mRNAs *in vivo*, but these are first hints of possible regulations, which have to be investigated thoroughly.

mRNA	miRNA (mmu-)
Agpat5	miR-470
Cdh20	miR-30e, miR-200b
Elmo1	miR-742
Fbln2	miR-128
Fgl1	miR-26b
Fut10	miR-494, miR-712
Lep	miR-200a
Lpo	miR-467a
Marveld3	miR-19a
Pam	miR-743b, miR-881
Sall3	miR-301a
Sfrp1	miR-466b-3-3p
Slc7a2	miR-15a, miR-322, miR-466a-3p, miR-466b-3-3p, miR-497
Wrn	miR-203, miR-204
Zfp42	miR-465a-5p, miR-465b-5p
Zfp192	miR-19a, miR-83b-3p, miR-128, miR-140, miR-301a, miR-203, miR-351, miR-466a-3p, miR-466b-3-3p, 743b-3p

Table 3.5: **Database analyses using miRDB database**. Analyses revealed hypothetical matches between differently expressed mRNAs and mis-regulated miRNAs in *Tdrd6*$^{-/-}$ mice.

4. Discussion

As described previously (Vasileva et al. 2009), TDRD6 is a male germ cell specific protein and two different isoforms are expressed. The 250 kDa isoform is expressed in spermatocytes, the smaller isoform (230 kDa) mainly in round spermatids and localizes to the chromatoid body. Due to sequence analysis we hypothesize, that TDRD6 gets cleaved by Caspase I at the C-terminal end. So far, we could confirm that the cleavage takes place at the C-terminus, but still no details about the process of cleavage itself or the biological purpose are known. One interesting finding by our group is, that not only the full length TDRD6, but also a deletion mutant, where the approximately 20 kDa C-terminal end is missing, interact in direct *in vitro* protein interaction experiments with MILI and MIWI (Vasileva et al. 2009). This leads to the hypothesis, that both forms may affect MILI and MIWI localization and function.

The newly generated *Tdrd6*-deficient mice are normal, healthy mice, except their severe defects in spermatogenesis. Due to the absence of mature sperm, the mice are sterile. Since TDRD6 is not expressed in female mice, females do not show any abnormalities. The increase in apoptotic cells, which was observed in the first wave of spermatogenesis around day 19, is most probably due to overall changes in mRNA and miRNA expression patterns in the *Tdrd6*-deficient mice.

The *Tdrd6*$^{-/-}$ germ cells apparently develop normal until the transition from round to elongated spermatids, where an arrest between step 12 and 13 occurs. Due to defects in the chromatoid body assembly, the cells cannot go further in their maturation process. Chromatoid bodies in *Tdrd6*$^{-/-}$ mice are diffuse, disrupted and less condensed than their counterpart in wild-type mice. *Tdrd6*$^{-/-}$ CBs are in the same close proximity to the nuclear membrane and do not differ in their total size. But their interior is largely missing, and only a “ghost”-like structure remains. CBs exhibit defects in recruiting proteins, which are known to localize to this compartment. In *Tdrd6*$^{-/-}$ testis sections, proteins like MVH, MIWI and MAEL are expressed, but do not localize to the CB in round spermatids, which leads most probably to the disrupted appearance. We (Vasileva et al. 2009) and others (Hosokawa et al. 2007) showed that TDRD6 directly interacts with CB proteins like MVH, MILI and MIWI, and has most probably a role in building complexes and scaffolds. Tudor domain proteins are known to be involved in scaffolding through their tudor domains (Hirose et al. 2000; Hosokawa et al. 2007; Skorokhod et al. 2008). Since in the *Tdrd6*$^{-/-}$ mice all seven

tudor domains of TDRD6 are deleted, it is not unexpected, that *Tdrd6*$^{-/-}$ spermatids are not able to assemble the chromatoid body correctly.

In the literature (Ventela et al. 2003) it was described, that the chromatoid body moves within the cell, as well as through cytoplasmic bridges between spermatids. It would be interesting to investigate, if the CBs in the *Tdrd6*$^{-/-}$ spermatids are still able to move or if they are immobile due to their disrupted phenotype.

Chromatoid bodies play a role in extensive posttranscriptional storing and processing of mRNAs in male germ cells, due to involvement of small RNAs like microRNAs (miRNAs) and Piwi-interacting RNAs (piRNAs) (Kotaja and Sassone-Corsi 2007). Since in *Tdrd6*$^{-/-}$ mice the CB is not completely functional we investigated, whether miRNAs in testes show an altered expression profile. Indeed, approximately 10 % of all known miRNAs in mice were shown to be differently expressed in testes of *Tdrd6*$^{-/-}$ mice, with most of the miRNAs up-regulated. Since we observed an up-regulation of microRNA precursors as well, we can conclude, that transcription of miRNAs directly is affected.

An interesting question is, if miRNA precursor can be exported to the CB. Nothing is known, if the precursors remain in the nucleus, or are transported to the cytoplasm of the cell by mistake. So far, we analyzed only the expression of mature miRNAs from total testes RNA. Further analyses, e.g. *in situ* hybridization using probes for specific miRNAs, would be helpful to get information about the localization of mature miRNAs. Not only the mature transcripts of three investigated miRNAs are up-regulated, but also the corresponding precursors. An assumption would be, that TDRD6 plays an unexpected direct role in transcriptional regulation of miRNA gene expression, but since TDRD6 has not been seen in nuclei of cells, it is more likely due to an indirect effect of TDRD6, probably through a common transcriptional regulation by transcription factors (TFs). One hypothesis would be, that the responsible TFs are mis-regulated because of the disrupted CB itself. Pri-miRNAs are typically transcribed by RNA polymerase II or III and have promoter elements that are similar to those of protein-coding genes, a TATA box, CpG islands and a transcriptional start site (Cui et al. 2009). Promoter analyses of all investigated mis-regulated miRNA genes in the *Tdrd6*-deficient mice, did not reveal any common features, like transcription factors, transcriptional start sites or CpG islands. Furthermore, no similarities were found between all mis-regulated miRNAs in respect to their localization either intergenic or intronic in the genome. Since these analyses

were done with bioinformatic databases, which work on the basis of sequence homology, we cannot conclude about the real situation in the cell and possible common features, which are not detected by databases.

MiRNA genes lie in cluster of several genes on the chromosomes. Interestingly, not all miRNAs from one cluster are differently expressed. For example, only 9 of 13 miRNAs from one cluster on chromosome X, and only 3 of 8 miRNAs from a cluster of Chr 2, are up-regulated. The remaining miRNAs of these clusters are not affected. This supports either the hypothesis that miRNA genes within one cluster can be differently expressed (Song and Wang 2008), or the remaining miRNAs were not detected by any reason during the microarray analyses. One third of all mis-regulated miRNAs in *Tdrd6*$^{-/-}$ mice are located on Chr X. This chromosome is known to be rich in miRNAs specific for male germ cells, 19 % of all known mouse testis miRNAs are located to this chromosome (Ro et al. 2007b).

Through database analyses hypothetical targets can be predicted due to sequence homology between mature miRNA and mRNA. For each investigated miRNA more than 500 hypothetical target mRNAs are predicted. Several families of miRNAs are aberrantly regulated, including the miR-29, miR-34, and miR-463 families. The predicted targets of these miRNAs generally include many testis-specific RNAs. Interesting mRNA candidates could be investigated e.g. by immunoblotting, if the according protein is aberrantly expressed in the *Tdrd6*$^{-/-}$ mouse.

Vice versa, when analysing the mis-regulated mRNAs of the *Tdrd6*-deficient mouse for hypothetical sequence homology to all differently expressed miRNAs, matches for 16 mRNAs could be found. All listed miRNAs are up-regulated in the *Tdrd6*-deficient mouse. If a mature miRNA were more abundant in a cell, the corresponding target would be down-regulated. But some of the listed mRNAs are up-regulated in the *Tdrd6*$^{-/-}$ mouse (*Agpat5, Cdh20, Elmo1, Fbln2, Fgl1, Fut10, Lep, Sall3, Slc7a2, Wrn and Zfp192*). We have to take in consideration, that these results are just theoretically, based on sequence homology. Probably not all miRNAs are indeed responsible for the mis-regulation of the listed mRNAs *in vivo*, but these are first hints of possible regulations.

In the *Tdrd6*-deficient mouse, 36 % of all differently expressed genes are located in the centromer-proximal region of chromosome 8, and 11 % of the genes on the distal end of chromosome 1. Nothing is known so far about TDRD6 and its possible role in transcriptional regulation of specific chromosomes. Since it has not been seen in the nucleus itself, there is likely some indirect influence of TDRD6. One control experiment would be to investigate if the *Tdrd6*$^{-/-}$ mice exhibit rearrangement on Chr 1 or Chr 8 due to some undesirable effects. Chr 8 is a chromosome in the mouse genome where rearrangements seem to occur most frequently. Chr 8 trisomy is one of the most frequent abnormalities occurring in ES cell lines (Liu et al. 1997), and pericentric inversions have been reported (Ashley et al. 1993). A large repeated region has been identified in laboratory strains of mice, which comprises 60 to 80 copies of a partially characterized element. Most of these copies are clustered in the pericentromeric region of mouse Chr 8 (Boyle and Ward 1992).

To rule out the possibility of unspecific effects of chromosomal rearrangements, one has to analyze, if rearrangement occurred in the embryonic stem cells, due to some unknown reasons. One possible method to analyze the chromosomal structure in *Tdrd6*$^{-/-}$ mice is fluorescence *in situ* hybridization (FISH), using probes for specific regions on Chr 1 and 8. If the chromosomal structure of all *Tdrd6* progenies would be normal like in wild-type mice, one could conclude, that the phenotype of mis-regulated genes on Chr 1 and 8 is indeed due to the disruption of *Tdrd6*. One argument against the hypothesis of rearrangement in the ES cell clone is, that the obtained chimeras were crossed with different wild-type mice and within the mouse colony for more than five generations, before microarray analyses were done. In this analyses *Tdrd6*$^{+/-}$ and *Tdrd6*$^{-/-}$ mice from different breeding pairs were investigated and only the *Tdrd6*-deficient mice showed the “chromosome 1 and 8” phenotypes. Thus, it is more likely that this phenotype is indeed caused by the disruption of the *Tdrd6* gene.

One possible mechanism of mis-regulation of all genes on both chromosomes would be through common transcriptional regulations. Promoter analyses considering their transcription factor binding sites (TFBS) of 25 mis-regulated genes were performed, and 35 common transcription factors were found. When comparing the results of the TF binding site analyses from the mis-regulated genes with the control genes, no transcription factor was found that was specific for the mis-regulated genes. So far, we cannot conclude a mechanism of common transcriptional regulation of the

differently expressed genes in the *Tdrd6*-deficient mice. Further analyses have to be done, e.g. analyses of the expression pattern of certain transcription factors in the *Tdrd6*$^{-/-}$ mice. Chromatin-Immunoprecipitation (ChIP) would give information about direct binding of TFs to the promoter region of mis-regulated genes in the *Tdrd6*-deficient mice.

The affected regions on Chr 1 and 8 in the *Tdrd6*$^{-/-}$ mouse are orthologous to regions on the human chromosomes 1 and 2, as well as the short arm of the human chromosome 8 (Figure 4.1).

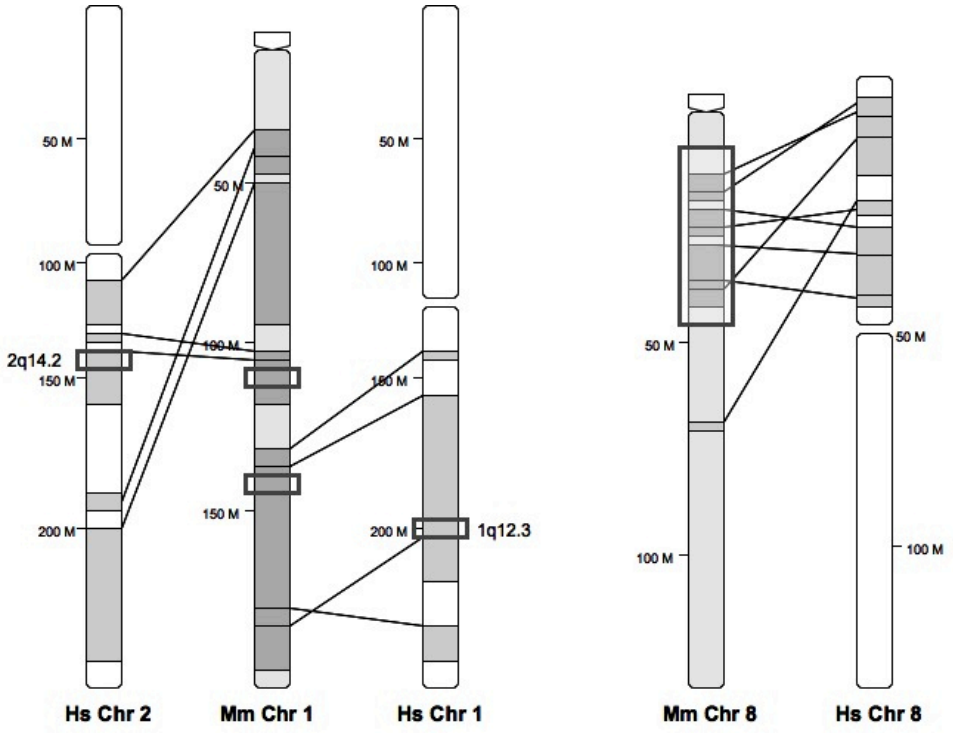

Figure 4.1: Presented are the mouse chromosomes 1 and 8 and their orthologous regions on the human chromosomes 1, 2, and 8. Encircled are the regions with the highest number of mis-regulated genes.

In a variety of human malignancies, aberrations and loss of heterozygosity (LOH) of human chromosomes are common. The most common chromosomal abnormalities are gains at 1q (q, long arm), 7p (p, short arm), 7q, 8q, and Xq, and losses at 8p, 10q, 13q, and 16q. The frequent rearrangement of chromosome band 1q12 constitutive heterochromatin in hematologic malignancies suggests that this rearrangement plays an important role in these diseases. The oncogenic mechanisms linked to 1q12 heterochromatin are unknown. Constitutive heterochromatin can epigenetically regulate gene function through the formation of

transcriptional-silencing compartments (Barki-Celli et al. 2005). Methylation studies of carcinomas of breast, liver and ovary have revealed an association between hypomethylation of this heterochromatic region on the long arm of chromosome 1 (1q12) and rearrangement within this region (Davidsson et al. 2007).

Genomic deletions involving the short arm of the human chromosome 8 are common in a wide range of epithelial malignancies including prostate (Macoska et al. 1994; Kagan et al. 1995), colorectal (Emi et al. 1992), breast (Yokota et al. 1999), and bladder (Takle and Knowles 1996; Wagner et al. 1997) carcinomas. In many of these cancer types, loss of heterozygosity is associated with a more aggressive tumour phenotype indicating the possible presence of a tumour suppressor (Knowles et al. 2005). An interesting rearrangement on Chr 8 in a human primary giant cell carcinoma of the lung is the joining of a LINE-1 family member to the 5'- upstream region of the *c-myc* gene (Iizuka et al. 1990). In breast cancer two regions at 8q11-q12 and 8q23-24 are commonly deleted (Dahiya and Deng 1998). Alterations of chromosome 8 are found in up to 50 % of prostate cancers (Schulz et al. 2007). Several genes located on chromosome 8p have been examined as candidate tumour suppressors, with one of the most promising being *c-Myc* (DeMarzo et al. 2003).

Fgl1 (fibrinogen-like 1) is a tumour-suppressor gene on the short arm of human Chr 8, which down-regulation in hepatocellular carcinoma is frequently associated with 8p allelic losses. Surprisingly, we found the mouse *Fgl1* mRNA up-regulated in the *Tdrd6*-deficient mice. Oncogenes like Inhibitor of kappaB kinase epsilon (*Ikbke*) and Zinc finger protein 42 (*Zfp42*) were shown to be down-regulated in the *Tdrd6*$^{-/-}$ mice.

These are not the only indications, that TDRD6 might play an unknown role in carcinogenesis. The human TDRD6 was initially found to be expressed in colon carcinoma cells (Scanlan et al. 2002). Meiosis/germ cell-specific genes like *Sycp3* are known, to cause cell transformation, when they are overexpressed in somatic cells (Adamah et al. 2006; Jessberger 2008). MiRNAs like the miR-34 family are known to play a role in tumorigenesis, by directly targeting the p53 tumour suppressor gene (He et al. 2007). The miR-34 family is up-regulated in the *Tdrd6*$^{-/-}$ mice. But if TDRD6 indeed plays a role in somatic carcinogenesis, possibly through mis-regulation of certain miRNAs, will be investigated in more detail, e.g. by screening different human tumour tissues for the expression of the mouse TDRD6. An antibody against the N-terminus of TDRD6 will be used, to detect both isoforms of the protein.

In many human cancers, the overall level of DNA cytosine methylation is decreased, even though specific sites may be hypermethylated (Robertson 2001). The increase in DNA methylation affects different types of repetitive sequences, such as retrotransposons and satellites, which contain most of the methylcytosines in the genome (Schulz 1998). At the same time that CpG islands become hypermethylated, the genome of the cancer cell undergoes a dramatic global hypomethylation. Although some cancer specimens seem to retain an overall DNA methylation level close to that of normal tissue, some show extensive hypomethylation, with up to 50 % decrease in an overall methylation. Pronounced global hypomethylation is associated with chromosomal instability in several human cancer types. For example the alterations on human chromosome 8 in prostate carcinoma, which were found to correlate with diminished methylation of repetitive LINE-1 sequences (Ehrlich 2002; Schulz et al. 2002). These sequences are highly methylated in normal somatic tissue including prostate. In the *Tdrd6*$^{-/-}$ mice no modified methylation pattern in the *Line-1* promoter region in comparison to wild-type mice was observed. This was in contrast to other chromatoid body components, like MIWI2, MILI and MAEL, which are known to be involved in transposon activation through methylation of CpG islands in the promoter region. This indicates that, despite malformed CBs and mislocalization of MIWI, MVH, and MAEL, protection from retrotransposons activation is still functional. And it emphasizes the assumption that TDRD6 may represent a new class of CB proteins, specifically involved in CB formation and small RNA transcription and processing.

If other genes in the *Tdrd6*-deficient mouse show abnormal methylation pattern in their promoter region, will be investigated in more detail, e.g. by bisulfite sequencing analyses of some mis-regulated genes in the *Tdrd6*$^{-/-}$ mouse, especially the genes on chromosomes 1 and 8.

5. Summary

Several tudor domain proteins exists in mammalian germ cells. We are interested in the male germ cell specific tudor domain containing protein 6 (TDRD6). It is composed of seven characteristic tudor domains, which are known to bind nucleic acids (mostly RNA), as well as some arginine-methylated proteins. Tudor domain containing proteins are suggested to build macromolecular complexes or scaffolds, through binding with their tudor domains. TDRD6 expression starts around day 16 in spermatogenesis, from primary spermatocytes to round spermatids. It exists as two different isoforms, in spermatocytes as a 250 kDa protein, and after development of the cells into haploid spermatids, as a prominent 230 kDa protein. Using two different antibodies against each terminus, we observed that the protein gets cleaved at the C-terminal end, possibly through Caspase I. In round spermatids TDRD6 is localized to the chromatoid body (CB), a male germ cell specific, electron-dense structure. It is in close proximity to the nucleus, and makes frequent contact with the nuclear pores, where an extensive exchange of material between nucleus and CB occurs. The CB consists mainly of RNA and various RNA-binding proteins, as well as small non-coding RNAs like microRNAs (miRNAs) and Piwi-interacting RNAs (piRNAs). These small non-coding RNAs behave as sequence-specific triggers for degradation and translational repression of mRNAs, which are stored in the CB. MiRNAs exist in clusters on the chromosomes and are transcribed into precursor miRNAs. They are exported into the CB, where they are processed into mature miRNAs. Mature miRNAs are incorporated into the RNA-induced silencing complex (RISC), which can regulate the translation of mRNAs. Chromatoid body components like MIWI, MIWI2 and MILI, all belonging to the Piwi protein family, are known to bind another class of small non-coding RNAs, the Piwi-interacting RNAs. These testis-specific RNAs are important to regulate transposon activity during germ cell development.

To analyze the function of TDRD6 during male germ cell development, a *Tdrd6*-deficient mouse model was generated, by disrupting most of exon 1, which implies deletion of all seven tudor domains and thus, leading to complete absence of TDRD6. The *Tdrd6*-deficent mice are viable and healthy, whereas the male mice are sterile, due to absence of mature sperm. The female mice are not affected, since TDRD6 is not expressed in females. The most striking intracellular phenotype of *Tdrd6*$^{-/-}$ mice is their highly aberrant architecture of chromatoid bodies in round

spermatids. *Tdrd6*$^{-/-}$ CBs appear as diffuse, disrupted, and less condensed structures. Their interior is largely missing, and only a “ghost”-like structure remains, expected to be significantly impaired in function. Other CB components like MVH, MIWI and MILI are expressed in *Tdrd6*$^{-/-}$ testes, but they cannot localize to the disrupted CBs. This suggests a role for TDRD6 in assembling the chromatoid body complex by recruiting other proteins. We investigated if the maintenance and processing of small RNAs is affected in the disrupted CB of the *Tdrd6*$^{-/-}$ mice. Approximately 10 % of all known murine miRNAs are differently expressed in *Tdrd6*-deficient mice, whereas most of the miRNAs are up-regulated, indicating less turnover, and thus, accumulation of mature miRNAs. But not only the mature miRNAs are differently expressed, also three investigated miRNAs showed abnormal expression of precursors. This leads to the assumption that TDRD6 most likely has an influence on transcriptional regulation of miRNA genes, most likely by an indirect effect, probably through transcriptional regulation. No common features in the promoter region of the investigated mis-regulated miRNAs were observed.

The chromatoid body in the *Tdrd6*-deficient mice is disrupted and seems to be not functionally. Since it is a place for mRNA storage and regulation, it was interesting to analyze, if testes cells show an abnormal expression pattern. In the *Tdrd6*$^{-/-}$ testes more than 100 genes are differently expressed. Unexpectedly, 36 % of all genes are located to the centromer-proximal region of Chr 8, and 11 % are located to the distal end of Chr 1. These regions are orthologous to regions on human chromosomes, which show an altered chromosomal structure in many different carcinomas, due to rearrangements and loss of heterozygosity. Genes like *Fgl1*, *Zfp42* and *Ikbke*, which are known to play a role in carcinogenesis, are differently expressed in the *Tdrd6*$^{-/-}$ mouse. Additionally, miRNAs like miR-34 and miR-29 are known to be involved in tumorigenesis and are mis-regulated in the *Tdrd6*-deficient mice. One possibility for mis-regulation of genes is transcriptional regulation through transcription factors (TF). Database analyses revealed no common TFs, which are specific for mis-regulated genes on Chr 8, as well as differently expressed genes from other chromosomes. Another possibility is, that mis-regulated miRNAs directly target specific mRNAs, and thus, leading to differently expression of them. Using database analyses, putative homologous miRNAs were found for 16 of the mis-regulated genes. These findings have to be analyzed in more detail.

In the *Tdrd6*$^{-/-}$ mice no modified methylation pattern in the *Line-1* promoter region was observed in comparison to wild-type mice. This was in contrast to other chromatoid body components, like MIWI2, MILI and MAEL, which are known to be involved in transposon activation through methylation of CpG islands in the promoter region. This highlights again, that TDRD6 may have a distinct role in germ cell development than other CB components. Whereas others regulated transposon activity, TDRD6 seems to have a scaffolding function and is important for the correct assembly of the chromatoid body, as well as small RNA transcription and processing. If TDRD6 plays any role in carcinogenesis will be investigated further in more detail.

6. Literature

Adamah, D.J., Gokhale, P.J., Eastwood, D.J., Rajpert De-Meyts, E., Goepel, J., Walsh, J.R., Moore, H.D., and Andrews, P.W. 2006. Dysfunction of the mitotic:meiotic switch as a potential cause of neoplastic conversion of primordial germ cells. *Int J Androl* **29**(1): 219-227.

Agilent. 2007. One-Color Microarray-Based Gene Expression Analysis. *Agilent Technologies*.

Anderson, R., Copeland, T.K., Scholer, H., Heasman, J., and Wylie, C. 2000. The onset of germ cell migration in the mouse embryo. *Mech Dev* **91**(1-2): 61-68.

Aravin, A., Gaidatzis, D., Pfeffer, S., Lagos-Quintana, M., Landgraf, P., Iovino, N., Morris, P., Brownstein, M.J., Kuramochi-Miyagawa, S., Nakano, T., Chien, M., Russo, J.J., Ju, J., Sheridan, R., Sander, C., Zavolan, M., and Tuschl, T. 2006. A novel class of small RNAs bind to MILI protein in mouse testes. *Nature* **442**(7099): 203-207.

Aravin, A.A. and Bourc'his, D. 2008. Small RNA guides for de novo DNA methylation in mammalian germ cells. *Genes Dev* **22**(8): 970-975.

Aravin, A.A., Naumova, N.M., Tulin, A.V., Vagin, V.V., Rozovsky, Y.M., and Gvozdev, V.A. 2001. Double-stranded RNA-mediated silencing of genomic tandem repeats and transposable elements in the D. melanogaster germline. *Curr Biol* **11**(13): 1017-1027.

Aravin, A.A., Sachidanandam, R., Bourc'his, D., Schaefer, C., Pezic, D., Toth, K.F., Bestor, T., and Hannon, G.J. 2008. A piRNA pathway primed by individual transposons is linked to de novo DNA methylation in mice. *Mol Cell* **31**(6): 785-799.

Aravin, A.A., Sachidanandam, R., Girard, A., Fejes-Toth, K., and Hannon, G.J. 2007. Developmentally regulated piRNA clusters implicate MILI in transposon control. *Science* **316**(5825): 744-747.

Ashley, T., Cacheiro, N.L., Russell, L.B., and Ward, D.C. 1993. Molecular characterization of a pericentric inversion in mouse chromosome 8 implicates telomeres as promoters of meiotic recombination. *Chromosoma* **102**(2): 112-120.

Bardsley, A., McDonald, K., and Boswell, R.E. 1993. Distribution of tudor protein in the Drosophila embryo suggests separation of functions based on site of localization. *Development* **119**(1): 207-219.

Barki-Celli, L., Lefebvre, C., Le Baccon, P., Nadeau, G., Bonnefoix, T., Usson, Y., Vourc'h, C., Khochbin, S., Leroux, D., and Callanan, M. 2005. Differences in nuclear positioning of 1q12 pericentric heterochromatin in normal and tumor B lymphocytes with 1q rearrangements. *Genes Chromosomes Cancer* **43**(4): 339-349.

Bastos, H., Lassalle, B., Chicheportiche, A., Riou, L., Testart, J., Allemand, I., and Fouchet, P. 2005. Flow cytometric characterization of viable meiotic and postmeiotic cells by Hoechst 33342 in mouse spermatogenesis. *Cytometry A* **65**(1): 40-49.

Behm-Ansmant, I., Rehwinkel, J., Doerks, T., Stark, A., Bork, P., and Izaurralde, E. 2006. mRNA degradation by miRNAs and GW182 requires both CCR4:NOT deadenylase and DCP1:DCP2 decapping complexes. *Genes Dev* **20**(14): 1885-1898.

Bellve, A.R., Millette, C.F., Bhatnagar, Y.M., and O'Brien, D.A. 1977. Dissociation of the mouse testis and characterization of isolated spermatogenic cells. *J Histochem Cytochem* **25**(7): 480-494.

Bourc'his, D. and Bestor, T.H. 2004. Meiotic catastrophe and retrotransposon reactivation in male germ cells lacking Dnmt3L. *Nature* **431**(7004): 96-99.

Boyle, A.L. and Ward, D.C. 1992. Isolation and initial characterization of a large repeat sequence element specific to mouse chromosome 8. *Genomics* **12**(3): 517-525.

Brahms, H., Meheus, L., de Brabandere, V., Fischer, U., and Luhrmann, R. 2001. Symmetrical dimethylation of arginine residues in spliceosomal Sm protein B/B' and the Sm-like protein LSm4, and their interaction with the SMN protein. *Rna* **7**(11): 1531-1542.

Branciforte, D. and Martin, S.L. 1994. Developmental and cell type specificity of LINE-1 expression in mouse testis: implications for transposition. *Mol Cell Biol* **14**(4): 2584-2592.

Braun, R.E. 1998. Post-transcriptional control of gene expression during spermatogenesis. *Semin Cell Dev Biol* **9**(4): 483-489.

Brenda, C. 1891. Neue Mitteilungen über die Entwicklung der Genitaldrüsen und die Metamorphose der Samenzellen. *Arch Anat Physiol*: 549-552.

Brennecke, J., Aravin, A.A., Stark, A., Dus, M., Kellis, M., Sachidanandam, R., and Hannon, G.J. 2007. Discrete small RNA-generating loci as master regulators of transposon activity in Drosophila. *Cell* **128**(6): 1089-1103.

Buhler, D., Raker, V., Luhrmann, R., and Fischer, U. 1999. Essential role for the tudor domain of SMN in spliceosomal U snRNP assembly: implications for spinal muscular atrophy. *Hum Mol Genet* **8**(13): 2351-2357.

Cai, X., Hagedorn, C.H., and Cullen, B.R. 2004. Human microRNAs are processed from capped, polyadenylated transcripts that can also function as mRNAs. *Rna* **10**(12): 1957-1966.

Carmell, M.A., Girard, A., van de Kant, H.J., Bourc'his, D., Bestor, T.H., de Rooij, D.G., and Hannon, G.J. 2007. MIWI2 is essential for spermatogenesis and repression of transposons in the mouse male germline. *Dev Cell* **12**(4): 503-514.

Carmell, M.A., Xuan, Z., Zhang, M.Q., and Hannon, G.J. 2002. The Argonaute family: tentacles that reach into RNAi, developmental control, stem cell maintenance, and tumorigenesis. *Genes Dev* **16**(21): 2733-2742.

Carthew, R.W. and Sontheimer, E.J. 2009. Origins and Mechanisms of miRNAs and siRNAs. *Cell* **136**(4): 642-655.

Chu, C.Y. and Rana, T.M. 2007. Small RNAs: regulators and guardians of the genome. *J Cell Physiol* **213**(2): 412-419.

Chuma, S., Hiyoshi, M., Yamamoto, A., Hosokawa, M., Takamune, K., and Nakatsuji, N. 2003. Mouse Tudor Repeat-1 (MTR-1) is a novel component of chromatoid bodies/nuages in male germ cells and forms a complex with snRNPs. *Mech Dev* **120**(9): 979-990.

Chuma, S., Hosokawa, M., Kitamura, K., Kasai, S., Fujioka, M., Hiyoshi, M., Takamune, K., Noce, T., and Nakatsuji, N. 2006. Tdrd1/Mtr-1, a tudor-related gene, is essential for male germ-cell differentiation and nuage/germinal granule formation in mice. *Proc Natl Acad Sci U S A* **103**(43): 15894-15899.

Cote, J. and Richard, S. 2005. Tudor domains bind symmetrical dimethylated arginines. *J Biol Chem* **280**(31): 28476-28483.

Cui, X.S., Zhang, D.X., Ko, Y.G., and Kim, N.H. 2009. Aberrant epigenetic reprogramming of imprinted microRNA-127 and Rtl1 in cloned mouse embryos. *Biochem Biophys Res Commun* **379**(2): 390-394.

Dahiya, R. and Deng, G. 1998. Molecular prognostic markers in breast cancer. *Breast Cancer Res Treat* **52**(1-3): 185-200.

Davidsson, J., Andersson, A., Paulsson, K., Heidenblad, M., Isaksson, M., Borg, A., Heldrup, J., Behrendtz, M., Panagopoulos, I., Fioretos, T., and Johansson, B. 2007. Tiling resolution array comparative genomic hybridization, expression and methylation analyses of dup(1q) in Burkitt lymphomas and pediatric high hyperdiploid acute lymphoblastic leukemias reveal clustered near-centromeric breakpoints and overexpression of genes in 1q22-32.3. *Human Molecular Genetics* **16**(18): 2215-2225.

Davis, B.N., Hilyard, A.C., Lagna, G., and Hata, A. 2008. SMAD proteins control DROSHA-mediated microRNA maturation. *Nature* **454**(7200): 56-61.

DeMarzo, A.M., Nelson, W.G., Isaacs, W.B., and Epstein, J.I. 2003. Pathological and molecular aspects of prostate cancer. *Lancet* **361**(9361): 955-964.

Deng, W. and Lin, H. 2002. miwi, a murine homolog of piwi, encodes a cytoplasmic protein essential for spermatogenesis. *Dev Cell* **2**(6): 819-830.

Dym, M. 1994. Spermatogonial stem cells of the testis. *Proc Natl Acad Sci U S A* **91**(24): 11287-11289.

Dym, M. and Fawcett, D.W. 1970. The blood-testis barrier in the rat and the physiological compartmentation of the seminiferous epithelium. *Biol Reprod* **3**(3): 308-326.

Ehrlich, M. 2002. DNA methylation in cancer: too much, but also too little. *Oncogene* **21**(35): 5400-5413.

Emi, M., Fujiwara, Y., Nakajima, T., Tsuchiya, E., Tsuda, H., Hirohashi, S., Maeda, Y., Tsuruta, K., Miyaki, M., and Nakamura, Y. 1992. Frequent loss of heterozygosity for loci on chromosome 8p in hepatocellular carcinoma, colorectal cancer, and lung cancer. *Cancer Res* **52**(19): 5368-5372.

Fabbri, M., Garzon, R., Cimmino, A., Liu, Z., Zanesi, N., Callegari, E., Liu, S., Alder, H., Costinean, S., Fernandez-Cymering, C., Volinia, S., Guler, G., Morrison, C.D., Chan, K.K., Marcucci, G., Calin, G.A., Huebner, K., and Croce, C.M. 2007. MicroRNA-29 family reverts aberrant methylation in lung cancer by targeting DNA methyltransferases 3A and 3B. *Proc Natl Acad Sci U S A* **104**(40): 15805-15810.

Faehnle, C.R. and Joshua-Tor, L. 2007. Argonautes confront new small RNAs. *Curr Opin Chem Biol* **11**(5): 569-577.

Feng, L.X., Chen, Y., Dettin, L., Pera, R.A., Herr, J.C., Goldberg, E., and Dym, M. 2002. Generation and in vitro differentiation of a spermatogonial cell line. *Science* **297**(5580): 392-395.

Feng, Q., Moran, J.V., Kazazian, H.H., Jr., and Boeke, J.D. 1996. Human L1 retrotransposon encodes a conserved endonuclease required for retrotransposition. *Cell* **87**(5): 905-916.

Findley, S.D., Tamanaha, M., Clegg, N.J., and Ruohola-Baker, H. 2003. Maelstrom, a Drosophila spindle-class gene, encodes a protein that colocalizes with Vasa and RDE1/AGO1 homolog, Aubergine, in nuage. *Development* **130**(5): 859-871.

Fujiwara, Y., Komiya, T., Kawabata, H., Sato, M., Fujimoto, H., Furusawa, M., and Noce, T. 1994. Isolation of a DEAD-family protein gene that encodes a murine homolog of Drosophila vasa and its specific expression in germ cell lineage. *Proc Natl Acad Sci U S A* **91**(25): 12258-12262.

Gadue, P., Huber, T.L., Paddison, P.J., and Keller, G.M. 2006. Wnt and TGF-beta signaling are required for the induction of an in vitro model of primitive streak formation using embryonic stem cells. *Proc Natl Acad Sci U S A* **103**(45): 16806-16811.

Gilbert, S. 2000. *Developmental Biology, 6th edition*.

Girard, A., Sachidanandam, R., Hannon, G.J., and Carmell, M.A. 2006. A germline-specific class of small RNAs binds mammalian Piwi proteins. *Nature* **442**(7099): 199-202.

Golumbeski, G.S., Bardsley, A., Tax, F., and Boswell, R.E. 1991. tudor, a posterior-group gene of Drosophila melanogaster, encodes a novel protein and an mRNA localized during mid-oogenesis. *Genes Dev* **5**(11): 2060-2070.

Gunawardane, L.S., Saito, K., Nishida, K.M., Miyoshi, K., Kawamura, Y., Nagami, T., Siomi, H., and Siomi, M.C. 2007. A slicer-mediated mechanism for repeat-associated siRNA 5' end formation in Drosophila. *Science* **315**(5818): 1587-1590.

Guo, J.P., Shu, S.K., He, L., Lee, Y.C., Kruk, P.A., Grenman, S., Nicosia, S.V., Mor, G., Schell, M.J., Coppola, D., and Cheng, J.Q. 2009. Deregulation of IKBKE is associated with tumor progression, poor prognosis, and cisplatin resistance in ovarian cancer. *Am J Pathol* **175**(1): 324-333.

Hajkova, P., Erhardt, S., Lane, N., Haaf, T., El-Maarri, O., Reik, W., Walter, J., and Surani, M.A. 2002. Epigenetic reprogramming in mouse primordial germ cells. *Mech Dev* **117**(1-2): 15-23.

Hamilton, A., Voinnet, O., Chappell, L., and Baulcombe, D. 2002. Two classes of short interfering RNA in RNA silencing. *Embo J* **21**(17): 4671-4679.

He, X., He, L., and Hannon, G.J. 2007. The guardian's little helper: microRNAs in the p53 tumor suppressor network. *Cancer Res* **67**(23): 11099-11101.

Hirose, T., Kawabuchi, M., Tamaru, T., Okumura, N., Nagai, K., and Okada, M. 2000. Identification of tudor repeat associator with PCTAIRE 2 (Trap). A novel protein that interacts with the N-terminal domain of PCTAIRE 2 in rat brain. *Eur J Biochem* **267**(7): 2113-2121.

Hofmann, M.C., Van Der Wee, K.S., Dargart, J.L., Dirami, G., Dettin, L., and Dym, M. 2003. Establishment and characterization of neonatal mouse sertoli cell lines. *J Androl* **24**(1): 120-130.

Hosokawa, M., Shoji, M., Kitamura, K., Tanaka, T., Noce, T., Chuma, S., and Nakatsuji, N. 2007. Tudor-related proteins TDRD1/MTR-1, TDRD6 and TDRD7/TRAP: domain composition, intracellular localization, and function in male germ cells in mice. *Dev Biol* **301**(1): 38-52.

Huyen, Y., Zgheib, O., Ditullio, R.A., Jr., Gorgoulis, V.G., Zacharatos, P., Petty, T.J., Sheston, E.A., Mellert, H.S., Stavridi, E.S., and Halazonetis, T.D. 2004. Methylated lysine 79 of histone H3 targets 53BP1 to DNA double-strand breaks. *Nature* **432**(7015): 406-411.

Iizuka, M., Shiraishi, M., Yoshida, M.C., Hayashi, K., and Sekiya, T. 1990. Joining of the c-myc gene and a line 1 family member on chromosome 8 in a human primary giant cell carcinoma of the lung. *Cancer Res* **50**(11): 3345-3350.

Ikenishi, K. 1998. Germ plasm in Caenorhabditis elegans, Drosophila and Xenopus. *Dev Growth Differ* **40**(1): 1-10.

Jessberger, R. 2008. New insights into germ cell tumor formation. *Horm Metab Res* **40**(5): 342-346.

Jia, D., Jurkowska, R.Z., Zhang, X., Jeltsch, A., and Cheng, X. 2007. Structure of Dnmt3a bound to Dnmt3L suggests a model for de novo DNA methylation. *Nature* **449**(7159): 248-251.

Joyner, A.L. 2000. Gene Targeting, a practical approach. *Oxford University Press, USA*.

Jurka, J. 1997. Sequence patterns indicate an enzymatic involvement in integration of mammalian retroposons. *Proc Natl Acad Sci U S A* **94**(5): 1872-1877.

Kagan, J., Stein, J., Babaian, R.J., Joe, Y.S., Pisters, L.L., Glassman, A.B., von Eschenbach, A.C., and Troncoso, P. 1995. Homozygous deletions at 8p22 and 8p21 in prostate cancer implicate these regions as the sites for candidate tumor suppressor genes. *Oncogene* **11**(10): 2121-2126.

Kato, Y., Kaneda, M., Hata, K., Kumaki, K., Hisano, M., Kohara, Y., Okano, M., Li, E., Nozaki, M., and Sasaki, H. 2007. Role of the Dnmt3 family in de novo methylation of imprinted and repetitive sequences during male germ cell development in the mouse. *Hum Mol Genet* **16**(19): 2272-2280.

Kierszenbaum, A.L. and Tres, L.L. 1975. Structural and transcriptional features of the mouse spermatid genome. *J Cell Biol* **65**(2): 258-270.

Kim, J., Daniel, J., Espejo, A., Lake, A., Krishna, M., Xia, L., Zhang, Y., and Bedford, M.T. 2006. Tudor, MBT and chromo domains gauge the degree of lysine methylation. *EMBO Rep* **7**(4): 397-403.

Kim, V.N., Han, J., and Siomi, M.C. 2009. Biogenesis of small RNAs in animals. *Nat Rev Mol Cell Biol* **10**(2): 126-139.

Kimmins, S. and Sassone-Corsi, P. 2005. Chromatin remodelling and epigenetic features of germ cells. *Nature* **434**(7033): 583-589.

Kimura, M., Ishida, K., Kashiwabara, S., and Baba, T. 2009. Characterization of two cytoplasmic poly(A)-binding proteins, PABPC1 and PABPC2, in mouse spermatogenic cells. *Biol Reprod* **80**(3): 545-554.

Kiriakidou, M., Tan, G.S., Lamprinaki, S., De Planell-Saguer, M., Nelson, P.T., and Mourelatos, Z. 2007. An mRNA m7G cap binding-like motif within human Ago2 represses translation. *Cell* **129**(6): 1141-1151.

Knowles, M.A., Aveyard, J.S., Taylor, C.F., Harnden, P., and Bass, S. 2005. Mutation analysis of the 8p candidate tumour suppressor genes DBC2 (RHOBTB2) and LZTS1 in bladder cancer. *Cancer Lett* **225**(1): 121-130.

Komiya, T., Itoh, K., Ikenishi, K., and Furusawa, M. 1994. Isolation and characterization of a novel gene of the DEAD box protein family which is specifically expressed in germ cells of Xenopus laevis. *Dev Biol* **162**(2): 354-363.

Kotaja, N., Bhattacharyya, S.N., Jaskiewicz, L., Kimmins, S., Parvinen, M., Filipowicz, W., and Sassone-Corsi, P. 2006a. The chromatoid body of male germ cells: similarity with processing bodies and presence of Dicer and microRNA pathway components. *Proc Natl Acad Sci U S A* **103**(8): 2647-2652.

Kotaja, N., Lin, H., Parvinen, M., and Sassone-Corsi, P. 2006b. Interplay of PIWI/Argonaute protein MIWI and kinesin KIF17b in chromatoid bodies of male germ cells. *J Cell Sci* **119**(Pt 13): 2819-2825.

Kotaja, N., Macho, B., and Sassone-Corsi, P. 2005. Microtubule-independent and protein kinase A-mediated function of kinesin KIF17b controls the intracellular transport of activator of CREM in testis (ACT). *J Biol Chem* **280**(36): 31739-31745.

Kotaja, N. and Sassone-Corsi, P. 2007. The chromatoid body: a germ-cell-specific RNA-processing centre. *Nat Rev Mol Cell Biol* **8**(1): 85-90.

Kristensen, D., Nielsen, J., Skakkebaek, N., Graem, N., Jacobsen, G., Meyts, E., and Leffers, H. 2008. Presumed pluripotency markers UTF-1 and REX-1 are

expressed in human adult testes and germ cell neoplasms. *Human Reproduction* **23**(4): 775-782.

Kuhn, U. and Wahle, E. 2004. Structure and function of poly(A) binding proteins. *Biochim Biophys Acta* **1678**(2-3): 67-84.

Kuramochi-Miyagawa, S., Kimura, T., Ijiri, T.W., Isobe, T., Asada, N., Fujita, Y., Ikawa, M., Iwai, N., Okabe, M., Deng, W., Lin, H., Matsuda, Y., and Nakano, T. 2004. Mili, a mammalian member of piwi family gene, is essential for spermatogenesis. *Development* **131**(4): 839-849.

Kuramochi-Miyagawa, S., Kimura, T., Yomogida, K., Kuroiwa, A., Tadokoro, Y., Fujita, Y., Sato, M., Matsuda, Y., and Nakano, T. 2001. Two mouse piwi-related genes: miwi and mili. *Mech Dev* **108**(1-2): 121-133.

Kuramochi-Miyagawa, S., Watanabe, T., Gotoh, K., Totoki, Y., Toyoda, A., Ikawa, M., Asada, N., Kojima, K., Yamaguchi, Y., Ijiri, T.W., Hata, K., Li, E., Matsuda, Y., Kimura, T., Okabe, M., Sakaki, Y., Sasaki, H., and Nakano, T. 2008. DNA methylation of retrotransposon genes is regulated by Piwi family members MILI and MIWI2 in murine fetal testes. *Genes Dev* **22**(7): 908-917.

Lacham-Kaplan, O. 2004. In vivo and in vitro differentiation of male germ cells in the mouse. *Reproduction* **128**(2): 147-152.

Landgraf, P., Rusu, M., Sheridan, R., Sewer, A., Iovino, N., Aravin, A., Pfeffer, S., Rice, A., Kamphorst, A.O., Landthaler, M., Lin, C., Socci, N.D., Hermida, L., Fulci, V., Chiaretti, S., Foa, R., Schliwka, J., Fuchs, U., Novosel, A., Muller, R.U., Schermer, B., Bissels, U., Inman, J., Phan, Q., Chien, M., Weir, D.B., Choksi, R., De Vita, G., Frezzetti, D., Trompeter, H.I., Hornung, V., Teng, G., Hartmann, G., Palkovits, M., Di Lauro, R., Wernet, P., Macino, G., Rogler, C.E., Nagle, J.W., Ju, J., Papavasiliou, F.N., Benzing, T., Lichter, P., Tam, W., Brownstein, M.J., Bosio, A., Borkhardt, A., Russo, J.J., Sander, C., Zavolan, M., and Tuschl, T. 2007. A mammalian microRNA expression atlas based on small RNA library sequencing. *Cell* **129**(7): 1401-1414.

Lane, N., Dean, W., Erhardt, S., Hajkova, P., Surani, A., Walter, J., and Reik, W. 2003. Resistance of IAPs to methylation reprogramming may provide a mechanism for epigenetic inheritance in the mouse. *Genesis* **35**(2): 88-93.

Lasko, P.F. and Ashburner, M. 1988. The product of the Drosophila gene vasa is very similar to eukaryotic initiation factor-4A. *Nature* **335**(6191): 611-617.

Lee, Y., Kim, M., Han, J., Yeom, K.H., Lee, S., Baek, S.H., and Kim, V.N. 2004. MicroRNA genes are transcribed by RNA polymerase II. *Embo J* **23**(20): 4051-4060.

Lees-Murdock, D.J., De Felici, M., and Walsh, C.P. 2003. Methylation dynamics of repetitive DNA elements in the mouse germ cell lineage. *Genomics* **82**(2): 230-237.

Liang, L., Diehl-Jones, W., and Lasko, P. 1994. Localization of vasa protein to the Drosophila pole plasm is independent of its RNA-binding and helicase activities. *Development* **120**(5): 1201-1211.

Linder, B., Plottner, O., Kroiss, M., Hartmann, E., Laggerbauer, B., Meister, G., Keidel, E., and Fischer, U. 2008. Tdrd3 is a novel stress granule-associated protein interacting with the Fragile-X syndrome protein FMRP. *Hum Mol Genet* **17**(20): 3236-3246.

Liu, J., Carmell, M.A., Rivas, F.V., Marsden, C.G., Thomson, J.M., Song, J.J., Hammond, S.M., Joshua-Tor, L., and Hannon, G.J. 2004. Argonaute2 is the catalytic engine of mammalian RNAi. *Science* **305**(5689): 1437-1441.

Liu, X., Wu, H., Loring, J., Hormuzdi, S., Disteche, C.M., Bornstein, P., and Jaenisch, R. 1997. Trisomy eight in ES cells is a common potential problem in gene targeting and interferes with germ line transmission. *Dev Dyn* **209**(1): 85-91.

Luan, D.D. and Eickbush, T.H. 1995. RNA template requirements for target DNA-primed reverse transcription by the R2 retrotransposable element. *Mol Cell Biol* **15**(7): 3882-3891.

Lund, E., Guttinger, S., Calado, A., Dahlberg, J.E., and Kutay, U. 2004. Nuclear export of microRNA precursors. *Science* **303**(5654): 95-98.

Macoska, J.A., Trybus, T.M., Sakr, W.A., Wolf, M.C., Benson, P.D., Powell, I.J., and Pontes, J.E. 1994. Fluorescence in situ hybridization analysis of 8p allelic loss and chromosome 8 instability in human prostate cancer. *Cancer Res* **54**(14): 3824-3830.

Malik, H.S., Burke, W.D., and Eickbush, T.H. 1999. The age and evolution of non-LTR retrotransposable elements. *Mol Biol Evol* **16**(6): 793-805.

Mangus, D.A., Evans, M.C., and Jacobson, A. 2003. Poly(A)-binding proteins: multifunctional scaffolds for the post-transcriptional control of gene expression. *Genome Biol* **4**(7): 223.

Marcon, E., Babak, T., Chua, G., Hughes, T., and Moens, P.B. 2008. miRNA and piRNA localization in the male mammalian meiotic nucleus. *Chromosome Res* **16**(2): 243-260.

Maurer-Stroh, S., Dickens, N.J., Hughes-Davies, L., Kouzarides, T., Eisenhaber, F., and Ponting, C.P. 2003. The Tudor domain 'Royal Family': Tudor, plant Agenet, Chromo, PWWP and MBT domains. *Trends Biochem Sci* **28**(2): 69-74.

McLaren, A. 2000. Germ and somatic cell lineages in the developing gonad. *Mol Cell Endocrinol* **163**(1-2): 3-9.

Meister, G., Landthaler, M., Patkaniowska, A., Dorsett, Y., Teng, G., and Tuschl, T. 2004. Human Argonaute2 mediates RNA cleavage targeted by miRNAs and siRNAs. *Mol Cell* **15**(2): 185-197.

Mishima, T., Takizawa, T., Luo, S.S., Ishibashi, O., Kawahigashi, Y., Mizuguchi, Y., Ishikawa, T., Mori, M., Kanda, T., Goto, T., and Takizawa, T. 2008. MicroRNA (miRNA) cloning analysis reveals sex differences in miRNA expression profiles between adult mouse testis and ovary. *Reproduction* **136**(6): 811-822.

Mizuuchi, K. 1992. Transpositional recombination: mechanistic insights from studies of mu and other elements. *Annu Rev Biochem* **61**: 1011-1051.

Muller-Reichert, T., Hohenberg, H., O'Toole, E.T., and McDonald, K. 2003. Cryoimmobilization and three-dimensional visualization of C. elegans ultrastructure. *J Microsc* **212**(Pt 1): 71-80.

Nagamori, I. and Sassone-Corsi, P. 2008. The chromatoid body of male germ cells: epigenetic control and miRNA pathway. *Cell Cycle* **7**(22): 3503-3508.

O'Donnell, K.A. and Boeke, J.D. 2007. Mighty Piwis defend the germline against genome intruders. *Cell* **129**(1): 37-44.

Olsen, L.C., Aasland, R., and Fjose, A. 1997. A vasa-like gene in zebrafish identifies putative primordial germ cells. *Mech Dev* **66**(1-2): 95-105.

Ooi, S.K., Qiu, C., Bernstein, E., Li, K., Jia, D., Yang, Z., Erdjument-Bromage, H., Tempst, P., Lin, S.P., Allis, C.D., Cheng, X., and Bestor, T.H. 2007. DNMT3L connects unmethylated lysine 4 of histone H3 to de novo methylation of DNA. *Nature* **448**(7154): 714-717.

Ostertag, E.M. and Kazazian, H.H., Jr. 2001. Biology of mammalian L1 retrotransposons. *Annu Rev Genet* **35**: 501-538.

Pan, J., Goodheart, M., Chuma, S., Nakatsuji, N., Page, D.C., and Wang, P.J. 2005. RNF17, a component of the mammalian germ cell nuage, is essential for spermiogenesis. *Development* **132**(18): 4029-4039.

Parvinen, M. 2005. The chromatoid body in spermatogenesis. *Int J Androl* **28**(4): 189-201.

Parvinen, M. and Jokelainen, P.T. 1974. Rapid movements of the chromatoid body in living early spermatids of the rat. *Biol Reprod* **11**(1): 85-92.

Parvinen, M. and Parvinen, L.M. 1979. Active movements of the chromatoid body. A possible transport mechanism for haploid gene products. *J Cell Biol* **80**(3): 621-628.

Petersen, C.P., Bordeleau, M.E., Pelletier, J., and Sharp, P.A. 2006. Short RNAs repress translation after initiation in mammalian cells. *Mol Cell* **21**(4): 533-542.

Ponting, C.P. 1997. Tudor domains in proteins that interact with RNA. *Trends Biochem Sci* **22**(2): 51-52.

Reinhart, B.J. and Bartel, D.P. 2002. Small RNAs correspond to centromere heterochromatic repeats. *Science* **297**(5588): 1831.

Ro, S., Park, C., Sanders, K.M., McCarrey, J.R., and Yan, W. 2007a. Cloning and expression profiling of testis-expressed microRNAs. *Dev Biol* **311**(2): 592-602.

Ro, S., Park, C., Song, R., Nguyen, D., Jin, J., Sanders, K.M., McCarrey, J.R., and Yan, W. 2007b. Cloning and expression profiling of testis-expressed piRNA-like RNAs. *Rna* **13**(10): 1693-1702.

Robertson, K.D. 2001. DNA methylation, methyltransferases, and cancer. *Oncogene* **20**(24): 3139-3155.

Rodriguez, A., Griffiths-Jones, S., Ashurst, J.L., and Bradley, A. 2004. Identification of mammalian microRNA host genes and transcription units. *Genome Res* **14**(10A): 1902-1910.

Rongo, C. and Lehmann, R. 1996. Regulated synthesis, transport and assembly of the Drosophila germ plasm. *Trends Genet* **12**(3): 102-109.

Roussell, D.L. and Bennett, K.L. 1993. glh-1, a germ-line putative RNA helicase from Caenorhabditis, has four zinc fingers. *Proc Natl Acad Sci U S A* **90**(20): 9300-9304.

Rowold, D.J. and Herrera, R.J. 2000. Alu elements and the human genome. *Genetica* **108**(1): 57-72.

Russell, L.D. 1990. Histological and Histopathological Evaluation of the Testis. *Cache River Press*.

Saade, M., Irla, M., Govin, J., Victorero, G., Samson, M., and Nguyen, C. 2007. Dynamic distribution of Spatial during mouse spermatogenesis and its interaction with the kinesin KIF17b. *Exp Cell Res* **313**(3): 614-626.

Sambrook, J. and Russell, D.W. 2001. *Molecular cloning: a laboratory manual*, Edn. 3rd. *Cold Spring Harbor Laboratory Press*.

Sasaki, T., Shiohama, A., Minoshima, S., and Shimizu, N. 2003. Identification of eight members of the Argonaute family in the human genome small star, filled. *Genomics* **82**(3): 323-330.

Sassaman, D.M., Dombroski, B.A., Moran, J.V., Kimberland, M.L., Naas, T.P., DeBerardinis, R.J., Gabriel, A., Swergold, G.D., and Kazazian, H.H., Jr. 1997. Many human L1 elements are capable of retrotransposition. *Nat Genet* **16**(1): 37-43.

Sassone-Corsi, P. 2002. Unique chromatin remodeling and transcriptional regulation in spermatogenesis. *Science* **296**(5576): 2176-2178.

Scanlan, M.J., Welt, S., Gordon, C.M., Chen, Y.T., Gure, A.O., Stockert, E., Jungbluth, A.A., Ritter, G., Jager, D., Jager, E., Knuth, A., and Old, L.J. 2002.

Cancer-related serological recognition of human colon cancer: identification of potential diagnostic and immunotherapeutic targets. *Cancer Res* **62**(14): 4041-4047.

Schulz, W.A. 1998. DNA methylation in urological malignancies (review). *Int J Oncol* **13**(1): 151-167.

Schulz, W.A., Alexa, A., Jung, V., Hader, C., Hoffmann, M.J., Yamanaka, M., Fritzsche, S., Wlazlinski, A., Muller, M., Lengauer, T., Engers, R., Florl, A.R., Wullich, B., and Rahnenfuhrer, J. 2007. Factor interaction analysis for chromosome 8 and DNA methylation alterations highlights innate immune response suppression and cytoskeletal changes in prostate cancer. *Mol Cancer* **6**: 14.

Schulz, W.A., Elo, J.P., Florl, A.R., Pennanen, S., Santourlidis, S., Engers, R., Buchardt, M., Seifert, H.H., and Visakorpi, T. 2002. Genomewide DNA hypomethylation is associated with alterations on chromosome 8 in prostate carcinoma. *Genes Chromosomes Cancer* **35**(1): 58-65.

Selenko, P., Sprangers, R., Stier, G., Buhler, D., Fischer, U., and Sattler, M. 2001. SMN tudor domain structure and its interaction with the Sm proteins. *Nat Struct Biol* **8**(1): 27-31.

Sharbati-Tehrani, S., Kutz-Lohroff, B., Bergbauer, R., Scholven, J., and Einspanier, R. 2008. miR-Q: a novel quantitative RT-PCR approach for the expression profiling of small RNA molecules such as miRNAs in a complex sample. *BMC Mol Biol* **9**: 34.

Skorokhod, O., Nemazanyy, I., Breus, O., Filonenko, V., and Panasyuk, G. 2008. Generation and characterization of monoclonal antibodies to TDRD7 protein. *Hybridoma (Larchmt)* **27**(3): 211-216.

Smit, A.F. 1999. Interspersed repeats and other mementos of transposable elements in mammalian genomes. *Curr Opin Genet Dev* **9**(6): 657-663.

Smit, A.F. and Riggs, A.D. 1996. Tiggers and DNA transposon fossils in the human genome. *Proc Natl Acad Sci U S A* **93**(4): 1443-1448.

Smith, J.M., Bowles, J., Wilson, M., Teasdale, R.D., and Koopman, P. 2004. Expression of the tudor-related gene Tdrd5 during development of the male germline in mice. *Gene Expr Patterns* **4**(6): 701-705.

Song, G. and Wang, L. 2008. MiR-433 and miR-127 arise from independent overlapping primary transcripts encoded by the miR-433-127 locus. *PLoS ONE* **3**(10): e3574.

Soper, S.F., van der Heijden, G.W., Hardiman, T.C., Goodheart, M., Martin, S.L., de Boer, P., and Bortvin, A. 2008. Mouse maelstrom, a component of nuage, is essential for spermatogenesis and transposon repression in meiosis. *Dev Cell* **15**(2): 285-297.

Southern, E.M. 1975. Detection of specific sequences among DNA fragments separated by gel electrophoresis. *J Mol Biol* **98**(3): 503-517.

Sprangers, R., Groves, M.R., Sinning, I., and Sattler, M. 2003. High-resolution X-ray and NMR structures of the SMN Tudor domain: conformational variation in the binding site for symmetrically dimethylated arginine residues. *J Mol Biol* **327**(2): 507-520.

Steger, K. 2001. Haploid spermatids exhibit translationally repressed mRNAs. *Anat Embryol (Berl)* **203**(5): 323-334.

Takle, L.A. and Knowles, M.A. 1996. Deletion mapping implicates two tumor suppressor genes on chromosome 8p in the development of bladder cancer. *Oncogene* **12**(5): 1083-1087.

Tanaka, S.S., Toyooka, Y., Akasu, R., Katoh-Fukui, Y., Nakahara, Y., Suzuki, R., Yokoyama, M., and Noce, T. 2000. The mouse homolog of Drosophila Vasa is required for the development of male germ cells. *Genes Dev* **14**(7): 841-853.

Unhavaithaya, Y., Hao, Y., Beyret, E., Yin, H., Kuramochi-Miyagawa, S., Nakano, T., and Lin, H. 2009. MILI, a PIWI-interacting RNA-binding protein, is required for germ line stem cell self-renewal and appears to positively regulate translation. *J Biol Chem* **284**(10): 6507-6519.

Vasileva, A., Tiedau, D., Firooznia, A., Muller-Reichert, T., and Jessberger, R. 2009. Tdrd6 is required for spermiogenesis, chromatoid body architecture, and regulation of miRNA expression. *Curr Biol* **19**(8): 630-639.

Ventela, S., Toppari, J., and Parvinen, M. 2003. Intercellular organelle traffic through cytoplasmic bridges in early spermatids of the rat: mechanisms of haploid gene product sharing. *Mol Biol Cell* **14**(7): 2768-2780.

Wagner, U., Bubendorf, L., Gasser, T.C., Moch, H., Gorog, J.P., Richter, J., Mihatsch, M.J., Waldman, F.M., and Sauter, G. 1997. Chromosome 8p deletions are associated with invasive tumor growth in urinary bladder cancer. *Am J Pathol* **151**(3): 753-759.

Walsh, C.P., Chaillet, J.R., and Bestor, T.H. 1998. Transcription of IAP endogenous retroviruses is constrained by cytosine methylation. *Nat Genet* **20**(2): 116-117.

Wang, J. and Dreyfuss, G. 2001. Characterization of functional domains of the SMN protein in vivo. *J Biol Chem* **276**(48): 45387-45393.

Wang, J., Saxe, J.P., Tanaka, T., Chuma, S., and Lin, H. 2009. Mili interacts with tudor domain-containing protein 1 in regulating spermatogenesis. *Curr Biol* **19**(8): 640-644.

Wang, X. 2008. miRDB: a microRNA target prediction and functional annotation database with a wiki interface. *Rna* **14**(6): 1012-1017.

Whitcomb, J.M. and Hughes, S.H. 1992. Retroviral reverse transcription and integration: progress and problems. *Annu Rev Cell Biol* **8**: 275-306.

Winter, J., Jung, S., Keller, S., Gregory, R.I., and Diederichs, S. 2009. Many roads to maturity: microRNA biogenesis pathways and their regulation. *Nat Cell Biol* **11**(3): 228-234.

Wu, L., Fan, J., and Belasco, J.G. 2006. MicroRNAs direct rapid deadenylation of mRNA. *Proc Natl Acad Sci U S A* **103**(11): 4034-4039.

Yan, J., Yu, Y., Wang, N., Chang, Y., Ying, H., Liu, W., He, J., Li, S., Jiang, W., Li, Y., Liu, H., Wang, H., and Xu, Y. 2004. LFIRE-1/HFREP-1, a liver-specific gene, is frequently downregulated and has growth suppressor activity in hepatocellular carcinoma. *Oncogene* **23**(10): 1939-1949.

Yi, R., Qin, Y., Macara, I.G., and Cullen, B.R. 2003. Exportin-5 mediates the nuclear export of pre-microRNAs and short hairpin RNAs. *Genes Dev* **17**(24): 3011-3016.

Yokota, T., Yoshimoto, M., Akiyama, F., Sakamoto, G., Kasumi, F., Nakamura, Y., and Emi, M. 1999. Frequent multiplication of chromosomal region 8q24.1 associated with aggressive histologic types of breast cancers. *Cancer Lett* **139**(1): 7-13.

Yoon, C., Kawakami, K., and Hopkins, N. 1997. Zebrafish vasa homologue RNA is localized to the cleavage planes of 2- and 4-cell-stage embryos and is expressed in the primordial germ cells. *Development* **124**(16): 3157-3165.

7. Abbreviations

aa	amino acids
AE	axial element
bp	base pair
CB	Chromatoid body
cDNA	complementary DNA
Chr	chromosome
Cy3	Cyanine-3
DAPI	4’,6-diamidino-2-phenylindole
DNA	deoxyribonucleic acid
dpc	days post coitum
dpp	days postpartum
e.g.	for example
ES	embryonic stem (cells)
FITC	Fluorescein isothiocyanate
GST	Glutathione S-transferase
h	hours
HRP	Horseradish peroxidase
hs	*homo sapiens*
i.e.	id est (that is)
kb	kilo base
kDa	kilo Dalton
kg	kilogram
LTR	long terminal repeat
min	minutes
miRNA	microRNA
mg	milligram
ml	milliliter
mm	*mus musculus*
mRNA	messenger ribonucleic acid
nm	nanometer
ng	nanogram

nt	nucleotide
ORF	open reading frame
PCR	polymerase chain reaction
PGCs	primordial germ cells
piRNA	piwi-interacting RNA
pre-miRNA	preliminary miRNA
pri-miRNA	primery RNA
qRT-PCR	quantitative real time polymerase chain reaction
rasiRNA	repeat associated RNA
RISC	RNA induced silencing complex
RNA	ribonucleic acid
RT	room temperature
SC	synaptonemal complex
SDS-PAGE	sodium dodecyl sulfate polyacrylamide gel electrophoreses
Sec	second
siRNA	small interfering RNA
UTR	upstream translational region
UV	ultraviolet
vol	volume
µg	microgram
µl	microliter
µm	micrometer
x g	x-fold g-force

8. List of chemicals

Reagents	Provider	Cat #
100 bp DNA ladder	New England Biolabs	N3231L
100 mM dNTP Set	Invitrogen	10297-018
Accustain Harris Hematoxylin	Sigma-Aldrich	HHS16-500ML
Acetic acid (Glacial)	Merck	1.000.631.011
Acetone	Merck	1.000.141.011
Agarose	Sigma	A9539-500G
Albumin Bovine (BSA)	Sigma	A2153-100G
Ammonium sulfate	Roth	3746.1
APS Ammoniumperoxosulfate	Roth	9592.3
Bacto Yeast Extract	BD	212750
BioNickTM Labeling System	Invitrogen	18247-015
Boric acid	VWR	20.185.297
Bouin's solution	Sigma	HT10132-1L
Comassie Brilliant Blue	Merck	12553
Bromphenolblue	Fluka	273997
Calcium chloride	Merck	1.023.821.000
Chloramphenicol	Sigma	C0378-100G
Chloroform	Roth	3313.1
Colchicine	Sigma	C9754-1G
Collagenase type I	Gibco	9001-12-1.
Cot-1 DNA mouse	Invitrogen	18440-016
Cyanogen bromide-activated-SepharoseR 4 Fast Flow	Sigma	C5338-10G
DAPI (Diamidine-2-phenylindole) dihydrochloride	Sigma	D9542
Deoxycytidine 5'-triphosphate (a-32P), 250µCi (9.25 MBq)	PerkinElmer	NEG013H250UC
Deoxyribonucleic acid single stranded Salmon sperm testes	Sigma	D9156-1ML
DEPC Diethyl Pyrocarbonate	Sigma	1609-47-8
Dextransulfate sodium salt	Sigma	D8906-10G
Dimethyl sulfoxide	Sigma	D5879-100ML
DMEM + GlutaMAX	Invitrogen	31966-021
DNA Molecular Weight Marker X	Roche	11498037001
DNase I	Promega	M610A
DTT 1,4-Dithiothreit	Roth	6908.3
ECL Western Blotting	Pierce	1859701
Enzymes (PvuI, EcoRI, KpnI BglII, MspI, HpaI, HindIII)	NEB	
Ethanol	VWR	2 0821296
Ethidium Bromide	Merck	1.116.080.030
Ethylenediaminetetraacetic acid (EDTA)	Sigma	E5134-500G
Fetal calf serum (FCS)	Invitrogen	10270-106
Fixogum	Marabuwerke	290117000
Fluoromount-GTM	Southern Biotech	0100-01
Formaldehyde	Sigma	F8775-500ML
Formamide, deionized	Sigma	F9037-100ML

Freund's Adjuvant, Complete	Sigma	F5881-10ML
Freund's Adjuvant, Incomplete	Sigma	F5506-10ML
FISH Gelatin from cold water fish skin	Sigma	G7765-250ML
Glutathione reduced	Sigma	G4251-10G
Glutathione-Agarose	Sigma	G4510-10ML
Glycerol	Roth	3783.1
Glycine	Sigma	G8898-1KG
HBSS	Invitrogen	24020-091
HEPES	Gibco	15630-056
Hoechst No.33342 (bisBenzimide)	Sigma	B-2261-100MG
Hybond™-C super	Amersham	RPN203E
Hybond™-N+	Amersham	RPN203B
Hydrochloric acid 37%	Merck	1.003.171.000
Igepal CA630/ NP-40	Fluka	56741
Illustra Nick columns	Amersham	17-0855-01
IPTG Isopropyl ß-D-1-thiogalactopyranoside	Peqlab	37-2020
Isopropanol	Merck	1.096.341.011
Magnesium sulfate	Sigma	M8266-1KG
Methanol	Merck	1.060.091.011
Milk Powder nonfat dried	AppliChem	A0830-0500
Paraformaldehyde	Sigma	P6148-500G
PBS Phosphate buffered saline	BioChrom AG	L 18205
Penicillin/Streptomycin	BioChrom	A2213
Perfect Hyb™ Plus Hybridization buffer	Sigma	H7033-125ML
Periodic acid	Pharmacy	
PMSF phenylmethanesulphonylfluoride	Sigma	P7626-5G
Ponceau red	Roth	5938.2
Potassium acetate	Sigma	P1190
Potassium dihydrogen phosphate	Sigma	P5655
Potassium chloride	Roth	6781.1
Precision Plus Protein™ Standard	Bio-Rad	161-0373
Prestainded marker	Fermentas	SM0671
Prime It® RmT Random Primer Labeling Kit	Stratagene	300392
Primer p(dT)15 for cDNA synthesis	Roche	10814270001
Propidium iodide	Sigma	P4170-25MG
Protease Inhibitor Cocktail Complete Mini	Roche	11836153001
Protein A Agarose	Invitrogen	15918-014
Proteinase K	Peqlab	04-1070
Puromycin	Sigma	P7255
QuantiTectR SYBRR Green PCR Kit	Qiagen	204143
Random Primers	Promega	C1181
RNase A	Sigma	R4875-100MG
Roti-Histokitt II	Roth	T160.1
Roti-Phenol	Roth	0038.1
Rotiphorese Gel 30	Roth	3029.2
Roti-Quant	Roth	K015.1

RPMI 1640	Invitrogen	21875-034
Schiff's Reagent	Pharmacy	
SDS Sodium dodecylsulfate	Roth	2326.2
Sodium Azide	Sigma	S8032
Sodium Chloride	Roth	3957.1
Sodium citrate	Fluka	71406
Sodium deoxycholate	Sigma	G6750-100G
Sodium DL-lactate	Sigma	L4263-500ML
Sodium fluoride	Sigma	S7920
Sodium hydroxid	Sigma	S8045
Sodium metabisulfite	Fluka	71928
Sodium hydrogen phosphate Na2HPO4	Roth	P030.2
Sodium Orthovanadate	Sigma	S6508-10G
Sodium Pyruvate	Gibco	11360
Sodium thiocyanate	Fluka	71938
ß-ME mercaptoethanol	Sigma	M6250-100ML
Super Script TM II Reverse Transcriptase	Invitrogen	18064-022
TACS^{TM} 2 TdT *In Situ* Apoptosis Detection Kit	Trevigen	4810-30-K
Taq DNA Polymerase	Invitrogen	10342-020
TEMED	Bio-Rad	161-0801
Tissue Tek O.C.T.TM Compound	Sakura	623010015
TLCK Tosyl-L-Lysine chloromethyl ketone hydrochloride	BioChemika	90182
Trichloroacetic acid	Merck	807
Tris	Roth	5429.3
Triton® X-100	Sigma	T9284-100ML
Trizol® reagent	Invitrogen	15596-018
Trypsin/EDTA	BioChrom	L2143
Trypton	Biodeal	CH1008,1000
Tween® 20	Serva	37470
Urea	Fluka	51456
Xylene cyanole	Sigma	X-4126

Erklärung entsprechend §5.5 der Promotionsordnung

Hiermit versichere ich, dass ich die vorliegende Arbeit ohne unzulässige Hilfe Dritter und ohne Benutzung anderer als der angegebenen Hilfsmittel angefertigt habe; die aus fremden Quellen direkt oder indirekt übernommenen Gedanken sind als solche kenntlich gemacht. Die Arbeit wurde bisher weder im Inland noch im Ausland in gleicher oder ähnlicher Form einer anderen Prüfungsbehörde vorgelegt.
Die Dissertation wurde von Prof. Dr. Rolf Jessberger, Institut für Physiologische Chemie der Medizinischen Fakultät Carl Gustav Carus der Technischen Universität Dresden, betreut und im Zeitraum von Oktober 2005 bis September 2009 verfasst.
Meine Person betreffend erkläre ich hiermit, dass keine früheren erfolglosen Promotionsverfahren stattgefunden haben.
Ich erkenne die Promotionsordnung der Fakultät für Mathematik und Naturwissenschaften, Technische Universität Dresden, an.

Dresden, den 30.06.2009

Acknowledgements

Foremost, I would like to gratefully thank Prof. Rolf Jessberger for providing me with the opportunity to complete my Ph.D. thesis in the Institute of Physiological Chemistry of the Medical faculty of the Technical University, Dresden. He has been very interested in my work and has always been available to advise me. I am very grateful for his patience, motivation, and enthusiasm.

I would like to thank Prof. Gerhard Rödel for supervision of this thesis.

Especially, I want to thank Dr. Ana Vasileva from MSSM, NY. I appreciate all her contributions of time, ideas, and help to make my Ph.D. experience productive and stimulating. The joy and enthusiasm she has for her research was always motivational for me.

I am very grateful to Thomas Müller-Reichert and Jana Mäntler from the EM facility in the Max-Planck-Institute for their splendid guidance with the electron microscope, as well as Ronald Naumann from the transgenic core facility for his great support, handling the ES cells and construction of the *Tdrd6*-deficient mice.

I would also like to acknowledge Sandra Martin from the University of Colorado for providing the Line-1 antibody.

I thank all my colleagues for the exciting and stimulating time during the last four years and the nice atmosphere in the lab. A special thank to Sabine Kamionka for her help with the mice.

I want to express my grateful thank to Estelle Festor and Dr. Caroline Adelfalk, as well as the remaining “SMCler” for an awesome time. I enjoyed the many hours of discussion in the lab, along with entertaining lunch and coffee breaks (not to forget the cakes and chocolate, thanks Caroline).

Finally, I owe special gratitude to my parents and my whole family for continuous and unconditional support, especially to Maximilian Anheier for his enduring patience and understanding during this part of my life.